

Catalytic Microreactors for Aqueous Phase Reactions – Carbon Nano Fibers as Catalyst Support



Digvijay Bhagwan Thakur

Catalytic Microreactors for Aqueous Phase Reactions – Carbon Nano Fibers as Catalyst Support

Graduation committee

Prof. Dr. Ir. B. Poelsema, chairman	University of Twente
Prof. Dr. Ir. L. Lefferts, promoter	University of Twente
Dr. K. Seshan, assistant promoter	University of Twente
Prof. Dr. J.G.E. Gardeniers	University of Twente
Prof. Dr. A.J.H.M. Rijnders	University of Twente
Prof. Dr. Ir. J.C. Schouten	Technical University of Eindhoven
Dr. J.H. Bitter	Utrecht University
Prof. Dr. D. Chen	Norwegian University of Science and Technology

The research described in this thesis was carried out at the Catalytic Processes and Materials group of the MESA+ Institute for Nanotechnology and Faculty of Science and Technology of the University of Twente, P.O. Box 217, 7500 AE Enschede, The Netherlands.



This Project was financially supported by 'MicroNed Program' under work package II-G-2 & 3 of cluster II: SMACT (Smart Microchannel Technology).

Cover design: Aabha and Digvijay Thakur.

Printed by: *Gildeprint*, Enschede, The Netherlands

Copyright © 2010 by Digvijay Bhagwan Thakur

All rights reserved. No part of this book may be reproduced or transmitted in any form, or by any means, including, but not limited to electronic, mechanical, photocopying, recording, or otherwise, without the prior permission of the author.

ISBN: 978-90-365-3100-9

Author's email: thakurdb@gmail.com

CATALYTIC MICROREACTORS FOR AQUEOUS PHASE REACTIONS – CARBON NANO FIBERS AS CATALYST SUPPORT

DISSERTATION

to obtain
the degree of doctor at the University of Twente,
on the authority of the rector magnificus,
prof. dr. H. Brinksma,
on account of the decision of the graduation committee
to be publicly defended on
Friday October 29th, 2010 at 15:00 hrs

by

Digvijay Bhagwan Thakur

born on April 24th, 1979
in Nasik, India

This dissertation has been approved by the promoter

Prof. Dr. Ir. L. Lefferts

and the assistant promoter

Dr. K. Seshan

To my Mother, Father, Aabha and my Teachers

“Take the first step in faith.
You don’t have to
see the whole staircase,
just take the first step.”

- *Dr. Martin Luther King, Jr.*

“Unity can only be manifested by the Binary.
Unity itself and the idea of Unity are already two.”

- *Buddha*

Summary

Microfabrication techniques are increasingly used in different fields of chemistry to realize structures with capabilities exceeding those of conventional macroscopic systems. Microfabricated chemical systems have a number of advantages for chemical synthesis, chemical kinetics studies and process development. Currently, there is tremendous interest to develop microstructured catalytic reactors for multiphase and/or heterogeneously catalyzed liquid phase reactions, comprising modified catalytic coatings on their internals. The use of structured catalyst supports, *i.e.* rigid, orderly arranged support materials such as carbon nanofibers (CNFs), is a prospective option in this respect.

This thesis describes various aspects of the development of carbon nanofiber supported catalyst layers on structured internals of microreactors made from silicon technology based materials (*e.g.* fused silica and/or silicon). These microreactors are intended to be used for heterogeneously catalyzed liquid phase reactions, in this case for aqueous phase removal of nitrite and bromate to evaluate the performance of such systems and demonstrate their benefit over conventional catalyst support material.

The synthesis of stable carbon nanofiber layer on flat substrates (representing surfaces of microreactor channel walls) is a requisite for obtaining the know-how to translate it for preparing these layers inside microreactor channels. Chapter 2 is a detailed study of CNF synthesis using thin metal film configurations with nickel (Ni) as growth catalyst and different metals (*i.e.* Ti, Ti-W and Ta) as adhesion layer between nickel and fused silica substrates. Although CNFs could be synthesized on 25 nm nickel with a titanium adhesion layer (10-200 nm), titanium is not a good adhesion material. The use of a 10 nm thick adhesion layer of titanium-tungsten or tantalum resulted in the formation of well-attached CNF-layers. The carbon nanofibers in these layers were entangled, quasi-crystalline and showed tip-type growth mode. Although for both metal layer configurations, *i.e.* Ni/Ti-W and Ni/Ta, the thickness of the CNF layer was similar under the same growth conditions, the diameter of the fibers was smaller in case of Ni/Ta (20-50 nm) compared to Ni/Ti-W (80-125 nm). This is found to be related to the grain size of the nickel nanoparticles formed during the reduction treatment prior to the CNF synthesis step.

The work presented in chapter 3 describes essential understanding about tuning and/or optimization of the overall CNF layer morphology, by evaluating the influence of various growth parameters during catalytic thermal chemical vapour deposition of Ni/Ti-W and Ni-Ta on fused silica and oxidized silicon substrates. It was found that the most important parameters were ethylene concentration and addition of hydrogen to the reactant mixture. Open, structured CNF layers with entangled morphology were formed for ethylene concentrations ≥ 25 vol.%. Moreover, addition of hydrogen to ethylene significantly enhanced the rate of formation of CNFs, and at the same time resulted in reduced average diameter of the fibers. Additionally, the choice of adhesion layer material (*i.e.* Ti-W and /or Ta) in combination with feed composition during C-TCVD was found to play a crucial role in the existence of a thick 'dense' C-layer between the substrate and the 'open' CNF layer.

Thus optimized CNF layers can be used as a structured catalyst support in microreactors. Chapter 3 further illustrates the effective utilization of structured features such as arrays of micromachined pillars, to fill the volume of microreactor channel with CNF layers. Eventually, the suitable combination of interpillar spacing and CNF layer thickness demonstrated successful filling of channel volume.

In chapter 4 the preparation and characterization of a CNF supported catalyst layer on flat surfaces and inside microchannels has been shown. Ruthenium catalytic nanoparticles on carbon nanofiber support layers were realized *via* homogeneous deposition precipitation and pulsed laser deposition. CNF layers are functionalized by oxidation with nitric acid to facilitate Ru deposition. Besides removal of exposed nickel (used for CNF-growth), an acid treatment forms oxygen-containing groups on the surfaces of CNFs (mainly carboxyl and hydroxyl groups). Ruthenium was anchored on oxidized CNF layers by means of HPD and PLD. Critical issues for a good dispersion of the particles and a sharp size distribution are the pH of the precursor solution (HDP) and the reduction treatment after deposition (PLD). Both optimized deposition methods resulted in a ruthenium loading of 2.3 ± 0.1 wt.% (HDP had a narrower particle size distribution). The presence of nanoparticles across the complete thickness of the CNF layers was found to be uniform when HDP was used to deposit Ru on CNF layers. A catalytic microreactor module containing Ru particles attached to carbon nanofibers which fill the entire reactor volume keeping the highly porous and/or open structure, is achieved.

In chapter 5, Carbon nanofiber supported palladium (Pd) catalyst layers synthesized inside silicon based microreactors were used for studying the reduction of aqueous nitrite solution. Nitrite hydrogenation is known to be kinetically fast reaction, hence ideal for demonstrating performance of synthesized CNF layers inside microreactor systems. The catalyst layers were prepared *via* incipient organic impregnation method using palladium acetylacetonate precursor solution in toluene. A relatively large average particle size of Pd (~7-9 nm) was obtained with uniform distribution across the CNF layers. The mass transfer properties, both external and internal, were probed and the intrinsic rates of nitrite conversion (TOF) were found to be independent of the, (i) linear velocity higher than 90 cm/min (flow rate of 50 μ L/min for the current microreactor module), and (ii) CNF layer thickness below ~13 μ m, indicating the absence of any mass transfer limitations. Thus optimized CNF layers were applied for performing a heterogeneously catalyzed liquid phase reaction, *i.e.* aqueous phase bromate reduction.

Chapter 6 presents results of systematic study of aqueous phase bromate reduction using carbon nanofiber supported ruthenium catalyst layers integrated in silicon based microreactors. These results clearly show a promising catalytic performance in eliminating bromate contamination from aqueous solutions *via* red-ox mechanism of ruthenium based catalyst. It was demonstrated that a CNF based catalyst is indeed highly active for bromate reduction, resulting in TOFs larger in comparison to conventional powdered catalyst *i.e.* Ru/activated carbon. This enhanced catalytic performance is due to improved mass transfer properties of entangled CNF layers with macroporous (open) structure, which offer low tortuosity and subsequently enhanced accessibility to all the Ru active sites, in contrast to the poor accessibility of active sites in the case of microporous AC support material. This benefit is crucial to in particular heterogeneously carried liquid phase reactions where mass transfer limitations are important factor. Although a high catalytic activity was shown, a gradual deactivation of the Ru/CNF catalyst was observed under current experimental conditions. Further investigation of used catalyst showed that severe sintering took place and confirmed no deposition of coke or amorphous carbon on Ru catalyst. Specific characterization using XPS indicate the formation of Ru(OH)_x species as an additional cause of deactivation. The use of higher alcohols indeed limited the extent of deactivation by controlling hydroxylation of Ru.

It is proposed that aqueous phase bromate removal is carried out by heterogeneous redox catalysis *via* bromate reduction to bromide, mainly by RuO_2 which itself gets oxidized to a higher oxidation state and react with alcohol to be recycled after being reduced in the process. In general, Ru supported on CNF layers inside microreactor systems offers a promising option in terms of efficiency and offer a “green” method for removal of drinking water pollutants such as bromate.

It is expected that this novel approach of constructing microreactors comprising stable and well-defined layers of carbon nanofibers as a structured catalyst support will allow efficient use of catalysts in fluid-solid reactions carried within microreaction systems.

Samenvatting

In meerdere gebieden van de chemie worden steeds vaker systemen gebruikt die gemaakt zijn met microfabricage technieken, daar met deze technieken structuren gemaakt kunnen worden die de capaciteiten van conventionele macroscopische systemen overtreffen. Ten opzichte van conventionele systemen hebben deze zogenaamde microsystemen een aantal voordelen, welke vooral gebruikt kunnen worden voor chemische synthese, kinetiek studies en proces ontwikkeling. Momenteel is er grote interesse in het ontwikkelen van katalytische microreactoren die toegepast kunnen worden voor meer-fasige en heterogeen gekatalyseerde vloeistof reacties, waarbij de katalysator aan de wanden van de microreactor is aangebracht. Voor dit laatste is het gebruik van sterke, geordende ondersteunings-materialen zoals koolstof nanofibers een veelbelovende optie.

In dit proefschrift zijn verschillende aspecten van de ontwikkeling van op koolstof nanofibers gebaseerde katalysator ondersteuningsmaterialen beschreven, die vervolgens geïntegreerd zijn in de interne structuren van microreactoren gemaakt van silicium en/of kwartsglas. Deze microreactoren zijn bedoeld voor het efficiënt uitvoeren van heterogeen gekatalyseerde vloeistof reacties, bijvoorbeeld de verwijdering van nitriet en bromaat. Dergelijke toepassingen tonen tevens het voordeel aan van deze koolstofmaterialen ten opzichte conventionele materialen.

De synthese van stabiele koolstof nanofibers op vlakke substraten (die de wanden van kanalen in een microreactor representeren) is beschreven in hoofdstuk 2. In dit hoofdstuk wordt in detail de synthese van fibers op verschillende dunne metaallaagjes beschreven, waarbij nikkel (Ni) de groeikatalysator is voor nanofibers en tantaal (Ta), titaan (Ti) of titaan-wolfraam (Ti-W) het adhesie metaal tussen het kwartsglas en de nikkel laag. Hoewel het mogelijk is om nanofibers te groeien op 25 nm nikkel met een hechtlaag van titaan (dikte 10-200 nm), is titaan geen goed hechtmateriaal: de nanofibers laten los van het kwartsglas. Bij toepassing van tantaal of titaan-wolfraam blijven de gesynthetiseerde nanofibers vastzitten op het substraat. In beide gevallen zijn de fibers in elkaar verstrengeld, quasi-kristallijn en gegroeid volgens het punt/top principe. Hoewel voor beide metaallagen (Ni/Ta en Ni/Ti-W) de dikte van de nanofiberlaag identiek is voor gelijke synthese condities, is de diameter van de fibers in

het geval van Ni/Ta kleiner dan voor Ni/Ti-W, te weten 20-50 nm en 80-125 nm. Dit verschil is nauw gerelateerd aan de grootte van de nanodeeltjes die gevormd worden tijdens de reductie behandeling van de metaallaag.

In hoofdstuk 3 wordt opgedane kennis beschreven omtrent de groei en optimalisatie van de morfologie van de laag van koolstof nanofibers. De invloed van verschillende parameters van het katalytisch-thermische *chemical vapor deposition* proces voor de synthese van nanofibers is onderzocht voor Ni/Ti-W en Ni/Ta op kwartsglas en geoxideerd silicium. Gebleken is dat de ethyleen concentratie en het toevoegen van waterstof aan ethyleen de parameters zijn die de grootste invloed hebben op het groeiproces. Ethyleen concentraties ≥ 25 vol.% leiden tot het ontstaan van verstengelde koolstof fibers, waarbij het geheel een 'open' netwerk van nanofibers is. Het toevoegen van waterstof aan ethyleen heeft een sterke toename van de groeisnelheid van de nanofibers tot gevolg, en tevens een afname van de gemiddelde diameter van de fibers. Verder beïnvloedt de gebruikte hechtlaag (Ti-W of Ta) in combinatie met genoemde parameters het al dan niet aanwezig zijn van een zogenaamde 'dichte' C-laag tussen het substraat en de 'open' laag van nanofibers. Met deze optimale parameters is vervolgens een efficiënt bed van nanofibers gemaakt in de vloeistofkanalen van een microreactor. Door het wederzijds afstemmen van de groeiparameters en afstand tussen micropilaren (welke in geordende arrays in het kanaal aanwezig zijn), is het mogelijk om de ruimtes tussen de pilaren volledig te vullen met genoemde 'open' laag van nanofibers, die vervolgens gebruikt kunnen worden als ondersteuningsmateriaal voor katalysatoren.

In hoofdstuk 4 is beschreven hoe dergelijke nanofiberlagen gebruikt kunnen worden als drager van een katalysator. Het aanbrengen van ruthenium (Ru) nanodeeltjes is gedaan door middel van homogene depositie-precipitatie (HDP) alsmede gepulseerde laser depositie (PLD). Alvorens Ru te deponeren zijn de nanofibers gefunctionaliseerd met salpeterzuur. Naast het oplossen van vrijliggende nikkeldeeltjes (die gebruikt zijn voor het groeien van de nanofibers), leidt een dergelijke zuurbehandeling de vorming van zuurstofbevattende groepen aan het oppervlak van de fibers (voornamelijk carboxyl en hydroxyl groepen). Aan deze geoxideerde fibers is ruthenium gekoppeld met genoemde technieken. Kritische zaken voor een goede dispersie van de deeltjes en een juiste distributie zijn de zuurgraad van de precursor oplossing (HDP) en een reductiestap na depositie (PLD). Met beide technieken is een

ruthenium lading van 2.3 ± 0.1 wt.% bereikt, waarbij de HDP-methode een smallere verdeling van de deeltjesgrootte had. In het geval van HDP zijn de Ru-nanodeeltjes homogeen verdeeld over de gehele dikte van de nanofiberlaag. Ru-depositie middels HDP is tevens succesvol uitgevoerd op nanofiberlagen in kanalen van microreactoren, welke middels plaatsing in een module getest kunnen worden.

In hoofdstuk 5 is aangetoond hoe nanofiberlagen in microreactoren gefunctionaliseerd kunnen worden met palladium (Pd), en vervolgens hoe deze toegepast zijn voor de reductie van een waterige nitriet oplossing. Daar het bekend is dat nitriet hydrogenering een kinetisch snelle reactie is, is deze reactie ideaal voor het aantonen van de kwaliteit en bekwaamheid van microreactoren met daarin nanofibers als ondersteuning voor katalyse materialen. Op de fibers is palladium aangebracht middels een organische impregnatie methode, waarvoor een precursor oplossing van palladium acetylacetonaat in toluen gebruikt is. Dit leidt tot een relatief grote Pd-deeltjes (7-9 nm), maar de deeltjes zijn homogeen verdeeld over de dikte van de nanofiberlaag. Vervolgens zijn massa-overdracht eigenschappen in een microreactor onderzocht, en daaruit bleek dat de intrinsieke snelheden van nitriet omzetting constant zijn (d.w.z. afwezigheid van massa-overdrachts beperkingen) voor lineaire vloeistofsnelheden tot 90 cm/min en nanofiber-laagdiktes tot ~ 13 μm .

Microreactoren met daarin nanofiberlagen die gefunctionaliseerd zijn met ruthenium zijn gebruikt voor vloeistoffase bromaat reductie, welke beschreven is in hoofdstuk 6. De resultaten tonen een veelbelovende katalytische performance voor het verwijderen van bromaat vervuiling uit wateroplossingen middels het redox mechanisme van de ruthenium katalysator. Aangetoond is dat de ruthenium gefunctionaliseerde nanofiberlagen een hoge activiteit hebben voor het reduceren van bromaat, en hogere TOF-waarden hebben dan conventionele poeder katalysatoren. Deze betere katalytische performance is het gevolg van verbeterde massa-overdracht eigenschappen van de verstengelde nanofibers, en dus goede toegankelijkheid van de actieve Ru deeltjes (dit is niet het geval voor meer conventionele katalysatordragers). Dit is met name van belang voor heterogeen gekatalyseerde vloeistof reacties waarin normaliter massa-overdracht beperkingen een rol spelen. Hoewel een initieel hoge katalytische activiteit gevonden is, daalt deze activiteit als gevolg van sintering en niet vanwege de vorming cokes of amorf carbon op de Ru-deeltjes. Daarnaast is met XPS aangetoond dat het ontstaan van $\text{Ru}(\text{OH})_x$ ook een reden van deactivatie, en kan door

het gebruik van andere alcoholen de mate van deactiviteit van de katalysator beperkt worden. Geponeerd is dat het verwijderen van bromaat (in vloeistoffen) geschiedt door heterogene redox katalyse: bromaat reduceert tot bromide, in hoofdzaak door RuO_2 welke zelf tot een hogere toestand oxideert en met alcohol reageert na reductie in het proces.

Geconcludeerd is dat microreactoren met ruthenium-gefunctionaliseerde nanofiberlagen een veelbelovend alternatief zijn voor het efficiënt en ‘groen’ verwijderen van vervuilingen uit drinkwater, zoals bromaat. Het is de verwachting dat dergelijke nieuwe benaderingen van het gebruik van stabiele en goed-gedefinieerde koolstof nanofiberlagen in microreactoren als dragermateriaal voor katalysatoren leiden tot een efficiënt gebruik van katalysatoren voor meerfasige reacties.

Contents

1. General Introduction	1
1.1 Catalysis - at the heart of modern chemical industry	3
1.2 Conventional multiphase reactor technology	4
1.3 Microreaction technology - General introduction	6
1.4 Integration of catalyst layer (solid phase) inside multiphase microreactors	8
1.5 Carbon nanofibers (CNF) – Novel structured catalyst support	9
1.5.1 General introduction	9
1.5.2 CNF as a catalyst support for liquid phase reactions in microreactors	12
1.5.3 Synthesis of CNFs on fused silica and silicon based substrates	13
1.6 Nitrite and bromate removal from aqueous solutions	15
1.7 Scope of the thesis	17
References	19
 2. Growth of Stable Carbon Nanofiber Layers on Fused Silica Substrates: On the Use of Ti, Ti-W and Ta as Adhesion Layers	 25
2.1 Introduction	27
2.2 Experimental	28
2.3 Results and discussion	31
2.4 Conclusions	40
References	41
 3. Carbon Nanofiber Layers to be used in Silicon based Microreactors: Influence of Growth Parameters on Carbon Nanofiber Morphology	 45
3.1 Introduction	47
3.2 Experimental	50
3.3 Results and discussion	53
3.4 Conclusions and outlook	65
References	66

4. Ruthenium Catalyst on CNF Support Layers for Si-based Structured Microreactors, Part I: Preparation and Characterization	71
4.1 Introduction	73
4.2 Experimental	74
4.3 Results and discussion	77
4.4 Conclusions	89
Appendix	90
References	92
5. Palladium Catalyst on Carbon Nanofiber Support Layers for Si-based Structured Microreactors: Catalytic Reduction of Nitrite Contaminants in Aqueous Phase	95
5.1 Introduction	97
5.2 Experimental	98
5.3 Results and discussion	101
5.4 Conclusions	107
References	107
6. Ruthenium Catalyst on CNF Support Layers for Si-based Structured Microreactors, Part II: Catalytic Reduction of Bromate Contaminants in Aqueous Phase	109
6.1 Introduction	111
6.2 Experimental	112
6.3 Results and discussion	114
6.4 Conclusions	126
References	127
7. Conclusions and Recommendations	131
References	138
List of Publications and Conference Presentations	139
Acknowledgements	143

Chapter 1

General Introduction

Abstract

Microfabrication techniques are increasingly used in different fields of chemistry to realize structures with capabilities exceeding those of conventional macroscopic systems. Microfabricated chemical systems are expected to have a number of advantages for chemical synthesis, chemical kinetics studies and process development. Currently, there is tremendous interest to develop microstructured catalytic reactors for multiphase and/or heterogeneously catalyzed liquid phase reactions, comprising modified catalytic coatings on their internals. The use of structured catalyst supports, i.e. rigid, orderly arranged support materials such as carbon nanofibers (CNFs), is a prospective option in this respect.

1.1 Catalysis – at the heart of modern chemical industry

In the chemical industry the ability to carry out chemical reactions at a large scale with high yields of useful products and at the same time achieving economic efficiency is extremely important. Generally, chemical processes convert readily available starting materials to more valuable product molecules. At the heart of most of these processes are catalytic materials, which are utilized to accelerate chemical transformations so that reactions proceed in a highly efficient manner, achieving high yields of desirable products and avoiding unwanted by-products. Catalysts often allow more economical and environmentally benign production routes compared to classical stoichiometric procedures. Approximately 85-90% of the products of the chemical industry are made applying catalysts. Catalysis is so pervasive that subareas are not readily classified. However, the three main fields of applications where catalysts are crucial can be identified as *(i)* production of transportation fuels, *(ii)* production of bulk and fine chemicals, and *(iii)* abatement of pollution in end-of-pipe solutions (such as automotive and industrial exhaust). The total annual catalyst demand from chemical, petroleum refining, and polymer firms in 2007 was close to \$ 13.5 billion, with an expected increase of 6% per year to \$16.3 billion by 2012 [1].

Industrial chemical reactions involving more than one phase have become rather a rule than exception. Catalytic multiphase reactions involving fluid-fluid (homogeneously catalyzed), fluid-solid and three phase reactions (heterogeneously catalyzed) account for more than 85% of industrial chemical processes. Typical application areas include the manufacture of petroleum-based products and fuels, production of commodity and specialty chemicals, pharmaceuticals, polymers, herbicides and pesticides, refining of ores and pollution abatement. The reactors utilized to perform such reactions are categorized as multiphase reactors. These are reactor systems in which gas and/or liquid phase reactants are contacted with solid phase which mostly is a catalyst.

Selection of a multiphase reactor configuration for a given reaction system requires various parameters to be considered such as, *(i)* the number of phases involved, *(ii)* the differences in the physical properties of the participating phases, *(iii)* the inherent nature of reaction (described by stoichiometry of reactants, intrinsic reaction rates, isothermal or adiabatic conditions *etc.*), *(iv)* post-reaction separation, *(v)* required residence time, and *(vi)* the heat and mass transfer characteristics of the reactor. The initial four aspects are usually controlled to a limited extent only, while the remaining

aspects are helpful as design variables for optimizing the reactor performance [2]. Higher rates of heat and mass transfer improve effective rates and selectivities, in particular for fast catalytic reactions. Transport processes can be made efficient by enhanced heat and mass exchange, which depend upon higher interfacial surface areas and short diffusion paths. These are easily attained in microstructured reactors comprising fluid channels with lengths in the millimeter-to-centimeter range and cross-sectional dimensions in the range sub-micrometer to sub-millimeter [3, 4]. A comparison between conventional multiphase reactor systems and microstructured reactors illustrates the benefits of latter, in particular for heterogeneously catalyzed multiphase reactions.

1.2 Conventional multiphase reactor technology

Conventional multiphase reactor technologies, involving liquid and gas phase reactants and solid phase catalyst, comprise different types of reactors. Among them most commonly used are the agitated tank slurry reactor, the bubble column slurry reactor and the packed/trickle bed reactor (*Fig.1.1*). The general advantages as well as their limitations are listed in *Table 1.1*. Slurry reactors (agitated tank and/or bubble column) comprise small catalyst particles suspended in liquid phase reactant through, which reactive gas is dispersed. The small catalyst particles (diameter \sim tens of microns) ensure short diffusional distances, providing better mass transfer properties for multiphase reactions and hence efficient utilization of the catalyst. However, catalyst separation is difficult and a filtration step is necessary for separating the fine catalyst particles from the products. Moreover, attrition of catalyst particles can lead to loss of active metal and consequently deteriorate the performance of the catalyst over time. Trickle bed reactors are relatively simple and essentially consist of packed bed of catalyst pellets through which gas and liquid reactants flow co- or countercurrently. They are easy to operate and more suitable for the reactions which require relatively high amounts of catalyst; in contrast to slurry reactors which can hold relatively smaller amounts of catalyst. The relatively longer residence time in the reactor (owing to plug flow behavior) makes it suitable for achieving higher conversions, an advantage particularly for slow reactions [2, 5]. The catalyst pellet size typically used to prepare a packed bed is relatively large (4–10 mm) as a precaution for avoiding large pressure drops across the packed bed. However, this also leads to poor performance in terms of intraparticle mass transfers due to long diffusional distances existing in larger catalyst particles. Additionally, heat

management and liquid flow maldistribution are two common problems observed in this type of reactor [6], which could lead to local ‘hot spots’ resulting not only into a decreased selectivity of the reaction and reduced catalyst life, but also to side reactions which may cause reactor runaway [7].

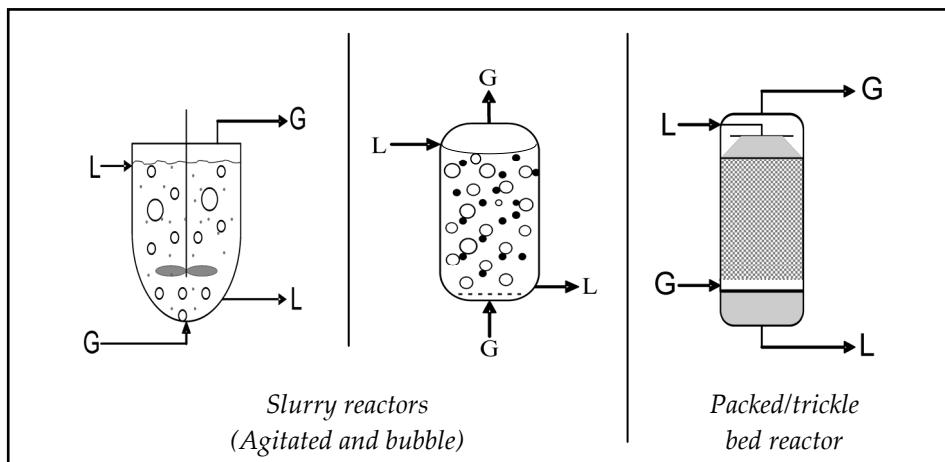


Figure 1.1: Most commonly used conventional multiphase reactor configurations

Table 1.1: General advantages and limitations of slurry and packed bed reactors [2]

Reactors	Advantages	Limitations
Slurry reactors (agitated tank and bubble column)	<ul style="list-style-type: none"> • efficient utilization of catalyst • good liquid-solid mass transfer • good heat transfer characteristics 	<ul style="list-style-type: none"> • moderate gas-liquid mass transfer • catalyst separation is difficult and a filtration step is necessary • low selectivity in continuous mode due to back mixing
Packed bed reactor	<ul style="list-style-type: none"> • easy to operate • can accommodate high amounts of catalyst • suitable for slow reactions 	<ul style="list-style-type: none"> • flow maldistribution • higher pressure drop • possibilities of hot spot formation

1.3 Microreaction technology – General introduction

Advances in MEMS (micro-electromechanical systems) have enabled selected ‘*Lab-on-a-chip*’ technologies and microfluidics to be instrumental for recent developments in analytical chemistry and molecular biology, which have also coincided with the efforts on research in chemical process miniaturization [8]. That is, reducing the characteristic length scale of the unit operation to improve mass and heat transfer, and consequently the whole process performance. Recently developed microfabrication technologies can now be applied to many disciplines, which have all contributed to the rapidly moving miniaturization of chemical and biotechnological processes. Up to now, the greatest research efforts in the field of microscale devices were in the analytical area [9, 10]. For the electronics industry, silicon microchips were an ideal subject for miniaturization, with the added possibility of increasing their capacity and functionality. The same approach has been implemented in chemical and biochemical engineering, so that sample preparation, mixing, reactions and separations can all be performed on an integrated microfabricated device. Miniaturization, in conjunction with integration of multiple functionalities can enable the construction of structures that exceed the performance of traditional macroscopic systems, can provide a number of new functionalities, and offer the potential of low-cost mass production [11].

Microreactors are nowadays regarded as a separate class of chemical reactors, characterized by small dimensions, *i.e.* reactors with a channel hydraulic diameter of 100 - 300 μm and a channel length of 1 - 50 mm [3, 4]. Microfabricated chemical reactor technology offers numerous advantages in processing of fine chemicals when compared with traditional batch-wise synthesis in stirred vessels. The improved mass and heat transfer properties (see *Fig. 1.2 [2]*) typical of microfluidic systems (due to their small dimensions, producing high surface-to-volume ratios in the order $10^4 \text{ m}^2/\text{m}^3$), enable the use of more intensive reaction conditions that result in higher yields than those obtained with conventional size reactors [12, 13]. Residence time and heat management can be properly tuned in microreactors to avoid secondary reactions and preventing thermal runaway during reactions *i.e.* safer operation. This leads to a higher selectivity to desired products, and thus to higher quality products [14, 15]. In this way, microreaction technology contributes to reducing the size of (fine) chemical manufacturing plants, which reduces risks and hazards, an important aspect of ‘green’ chemistry, *i.e.* chemistry designed to reduce or eliminate the use and generation of hazardous substances.

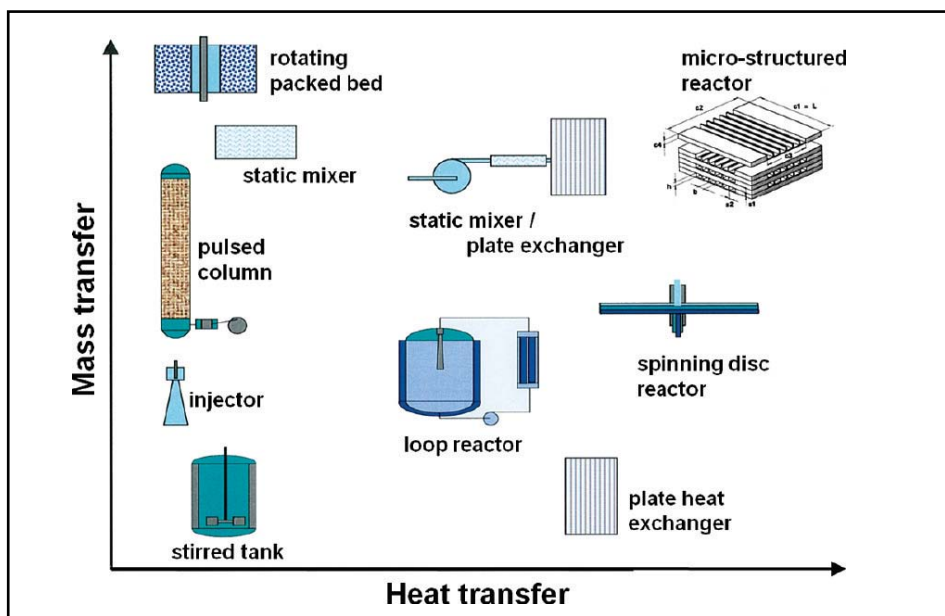


Figure 1.2: Benchmarking of the microreactor [2]

Generally, microreactors are operated in the laminar flow regime where the internal hydrodynamics, including heat and mass transfer characteristics, are well known. Therefore, under such circumstances, microreactors are also very suitable for measuring intrinsic reaction kinetics because mass and heat transport limitations can either be circumvented or they can be accurately accounted for. In this way, microreactors have also great potential in scientific research and in process development (*e.g.*, high throughput screening and synthesis, and small scale experimentation). For the production of fine chemicals and pharmaceuticals, many novel process routes and processing architectures can be envisaged [16, 17]. Major incentives for this can be found in the need for considerable shorter time-to-market, as well as improving the product/waste ratio for the current chemical routes, which is often below 0.01. Moreover, the future fine chemicals industry needs to become more flexible to be able to manufacture products in various quantities just in time and close to the raw materials source or at the location of use. Microreactors offer this capability to carry out flexible on-site production of fine chemicals at the point of demand. This is especially important, when products are not stable. Various industries can directly benefit from the use of microreactor technology: an example is the fine chemicals industry which

often involves multiphase reactions. Multifluid microreactors encompass gas-liquid, liquid-liquid and gas-liquid-liquid reactors [18]. An important class of multiphase reactors is fluid–solid reactors used to perform gas-liquid-solid (*G-L-S*) reactions which essentially involve a solid phase catalyst where the reaction takes place, which is generally incorporated inside the structured internal of reactor, such as microchannels either as a packed bed or a coating. These catalytic reactions, however, pose a substantial challenge in achieving an efficient contact between the different phases and mass transfer [19-21].

1.4 Integration of catalyst layer (solid phase) inside multiphase microreactors

Conventionally, integration of a (solid) catalyst layer inside microreactor channels can be achieved in two ways, *i.e.* (i) by using a micro packed-bed of powdered catalyst [22-24], or (ii) by using a thin layer of catalyst coated on the inner wall of a microchannel [25-27]. However, use a powdered catalyst packed-bed might result in large pressure drops across the bed since the size is scaled down, as predicted by the Ergun equation [28]. Also, channeling at the wall-particle interface becomes increasingly likely for creeping flow in microreactors. Nevertheless, one benefit of packed bed reactors is that commercial catalyst formulations that have already been optimized can be used. An alternative approach to the use of a catalyst packed bed is deposition of a thin catalyst film, typically *via* very-large-scale integration (VLSI) manufacturing methods used for mass production of integrated circuits (ICs), such as physical and/or chemical vapor deposition (PVD/CVD)[29]. However, a thin catalyst coating usually fails to utilize the entire volume of the reactor channel effectively and may not provide the high surface area required for catalytic reactions. Most of these problems can be overcome by introducing nanoscale structural features in the microchannels. For microsystems, various possibilities have been explored, such as use of porous anodic alumina layers [30, 31], walls coated with porous materials such as zeolites [32, 33], and black or porous silicon [8, 34]. However, these methods of creating porous structures are mostly limited to sub micron layers. *Table 1.2* enlists various techniques reported in literature to enhance the catalytic surface area in microreactors.

An exciting option in this regard is the use of rigid, porous and orderly arranged catalyst supports based on nanofibers, which due to their tunable morphology and surface properties can be an effective material to be used as catalyst support material.

Carbon nanostructures, such as carbon nanofibers and/or tubes (CNFs/CNTs), are promising candidates for this purpose, onto which metallic catalytic active phase (*e.g.* platinum (Pt) or palladium (Pd) nanoparticles) can be deposited.

Table 1.2: Various techniques used to enhance the catalytic surface area in microreactors [2]

Techniques	Coating layer
<i>Metal oxide coatings</i>	
• Anodic oxidation of aluminum	- Alumina ^[35]
• Anodic oxidation of AlMg microreactor wall	- Alumina ^[27]
• Sol-gel technique	- Alumina ^[36] , silica ^[37] , titania ^[38]
• High temperature treatment of Al containing steel	- Alumina ^[39]
• Wash-coating	- γ -alumina ^[40]
• Electrophoretic deposition	- Al ₂ O ₃ , ZnO, CeO ₂ ^[41]
• Zeolite coated microchannel reactors	- Zeolite ^[42, 43]
• Direct formation of zeolite crystal on metallic structure	- Zeolite ^[44-46]
• Chemical vapor deposition	- Alumina ^[47]
• Flame spray	- Au/TiO ₂ ^[48]
<i>Carbon based coatings</i>	
• Carbonization of polymers	- Carbon coating ^[49]

1.5 Carbon nanofibers (CNF) – Novel structured catalyst support

1.5.1 General introduction

The deterministic synthesis of nanomaterials with predefined structure and functionality plays a pivotal role in nanotechnology [50]. Out of several potential nanomaterials, nanostructured carbon materials such as carbon nanofibers and/or nanotubes (CNFs/CNTs) have emerged as the most promising candidates for various nano- and microsystem based applications due to their wide ranging properties [51]. Applications of carbon nanofibers (CNFs) and/or carbon nanotubes (CNTs) include emitters for field emission displays [52], composite reinforcing materials [53], hydrogen storage [54], bio- and chemical sensors [55, 56], nano- and microelectronic devices [57, 58].

The history of CNFs dates back to a U.S. patent published in 1889 [59], which reports the growth of carbon filaments and possibly that of carbon nanofibers from carbon-containing gases using iron as catalyst. In 1969, Robertson [60] recognized that

the interaction of metal surfaces and methane led to formation of graphitic carbon at relatively low temperatures. Baker *et al.* further showed in 1972 that carbon nanostructured materials can be synthesized using supported transition metal catalyst such as Ni, Co and Fe [61]. In 1976, Oberlin, Endo and Koyama reported CVD growth of nanometer-scale carbon fibers [62]. In following years detailed studies of CNFs were essentially motivated due to undesirable deposition of carbon on the surface of steam crackers during the production of olefins [63]. Two foremost events significantly boosted the research in carbon nanostructure field on global scale. The first was in 1985 when a new form of carbon, Buckminsterfullerene C_{60} was discovered by Robert Curl, Harold Kroto and Richard Smalley [64]. The second event was the discovery of multi-wall carbon nanotubes (MWCNTs) by Iijima in 1991 [65].

In principle, CNFs are filamentous nanostructures which are grown by the diffusion of carbon, *via* catalytic decomposition of carbon containing gases or vaporized carbon from arc discharge or laser ablation, through a metal catalyst following its subsequent precipitation as graphitic filaments (see *Fig. 1.3 [66]*).

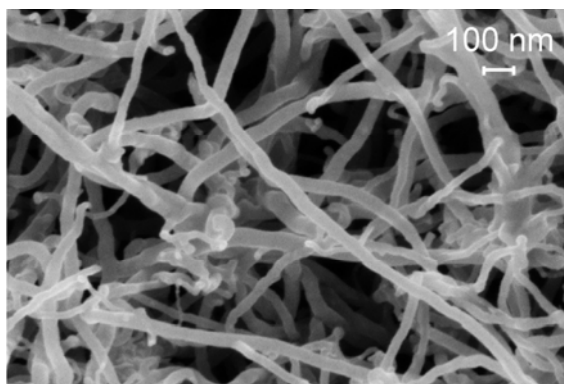


Figure 1.3: High resolution SEM image of entangled carbon nanofibers [66]

Based on their structural features, carbon nanofibers (CNFs) can be described as cylindrical or conical structures that have diameters varying from a few to hundreds of nanometers (0.4 to 500 nm) and lengths ranging from less than a micron to millimeters. They have varying internal structures depending on the arrangements of “graphene sheets”. The graphene sheets can be defined as a hexagonal network of covalently bonded sp^2 hybridized carbon atoms or a single two-dimensional (2D) layer of a three-dimensional (3D) graphite (*Fig. 1.4a*). The angle between the fiber axis and the graphene sheets determines two distinct types of carbon nanofibers that are commonly observed.

The first type of carbon nanofiber consists of stacked curved graphene layers that form cones or cups. The stacked cone structure is often described as herringbone (or fishbone) due to their resemblance with fish skeleton with the graphene sheets stacked at an angle of $\sim 45^\circ$ to the fiber axis (Fig. 1.4b, [51]). The second type of CNF consists of graphene sheets stacked on top of each other at an angle of $\sim 90^\circ$ to the fiber axis (Fig. 1.4c [67]).

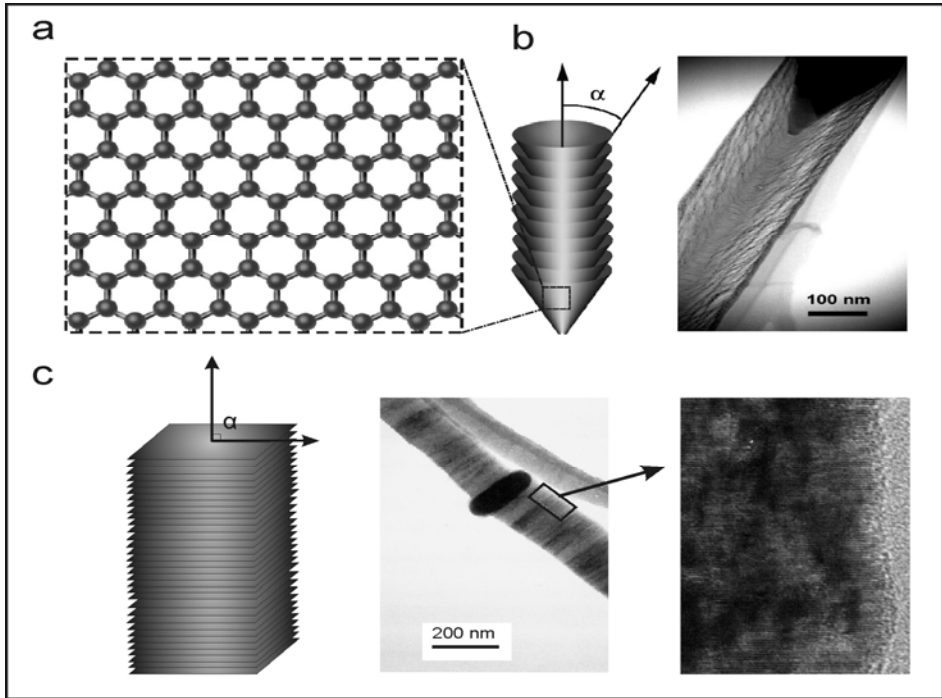


Figure 1.4: Schematic structure of carbon nanofibers, (a) Graphene layer, (b) stacked cone herringbone nanofiber ($\alpha = \sim 45^\circ$) and a high-resolution micrograph of the same [51], (c) the arrangement of the graphite platelets stacked in a direction perpendicular to the fiber axis ($\alpha = \sim 90^\circ$) [67]; in both cases the distance between two stacked graphene sheets is 0.34 nm.

The synthesis of carbon nanostructures can be achieved *via* arc discharge [68], laser ablation [69] and chemical vapor deposition (CVD) methods (*e.g.* catalytic thermal CVD and plasma enhanced CVD) [51, 70, 71]. The catalytic thermal chemical vapor deposition (C-TCVD) method is a versatile technique and a relatively cheap method for large-scale applications [63, 72, 73], and therefore most often used for CNF-synthesis.

The C-TCVD method utilizes decomposition of carbon-containing gases on catalytically active components, *e.g.* transition metals such as nickel (Ni), cobalt (Co) and iron (Fe) or alloys of these materials (due to their ability to dissolve carbon and/or form metal carbides) [51]. Hydrocarbon gases such as methane (CH_4), acetylene (C_2H_2), ethylene (C_2H_4), ethane (C_2H_6), or other C-sources as carbon monoxide (CO) or synthesis gas ($\text{CO} + \text{H}_2$) can be used to obtain CNF growth on these metal catalysts at temperatures between 400 and 1000 °C [63].

1.5.2 CNF as a catalyst support for liquid phase reactions in microreactors

Carbon nanostructures offer numerous advantages as catalyst supports for chemical reactions *viz.*, (i) corrosion resistance to acid or base medium, (ii) high length (μm)-to-diameter (nm) ratio and high surface area, (iii) absence of micro porosity, (iv) possibility to tune the surface chemistry, and (v) easy recovery of precious metal catalysts supported on them by simply burning the carbon skeleton [74-76]. Moreover, it has also been claimed that the performance of CNF supported catalysts can be influenced by adsorption of reactants on the CNF support. For example, for the liquid phase hydrogenation of cinnamaldehyde over Pt/CNF catalyst, it was demonstrated that catalytic action of Pt is influenced by the amount of cinnamaldehyde adsorbed on the support in the vicinity of Pt particles [72].

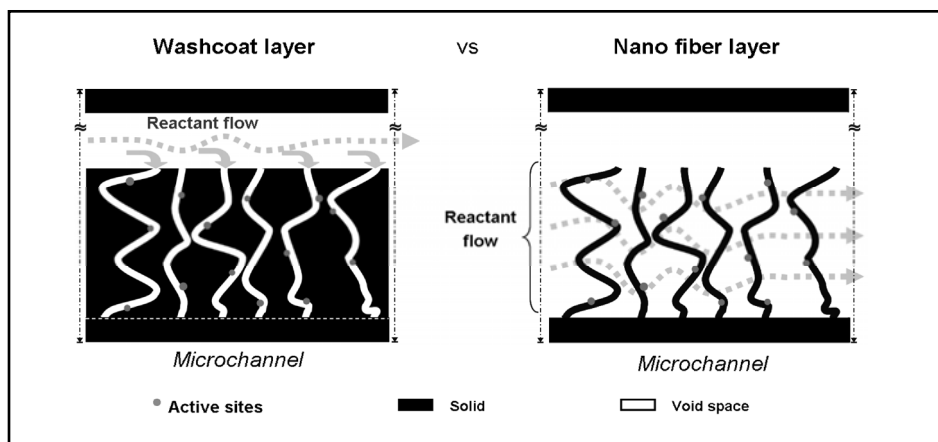


Figure 1.5: A schematic representation of reactant flow inside microchannel coated with washcoat layer (left) versus carbon nanofiber layer (right), illustrating a virtually reverse configuration in term of accessibility of the supported active sites

The small dimensions of carbon nanostructures and the above-mentioned advantages as catalyst support motivate integration of CNFs and/or CNTs as structured catalyst support layers in miniaturized reaction systems, *i.e.* microreactors. *Figure 1.5* exemplifies the advantage of integrating a layer of carbon nanostructures in a microreactor channel as an alternative to a washcoated layer. A CNF layer has easier accessibility of active sites for reactant molecules due to its open structure, as a consequence of which diffusion problems are avoided, particularly in the case of liquid phase reactions which exhibit relatively lower values of mass transfer coefficients (by a factor of 10^4 [77]) than gas phase reactions [78, 79].

1.5.3 Synthesis of CNFs on fused silica and silicon based substrates

A range of structured materials including monoliths [80], foams [76, 79, 81, 82], filters [83], glass and carbon fibers [84, 85] and cloths [86] have been used for the synthesis of CNF layers for catalytic application in conventional reactor systems. However, a microstructured reactor, especially that are silicon-technology based (*i.e.* made from materials such as silicon, Pyrex, Borofloat glass, quartz, fused silica *etc.*) requires the application of techniques which are suitable for deposition and/or synthesis of stable and uniform CNF layers on microreactor channel wall surfaces. However, synthesis of CNF/CNT based catalyst layers has rarely been achieved [87]. Thus, details on synthesizing stable and well-defined CNF layers in microreactor channels, their subsequent functionalization and deposition of catalytic phase for liquid phase reactions, are missing. An abundant amount of literature is available on the synthesis of carbon nanostructures on flat substrates using thin metal films of growth catalyst (*e.g.* Ni, Fe, Co *etc.*). These metal films are deposited using typical physical vapor deposition (PVD) techniques, *e.g.* e-beam evaporation and/or sputtering [51, 88, 89]. *Figure 1.6* schematically illustrates CNF synthesis on flat substrates using metal thin films. It primarily involves three major steps *viz.* (i) deposition of a stable metal thin film, (ii) dewetting (disintegration) of the as-deposited continuous metal film to create nucleation sites (nanoparticles) for facilitating CNF growth, (iii) catalytic thermal chemical vapor deposition (C-TCVD) of carbon containing gas at elevated temperatures to synthesize the CNFs. The C-TCVD step individually involves three sequential sub-steps based on a general mechanism proposed by various researchers *i.e.*, (i) decomposition of a carbon-containing gas exposed to the surface of a metal particle, (ii) dissolution of carbon in the metal particle (since transition metals have the ability to dissolve carbon and form metal carbide, mentioned earlier in *section 1.5.1*), and

diffusion of the dissolved carbon through the particle, and (iii) precipitation and/or growth of stacked layers of graphene sheets in the form of CNF on the opposite side of metal particle (as shown in *Fig. 1.6*-step 3).

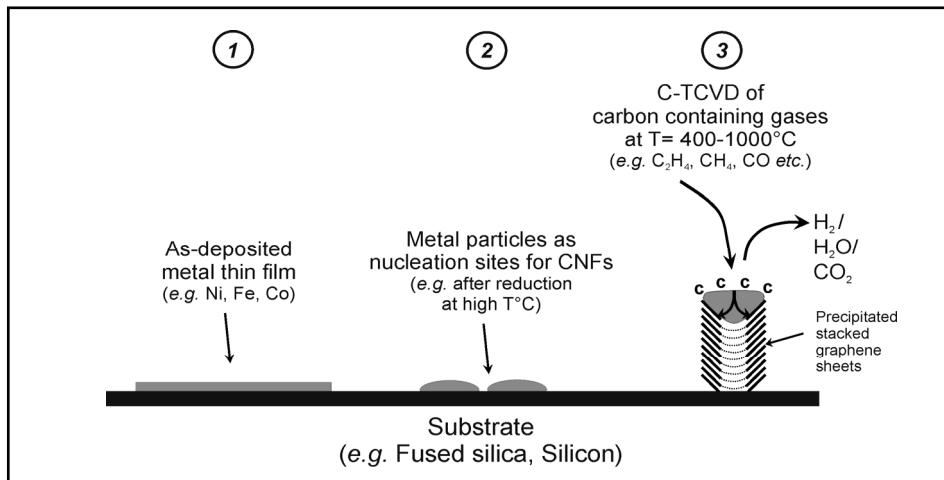


Figure 1.6: Schematic representation of CNF synthesis on flat surfaces via three essential steps viz. (i) metal thin film deposition, (ii) creation of metal particles as nucleation sites for CNF growth, (iii) C-TCVD of carbon containing gas at elevated temperatures to synthesize CNFs.

Good adhesion of synthesized CNF layers on structured internals of silicon microreactors is important to ensure that attrition losses of CNFs due to shear forces exerted by fluids flowing through the entangled CNF layers are minimized. Prior to formation of such stable CNF layers, the stability of thin metal film on substrates itself can be a critical issue. It is known that thin films of physical vapor deposited metal, such as nickel, do not adhere well to materials commonly used for silicon-technology based microreactors (*i.e.* silicon, Pyrex, Borofloat glass, quartz, fused silica), as a consequence of which an intermediate layer between the nickel and the substrate material has to be used [51].

Detailed studies of CNF synthesis using thin metal film configurations, including various aspects such as adhesion layer thickness, stability at high CNF growth temperatures and subsequent influence on the morphology of CNF layer formed, still needed to be carried out and is one of the objectives of research performed in this work. There are, however, additional critical issues which have to be addressed in order to

obtain microreactors of which the flow channels are filled with an efficient CNF-based catalyst support, *i.e.* a layer of entangled CNFs ‘jungle’ as shown in *Fig. 1.3*. These are, (i) deposition of a well adhered metal layer (*e.g.* Ni [25, 51]) required for the synthesis of CNFs, (ii) good attachment of the synthesized CNF layer to the microchannel walls, (iii) controllable CNF growth, (iv) efficient utilization of the microchannel volume to obtain a high surface area for active metal deposition, (v) preparation of CNF-based catalyst layer by deposition of stable and well dispersed active metal particles, and finally (vi) evaluation of the catalytic performance of these synthesized and functionalized CNF layers by means of appropriate aqueous phase reactions.

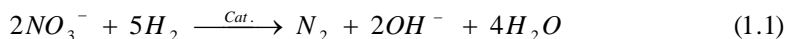
1.6 Nitrite and bromate removal from aqueous solutions

There is continuous and strict demand to achieve high water purity levels for both industrial and domestic use. Recent increase in the levels of concentration of nitrate and/or nitrite and bromate has raised concerns. The sources of these contaminants in water originate from excessive fertilization, industrial effluents *etc.* in the case of nitrate/nitrites, whereas bromate contamination is a consequence of undesirable disinfection by-products generated during water purification treatment processes. Bromate is frequently detected in drinking water, and originates from ozonation of bromide-containing source waters [90-92].

Even though nitrate ions (NO_3^-) do not exhibit toxicity, their further transformation to nitrite (NO_2^-) by reduction, however, can be detrimental for human health. It is known to be a cause of blue baby syndrome in addition to hypertension, and is a precursor for the carcinogenic nitroso amine [93-95]. European Commission directives have restricted the nitrate and nitrite concentration levels in drinking water to 50 mg/L and 0.5 mg/L, respectively [95]. Various physicochemical techniques such as ion exchange, reverse osmosis, and electrodialysis are available for removal of nitrate ions contamination from water. However, they only accumulate and are not able to convert these ions into less harmful products/materials. The biological process, on the other hand, is slow and complicated [95].

It is known from literature that most of the drawbacks of above mentioned conventional methods can be overcome *via* application of catalytic de-nitrification of nitrates and nitrites from aqueous solution using hydrogenation over noble-metal solid catalysts [96]. Recent work in Lefferts’ group on catalytic hydrogenation of nitrites (an intermediate in nitrate hydrogenation) to nitrogen by using hairy foam based thin layer

Pd/CNF catalyst has shown promising results in terms of catalytic performance compared to the conventional catalyst, inside fixed bed reactor [97]. It is understood from literature that nitrite reduction to nitrogen *Eq. (1.2)*, which is the second step of nitrate hydrogenation *Eq. (1.1)*, is extremely fast and hence can easily induce internal concentration gradients due to mass transfer limitations.



Thus this is an ideal reaction system for testing the diffusion limitations along the CNF layers and hence suitability of them as catalyst support when synthesized inside microreactor channels. Tested CNF layers with optimized mass transport properties and exhibiting intrinsic catalytic activity can be evaluated additionally for another contaminant *i.e.* bromate using ruthenium (Ru) as active phase.

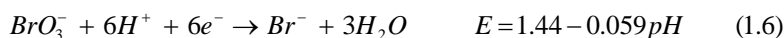
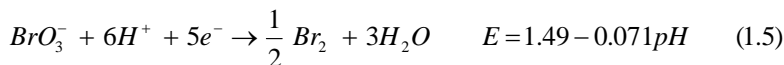
As mentioned earlier, bromate concentration levels have also been limited by various global agencies/organizations. The World Health Organization (WHO) and the United States' Environmental Protection Agency (EPA) have strictly regulated the bromate level in drinking water as the International Agency for Research on Cancer (IARC) has classified bromate as a Group 2B substance (*i.e.* possibly carcinogenic to humans) [98, 99]. This indeed demands development of an effective treatment method for the removal of bromate from drinking water [100]. Various techniques, such as biological [101, 102], photocatalytic [103, 104], electrochemical reduction [105] and more recently, catalytic hydrogenation [106], are available. A promising alternative for the removal of bromate pollution from drinking water is *via* heterogeneous redox catalysis without the requirement of using hydrogen [107, 108].



The main advantage of catalytic routes is the efficient and faster removal of water contaminants such as bromate under ambient conditions, particularly when compared to the conventional physicochemical methods. Furthermore, conventional methods concentrate removed contaminants in a secondary waste streams, which requires further treatment [97].

A review of literature cites only limited articles [13, 14] regarding the catalytic removal of BrO_3^- from aqueous solutions. It is reported by Grätzel *et al.* [13] that BrO_3^-

ion decomposition is thermodynamically allowed *via* red-ox reactions involving oxidation of water and subsequent reduction of bromate as below,



However, bromate ions are very stable in aqueous solutions, especially in the absence of oxidizable impurities or when protected from UV light. A dilute aqueous $HBrO_3$ solution does not undergo any decomposition even after several months of storage. The slow kinetics of the bromate reduction *via* the above redox cycle is due to the difficulty in the transfer of charges, which can be facilitated by the presence of connected electrodes. Accordingly, in the presence of typical electrode materials, in this case a Ru catalyst, RuO_2/TiO_2 [13], oxygen evolution was observed. Based on their studies with labeled oxygen (80% $H_2^{16}O$ and 20% $H_2^{18}O$) and that 20% $^{34}O_2$ was formed, they concluded that water is oxidized and is the source of oxygen.

However, Mills *et al.* [14] show that kinetics of the oxidation of water even in the presence of a RuO_2 catalyst is kinetically very slow ($0.05 \cdot 10^{-6} \text{ mol dm}^{-3} \text{ s}^{-1}$ at 30°C). Presence of an easily oxidizable water soluble organic component, *e.g.* MeOH, EtOH *etc.*, in the reaction medium enhances the rate of bromate decomposition. For example, Mills *et al.* reports that in the presence of MeOH a forty times improvement in rates in bromate conversion was observed compared to the situation when only water was present [14]. Carbon nanofiber supported ruthenium catalyst layers (Ru/CNF) present a novel option for treating bromate polluted water resources. In such a reactor, Ru metal particles are placed in space in the porous CNF layer, as in a frozen fluidized bed. Such an arrangement is expected to offer enhanced contact between bromate, reductant and Ru catalyst.

1.7 Scope of the thesis

The research objective of the work described in this thesis is to develop carbon nanofiber supported catalyst layers on structured internals of microreactors made from silicon technology based materials (*e.g.* fused silica and/or silicon). These microreactors are intended to be used for heterogeneously catalyzed liquid phase reactions, in this case for aqueous phase removal of nitrite and bromate.

The synthesis of stable carbon nanofiber layer on flat substrates (representing surfaces of microreactor channel walls) is a requisite for obtaining the know-how to translate it for preparing these layers inside microreactor channels. **Chapter 2** is a detailed study of CNF synthesis using thin metal film configurations with nickel (Ni) as growth catalyst and different metals (*i.e.* Ti, Ti-W and Ta) as adhesion layer between nickel and fused silica substrates. The study investigates various aspects such as stability of deposited metal films on the substrates and their interaction at elevated temperature (*i.e.* during treatment for obtaining Ni nanoclusters/particles and subsequent CNF growth). It will be illustrated further how the choice of adhesion metal influences and/or determines the morphology of CNF layers.

Chapter 3 describes the further investigation of CNF layer synthesis on oxidized silicon substrates towards their application in silicon technology based microreactors. The influence of various growth parameters on CNF morphology was investigated, *e.g.* ethylene concentration and addition of hydrogen to the reaction mixture, to be able to tune it for effective translation of CNF layer growth inside microreactor channels as a catalyst support. Moreover, implementation of this knowledge on the structured internals, *i.e.* well-defined arrays of Si-micropillars, of microreactors has been shown.

Thus prepared well-defined CNF layers were functionalized by depositing ruthenium active phase, the details of which are the described in **chapter 4**. The functionalization of CNF layers and the subsequent effect of it on physicochemical properties of CNFs has been illustrated in detail, followed by the details of preparation and characterization of ruthenium catalyst deposition on CNF layers *via* aqueous phase as well as physical vapor deposition based techniques. **Chapter 5** provides preliminary results of aqueous phase nitrite reduction, which is a kinetically fast reaction, hence probing the performance of CNF layers in terms of mass transfer properties in microreactor channels. **Chapter 6** discusses the results of testing Ru/CNF catalyst layers inside microreactors for aqueous phase bromate removal. These results highlight the better catalytic performance of CNF supported Ru catalyst when compared to the conventional powdered catalyst support such as activated carbon. **Chapter 7** summarizes the conclusions of the research towards development of stable and well-defined structured catalyst layers based on carbon nanofibers in microreactors, in order to perform liquid phase reactions, and is followed by recommendations for future applications.

References

- [1] A.E. Comyns, *Catalysts: industry growth spurs R&D investments, Focus on Catalysts*, (2009) 2-4.
- [2] M.N. Kashid, L. Kiwi-Minsker, *Ind. Eng. Chem. Res.* 48 (2009) 6465-6485.
- [3] W. Ehrfeld, V. Hessel, H. Lowe (Eds.), *Microreactors - New Technology for Modern Chemistry*, Wiley-VCH Weinheim, 2001.
- [4] G. Kolb, V. Hessel, *Chem. Eng. J.* 98 (2004) 1-38.
- [5] M.H. AlDahhan, F. Larachi, M.P. Dudukovic, A. Laurent, *Ind. Eng. Chem. Res.* 36 (1997) 3292-3314.
- [6] P.A. Ramachandran, R.V. Chaudhari, *Three phase catalytic reactors*, Gordon and Breach Science Publishers, New York, 1983.
- [7] P.C. Watson, M.P. Harold, *AIChE J.* 39 (1993) 989-1006.
- [8] M.W. Losey, R.J. Jackman, S.L. Firebaugh, M.A. Schmidt, K.F. Jensen, *J. Microelectromech. Sys.* 11 (2002) 709-717.
- [9] Y. Murakami, T. Takeuchi, K. Yokoyama, E. Tamiya, I. Karube, M. Suda, *Anal. Chem.* 65 (1993) 2731-2735.
- [10] J.P. Brody, P. Yager, *Sens. Actuators - A* 58 (1997) 13-18.
- [11] K.F. Jensen, *Chem. Eng. Sci.* 56 (2001) 293-303.
- [12] H. Lowe, W. Ehrfeld, *Electrochim. Acta* 44 (1999) 3679-3689.
- [13] M.T. Kreutzer, A. Gunther (Eds.), *Fluid-Fluid and Fluid-Solid Mass Transfer*, WILEY-VCH, 2009.
- [14] D.J. Adams, J.H. Clark, P.A. Heath, L.B. Hansen, V.C. Sanders, S.J. Tavener, *J. Fluorine Chem.* 101 (2000) 187-191.
- [15] L. Kiwi-Minsker, A. Renken, *Catal. Today* 110 (2005) 2-14.
- [16] P.D.I. Fletcher, S.J. Haswell, E. Pombo-Villar, B.H. Warrington, P. Watts, S.Y.F. Wong, X.L. Zhang, *Tetrahedron* 58 (2002) 4735-4757.
- [17] G.N. Doku, W. Verboom, D.N. Reinhoudt, A. van den Berg, *Tetrahedron* 61 (2005) 2733-2742.
- [18] V. Hessel, P. Angeli, A. Gavriilidis, H. Lowe, *Ind. Eng. Chem. Res.* 44 (2005) 9750-9769.
- [19] J. Kobayashi, Y. Mori, S. Kobayashi, *Chem. Asian J.* 1 (2006) 22-35.
- [20] J. Kobayashi, Y. Mori, K. Okamoto, R. Akiyama, M. Ueno, T. Kitamori, S. Kobayashi, *Science* 304 (2004) 1305-1308.
- [21] A. Gavriilidis, P. Angeli (Eds.), *Mixing and Contacting of Heterogeneous Systems*, WILEY-VCH, 2009.

- [22] S.K. Ajmera, C. Delattre, M.A. Schmidt, K.F. Jensen, *Stud. Surf. Sci. Catal.* 145 (2003) 97-102.
- [23] C.D. Baertsch, M.A. Schmidt, K.F. Jensen, *Chem. Commun.* (2004) 2610-2611.
- [24] K. Shah, R.S. Besser, *AIChE Annu. Meet., Conf. Proc. AIChE Annual Meeting*, Cincinnati, OH, United States, Oct. 30-Nov. 4, 2005, 36b/31-36b/38.
- [25] V. Meille, *Appl. Catal. A* 315 (2006) 1-17.
- [26] K. Haas-Santo, M. Fichtner, K. Schubert, *Appl. Catal. A* 220 (2001) 79-92.
- [27] K. Haas-Santo, O. Gorke, P. Pfeifer, K. Schubert, *Chimia* 56 (2002) 605-610.
- [28] H.S. Fogler, *Elements of Chemical Reaction Engineering*, 2nd ed., Prentice-Hall, Int., 1992.
- [29] J. Bravo, A. Karim, T. Conant, G.P. Lopez, A. Datye, *Chem. Eng. J.* 101 (2004) 113-121.
- [30] J.C. Ganley, E.G. Seebauer, R.I. Masel, *AIChE J.* 50 (2004) 829-834.
- [31] S.R. Deshmukh, A.B. Mhadeshwar, D.G. Vlachos, *Ind. Eng. Chem. Res.* 43 (2004) 2986-2999.
- [32] V. Sebastian, O. de la Iglesia, R. Mallada, L. Casado, G. Kolb, V. Hessel, J. Santamaria, *Microporous Mesoporous Mater.* 115 (2008) 147-155.
- [33] V. Valtchev, S. Mintova, M. Tsapatsis (Eds.), *Ordered Porous Solids*, Elsevier Publishing, 2009, 311-334.
- [34] M. Roumanie, C. Delattre, F. Mittler, G. Marchand, V. Meille, C. de Bellefon, C. Pijolat, G. Tournier, P. Pouteau, *Chem. Eng. J.* 135 (2008) S317-S326.
- [35] G. Wiessmeier, D. Honicke, J. Micromech. Microeng. 6 (1996) 285-289.
- [36] J.C. Ganley, K.L. Riechmann, E.G. Seebauer, R.I. Masel, *J. Catal.* 227 (2004) 26-32.
- [37] C.J. Brinker, G.W. Scherer, *Sol-Gel Science*, Academic Press, New York, 1990.
- [38] R.D. Gonzalez, T. Lopez, R. Gomez, *Catal. Today* 35 (1997) 293-317.
- [39] P. Reuse, *Production d'hydrogène dans un réacteur microstructure*. *Couplage thermique entre le steam reforming et l'oxydation totale du méthanol*, PhD thesis, EPFL, Lausanne, 2003.
- [40] A. Rouge, *Periodic operation of a microreactor for heterogeneously catalyzed reactions: the dehydration of isopropanol*, PhD thesis, EPFL, Lausanne, 2001.
- [41] P. Pfeifer, K. Schubert, G. Emig, *Appl. Catal. A* 286 (2005) 175-185.
- [42] J. Coronas, J. Santamaria, *Top. Catal.* 29 (2004) 29-44.
- [43] U. Hiemer, E. Klemm, F. Scheffler, I. Selvam, W. Schwieger, G. Emig, *Chem. Eng. J.* 101 (2004) 17-22.

- [44] E.V. Rebrov, G.B.F. Seijger, H.P.A. Calis, M.H.J.M. de Croon, C.M. van den Bleek, J.C. Schouten, *Appl. Catal. A* 206 (2001) 125-143.
- [45] B. Louis, L. Kiwi-Minsker, P. Reuse, A. Renken, *Ind. Eng. Chem. Res.* 40 (2001) 1454-1459.
- [46] B. Louis, P. Reuse, L. Kiwi-Minsker, A. Renken, *Appl. Catal. Ac* 210 (2001) 103-109.
- [47] M.T. Janicke, H. Kestenbaum, U. Hagendorf, F. Schuth, M. Fichtner, K. Schubert, *J. Catal.* 191 (2000) 282-293.
- [48] S. Thybo, S. Jensen, J. Johansen, T. Johannessen, O. Hansen, U.J. Quaade, *J. Catalysis* 223 (2004) 271-277.
- [49] S. Schimpf, M. Bron, P. Claus, *Chem. Eng. J.* 101 (2004) 11-16.
- [50] S. Helveg, C. Lopez-Cartes, J. Sehested, P.L. Hansen, B.S. Clausen, J.R. Rostrup-Nielsen, F. Abild-Pedersen, J.K. Nørskov, *Nature* 427 (2004) 426-429.
- [51] A.V. Melechko, V.I. Merkulov, T.E. McKnight, M.A. Guillorn, K.L. Klein, D.H. Lowndes, M.L. Simpson, *J. Appl. Phys.* 97 (2005) - 041301.
- [52] S.S. Fan, M.G. Chapline, N.R. Franklin, T.W. Tomblor, A.M. Cassell, H.J. Dai, *Science* 283 (1999) 512-514.
- [53] E. Hammel, X. Tang, M. Trampert, T. Schmitt, K. Mauthner, A. Eder, P. Potschke, *Carbon* 42 (2004) 1153-1158.
- [54] A.C. Dillon, K.M. Jones, T.A. Bekkedahl, C.H. Kiang, D.S. Bethune, M.J. Heben, *Nature* 386 (1997) 377-379.
- [55] W.J. Huang, S. Taylor, K.F. Fu, Y. Lin, D.H. Zhang, T.W. Hanks, A.M. Rao, Y.P. Sun, *Nano Lett.* 2 (2002) 311-314.
- [56] J. Kong, N.R. Franklin, C.W. Zhou, M.G. Chapline, S. Peng, K.J. Cho, H.J. Dai, *Science* 287 (2000) 622-625.
- [57] A.M. Fennimore, T.D. Yuzvinsky, W.Q. Han, M.S. Fuhrer, J. Cumings, A. Zettl, *Nature* 424 (2003) 408-410.
- [58] S.J. Tans, A.R.M. Verschueren, C. Dekker, *Nature* 393 (1998) 49-52.
- [59] T.V. Hughes, C.R. Chambers, *Manufacture of Carbon Filaments*, US Patent No. 405, 480, 1889.
- [60] S.D. Robertson, *Nature* 221 (1969) 1044-1046.
- [61] R.T.K. Baker, M.A. Barber, R.J. Waite, P.S. Harris, F.S. Feates, *J. Catal.* 26 (1972) 51-62.
- [62] A. Oberlin, M. Endo, T. Koyama, *Carbon* 14 (1976) 133-135.
- [63] K.P. De Jong, J.W. Geus, *Catal. Rev.-Sci. Eng.* 42 (2000) 481-510.

- [64] H.W. Kroto, J.R. Heath, S.C. O'Brien, R.F. Curl, R.E. Smalley, *Nature* 318 (1985) 162-163.
- [65] S. Iijima, *Nature* 354 (1991) 56-58.
- [66] D.B. Thakur, R.M. Tiggelaar, J.G.E. Gardeniers, L. Lefferts, K. Seshan, *Surf. Coat. Technol.* 203 (2009) 3435-3441.
- [67] N.M. Rodriguez, A. Chambers, R.T.K. Baker, *Langmuir* 11 (1995) 3862-3866.
- [68] T.W. Ebbesen, P.M. Ajayan, *Nature* 358 (1992) 220-222.
- [69] A. Thess, R. Lee, P. Nikolaev, H.J. Dai, P. Petit, J. Robert, C.H. Xu, Y.H. Lee, S.G. Kim, A.G. Rinzler, D.T. Colbert, G.E. Scuseria, D. Tomanek, J.E. Fischer, R.E. Smalley, *Science* 273 (1996) 483-487.
- [70] V. Ivanov, J.B. Nagy, P. Lambin, A. Lucas, X.B. Zhang, X.F. Zhang, D. Bernaerts, G. Vantendelo, S. Amelinckx, J. Vanlanduyt, *Chem. Phys. Lett.* 223 (1994) 329-335.
- [71] C.S. Cojocaru, A. Senger, F. Le Normand, J. Nanosci. Nanotechnol. 6 (2006) 1331-1338.
- [72] M.L. Toebes, Y.H. Zhang, J. Hajek, T.A. Nijhuis, J.H. Bitter, A.J. van Dillen, D.Y. Murzin, D.C. Koningsberger, K.P. de Jong, *J. Catal.* 226 (2004) 215-225.
- [73] Z.X. Yu, D. Chen, B. Totdal, T.J. Zhao, Y.C. Dai, W.K. Yuan, A. Holmen, *Appl. Catal. A* 279 (2005) 223-233.
- [74] C. Pham-Huu, N. Keller, L.J. Charbonniere, R. Ziessle, M.J. Ledoux, *Chem. Commun.* (2000) 1871-1872.
- [75] P. Serp, M. Corrias, P. Kalck, *Appl. Catal. A* 253 (2003) 337-358.
- [76] M.J. Ledoux, C. Pham-Huu, *Catal. Today* 102 (2005) 2-14.
- [77] W. Teunissen, A.A. Bol, J.W. Geus, *Catal. Today* 48 (1999) 329-336.
- [78] J.K. Chinthaginjala, K. Seshan, L. Lefferts, *Ind. Eng. Chem. Res.* 46 (2007) 3968-3978.
- [79] P.W.A.M. Wenmakers, J. van der Schaaf, B.F.M. Kuster, J.C. Schouten, J. Mater. Chem. 18 (2008) 2426-2436.
- [80] N. Jarrah, J.G. van Ommen, L. Lefferts, *Catal. Today* 79 (2003) 29-33.
- [81] N.A. Jarrah, F.H. Li, J.G. van Ommen, L. Lefferts, *J. Mater. Chem.* 15 (2005) 1946-1953.
- [82] A. Cordier, E. Flahaut, C. Viazzzi, C. Laurent, A. Peigney, *J. Mater. Chem.* 15 (2005) 4041-4050.
- [83] P. Tribolet, L. Kiwi-Minsker, *Catal. Today* 105 (2005) 337-343.

- [84] Z.R. Ismagilov, N.V. Shikina, V.N. Kruchinin, N.A. Rudina, V.A. Ushakov, N.T. Vasenin, H.J. Veringa, Catal. Today 102-103 (2005) 85-93.
- [85] S.S. Tzeng, K.H. Hung, T.H. Ko, Carbon 44 (2006) 859-865.
- [86] M. Cantoro, V.B. Golovko, S. Hofmann, D.R. Williams, C. Ducati, J. Geng, B.O. Boskovic, B. Kleinsorge, D.A. Jefferson, A.C. Ferrari, B.F.G. Johnson, J. Robertson, Diamond Relat. Mater. 14 (2005) 733-738.
- [87] N. Ishigami, H. Ago, Y. Motoyama, M. Takasaki, M. Shinagawa, K. Takahashi, T. Ikuta, M. Tsuji, Chem. Commun. (2007) 1626-1628.
- [88] C.J. Lee, T.J. Lee, J. Park, Chem. Phys. Lett. 340 (2001) 413-418.
- [89] C.J. Lee, J. Park, S. Han, J. Ihm, Chem. Phys. Lett. 337 (2001) 398-402.
- [90] H.S. Weinberg, C.A. Delcomyn, V. Unnam, Environ. Sci. Technol. 37 (2003) 3104-3110.
- [91] W.R. Haag, J. Hoigne, Environ. Sci. Technol. 17 (1983) 261-267.
- [92] M.S. Siddiqui, G.L. Amy, J. Am. Water Works Assoc. 85 (1993) 63-72.
- [93] L.W. Canter, *Nitrates in ground water*, CRC Press, Boca Raton, Florida, 1996.
- [94] C.S. Bruningfann, J.B. Kaneene, Veter. Human Toxicol. 35 (1993) 521-538.
- [95] A. Kapoor, T. Viraraghavan, J. Environ. Eng. 123 (1997) 371-380.
- [96] K.D. Vorlop, T. Tacke, Chem. Ing. Tech. 61 (1989) 836-837.
- [97] J.K. Chinthaginjala, J.H. Bitter, L. Lefferts, Appl. Catal. A (2010).
- [98] IARC, *Potassium Bromate (Summary Data Reported and Evaluation)*, IARC, Lyon, 1999.
- [99] World Health Organization, *Bromate in Drinking-water. Background Document for Preparation of WHO Guidelines for Drinking-water Quality*, World Health Organization Press, Geneva, 2008.
- [100] R. Butler, A. Godley, L. Lytton, E. Cartmell, Crit. Rev. Environ. Sci. Technol. 35 (2005) 193-217.
- [101] W.A.M. Hijnen, R. Voogt, H.R. Veenendaal, H. Vanderjagt, D. Vanderkooij, Appl. Environ. Microbiol. 61 (1995) 239-244.
- [102] C.G. van Ginkel, A.M. van Haperen, B. van der Togt, Water Res. 39 (2005) 59-64.
- [103] M. Siddiqui, W.Y. Zhai, G. Amy, C. Mysore, Water Res. 30 (1996) 1651-1660.
- [104] W.J. Huang, L.Y. Chen, Environ. Technol. 25 (2004) 403-412.
- [105] N. Kishimoto, N. Matsuda, Environ. Sci. Technol. 43 (2009) 2054-2059.
- [106] H. Chen, Z.Y. Xu, H.Q. Wan, J.Z. Zheng, D.Q. Yin, S.R. Zheng, Appl. Catal. B 96 (2010) 307-313.

- [107] D.H. Dung, W. Erbs, S.B. Li, M. Grätzel, Chem. Phys. Lett. 95 (1983) 266-268.
- [108] A. Mills, G. Meadows, Water Res. 29 (1995) 2181-2185.

Chapter 2

Growth of Stable Carbon Nanofiber Layers on Fused Silica Substrates: On the Use of Ti, Ti-W and Ta as Adhesion Layers

Abstract

Carbon nanofiber (CNF) layers were synthesized on fused silica substrates using a catalytic thermal chemical vapor deposition process (C-TCVD). The effects of various adhesion layers: titanium, titanium–tungsten and tantalum–under the nickel thin film on the attachment of carbon nanofibers and their morphological properties are presented. The diameter and the thicknesses of the CNF-coatings were analyzed by scanning electron microscopy, whereas the microstructure and crystallinity of the synthesized carbon nanofibers were investigated by transmission electron microscopy and Raman spectroscopy, respectively. Specific surface areas of CNF-coatings were determined with nitrogen adsorption–desorption isotherm measurements.

Using C-TCVD of ethylene at 700 °C (1 h), well-attached, entangled, quasi-crystalline platelet carbon nanofibers were synthesized with tip-type growth mode on 25 nm thick nickel films with an adhesion layer of 10 nm Ta or Ti–W. The thickness of CNF-coating was ~3.5 μm , and the diameter of the fibers depended on the composition of the metallic thin film stack: 20–50 nm for Ni/Ta and 80–125 nm for Ni/Ti–W.

2.1 Introduction

Due to their exceptional mechanical, electrical, physical and chemical characteristics carbon nanostructured materials are attractive for a variety of applications [1-5]. Applications of carbon nanofibers (CNFs) and carbon nanotubes (CNTs) include emitters for field emission displays [6, 7], composite reinforcing materials [8], hydrogen storage [9, 10], bio- and chemical sensors [11, 12], nano- and microelectronic devices [13, 14], and as catalyst support [15, 16]. The latter is because these structures offer numerous advantages as catalyst support, of which the most important ones are (i) corrosion resistance to acid or base medium, (ii) high surface area, (iii) absence of micro porosity, and (iv) the possibility to tune the surface chemistry of CNFs and CNTs [17-19].

Goal of this work was to investigate and control the properties of coatings of CNF layers synthesized *via* catalytic thermal chemical vapor deposition (C-TCVD) on nickel-based thin films deposited on flat fused silica substrates with different adhesion metals.

The C-TCVD method utilizes decomposition of carbon-containing gases on catalytically active components such as transition metals (*e.g.* nickel (Ni), cobalt (Co) or iron (Fe)) [20]. Hydrocarbon gases such as methane (CH_4), acetylene (C_2H_2), ethylene (C_2H_4), ethane (C_2H_6), or other C-sources as carbon monoxide (CO) or synthesis gas ($\text{CO} + \text{H}_2$) can be used to obtain CNF growth on these metal catalysts at temperatures between 400 and 1000 °C [20-22]. Controlled carbon nanofiber growth essentially concerns optimizing length, shape and diameter of the fibers, which influences the extent of fiber entanglement required for layer stability and the porosity of the layer. An efficient CNF-based catalyst support is a 'jungle' of entangled CNFs as shown in *Fig. 2.1* [23]. Good adhesion of these CNF-coatings is important to ensure that attrition losses of CNFs due to shear forces exerted by fluids flowing through the CNF-coating are minimized.

Thin films of physical vapor deposited nickel do, however, not adhere well to materials commonly used for silicon-technology based microreactors (*i.e.* silicon, Pyrex, Borofloat glass, quartz, fused silica), as a consequence of which an intermediate layer between the nickel and the substrate material has to be used [20]. Detailed studies on the adhesive strength of metallic thin films show that the optimal thickness of the adhesion layer is about 10-20 nm [24, 25]. Titanium (Ti) and tantalum (Ta) are proper adhesion metals for applications where the temperature exceeds 500 °C, *i.e.* the C-TCVD process used in this work (see *section 2.2*) [26-28]. In this work Ti, Ta and Ti-W are used as

adhesion metals for Ni thin-films onto which CNFs will be grown. Ti and Ti-W are selected because the synthesis of well-adhesive CNF-coatings is reported for Ni/Ti and Ni/Ti-W [29, 30], whereas Ta is selected because it is the best adhesion metal for high-temperature applications. Knowledge and control of the characteristics of CNF-coatings (*i.e.* fiber morphology, fiber diameter, thickness CNF-coating, specific surface area, adhesion quality of CNF-coating to substrate) synthesized on Ni-based thin films are essential for the development of efficient multiphase microreactors with CNF-based catalyst supports.

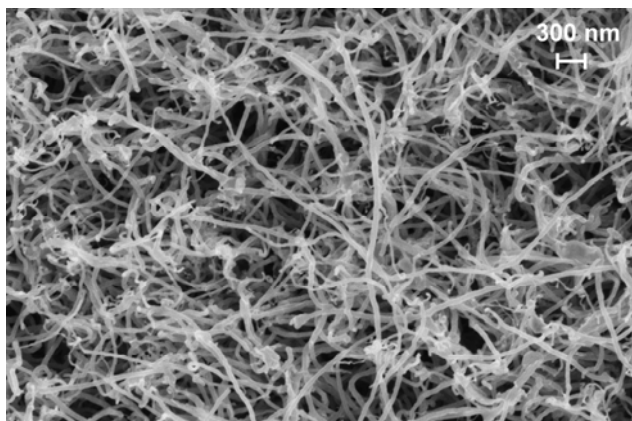


Figure 2.1: SEM image of entangled ('jungle') carbon nanofibers [23].

2.2 Experimental

2.2.1 Preparation of nickel-based thin films

Ni-based thin films for the synthesis of CNFs were deposited on fused silica substrates (Corning, UV Grade 7980F; diameter 100 mm, thickness $500 \pm 25 \mu\text{m}$, roughness as-fabricated $<1 \text{ nm}$). The substrates were ultrasonically cleaned in demineralized water (10 min), followed by immersion in fuming 100% nitric acid (Selectipur 100453, BASF) for 10 min, and boiling in 69% nitric acid (VLSI 116445, BASF) for 15 min, followed by quick dump rinsing in de-mineralized water and dry spinning. Within 30 minutes after these cleaning sequences the substrates were loaded into metal deposition systems.

Deposition of metals in a configuration shown in *Fig. 2.2* was done *via* evaporation and sputtering. On a Balzers BAK600 electron-gun evaporation system Ni/Ti and Ni/Ta films were deposited at pressures below 10^{-7} mbar. The purity of Ni target material was 99.99%, and at least 99.95% for adhesion metals Ti and Ta.

Evaporation rates for Ti and Ta were in the range 1-5 Å/s, whereas the growth rate for Ni was 10-15 Å/s. The thicknesses of evaporated films were controlled using an in-situ thickness monitor. Ni/Ti-W films were sputter-deposited on an AJA ATC 1500 sputtering system at an argon pressure of 6.7×10^{-3} mbar. The purity of the Ni target was >99.99% and >99.9% for Ti-W (target alloy composition: 30 at.% Ti and 70 at.% W), with sputter rates of *ca.* 2 nm/min (Ni: 200 W RF power, Ti-W: 200 W DC power). The thicknesses of sputtered metal films were controlled based on calibration runs performed prior to the actual deposition runs.

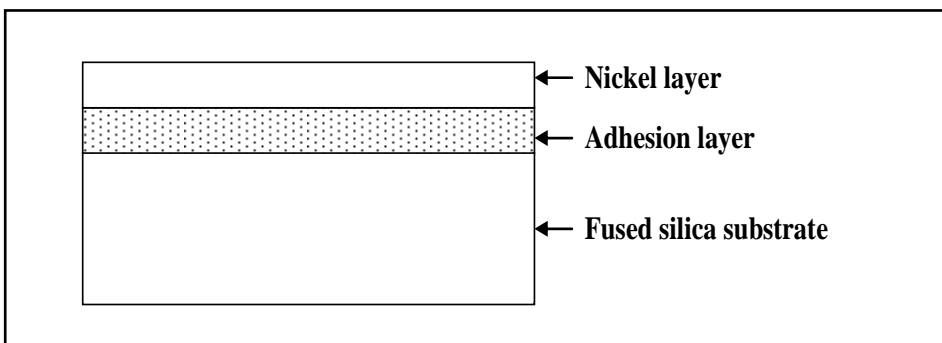


Figure 2.2: Schematic representation of the configuration of metal films for CNF-synthesis.

In order to avoid chipping, damaging and/or peeling of the thin films at locations where the substrates are cleaved during dicing, the substrates were lithographically patterned prior to metal deposition: squares of 8 mm \times 8 mm were defined in spin-coated photoresist (Olin, 907-12). The unmasked areas were etched in buffered hydrofluoric acid ($\text{NH}_4\text{F}:\text{HF}$ 1:7; VLSI 101171, BASF; etch rate of fused silica 60 nm/min). The depth of the recessed areas was identical to the thickness of the thin film to be deposited in the areas. After metal deposition, an ultrasonic lift-off step in acetone (>20 min; VLSI 100038, BASF) was carried out, followed by immersion in isopropanol (10 min; VLSI 107038, BASF), quick dump rinsing in de-mineralized water (10 min) and dry spinning. Finally, the substrates with the thin metal films were diced into samples of 1 cm \times 1 cm (Disco DAD-321 dicing machine). An overview of all prepared metal film configurations is given in *Table 2.1*.

Table 2.1: Specifications of metal films deposited on fused silica substrates by evaporation or sputtering.

Sample	Nickel layer Thickness [nm]	Adhesion layer	
		Material	Thickness [nm]
1.	25	None	—
2.	25	Ti	10
3.	25	Ti	200
4.	25 ^a	Ti-W ^a	10 ^a
5.	25	Ta	10

^a Sputtered metals

2.2.2 Synthesis of carbon nanofibers

Prior to CNF synthesis the nickel-based thin-film samples were first cleaned ultrasonically in acetone (5 min, Branson 200 ultrasonic cleaner) to remove organic contaminants, followed by washing with flowing deionized water (25 °C) and dried with pressurized technical air. Subsequently, the samples were reduced in a mixture of 20 vol.% H₂ in N₂ (99.999%, INDUGAS) with total flow rate of 50 ml/min, while increasing the temperature to 500 °C (ramp up 5 °C/min) and maintained at 500 °C for 2 h. This pretreatment is essential for the dewetting of the Ni thin film to produce nanoparticles which act as nucleation sites for CNF growth. After cooling down to room temperature, the samples were transferred to the CNF synthesis set-up for carrying out CNF synthesis. This procedure was selected because it is reported that reduction of ‘metal oxide’ during CNF synthesis to pure metallic phase produces smaller metal particles (compared to that obtained directly from pure metallic phase) as carbon is being deposited, which consequently resulted in thinner fibers and increased formation rates [31]. In the case of nickel thin films, exposure to environmental air after reduction pretreatment can be interpreted as (mild) oxidation of nickel nanoparticles: such an oxidation step prior to CNF synthesis is preferred, because it is assumed this leads to smaller grains, and thus smaller diameters of CNFs. The latter aspect is important for catalyst supports, because it results in high specific surface areas.

CNF synthesis was performed in a quartz reactor heated by a vertical furnace. The samples were heated in N₂ from room temperature to 700 °C at a rate of 5 °C/min, and at 700 °C exposed to a reactive gas mixture of 25 vol.% C₂H₄ in N₂ (99.95%, PRAXAIR) at a total flow rate of 100 ml/min. The reaction time at this temperature was one hour,

after which the samples were cooled down in N₂ to room temperature. The amount of carbon deposited on each sample was determined by measuring the increase in weight.

2.2.3 Characterization of metal and CNF-coatings

Prior to CNF-synthesis surface elemental analyses of as-deposited and reduced metal films were performed on a Quantera XPS system (Physical Electronics). The morphology of the synthesized CNF-coatings was investigated by scanning electron microscopy (HRSEM; LEO 1550) in conjugation with energy dispersive X-ray analysis (EDX; Thermo Noran Vantage system). Transmission electron microscopy (TEM; Philips CM300ST-FEG equipped with Gatan Ultrascan 1000 CCD camera) was used to study the nanostructure of the fibers. The surface area of the CNF-coatings was determined with the BET-method on data from N₂ adsorption-desorption isotherm (Micromeritics ASAP 2400 system). Room temperature Raman spectroscopy, (Senterra Raman microscope spectrometer), was used to determine the crystallinity of the CNF-coating [32, 33]. The adhesion of CNF-coatings to the fused silica substrate was tested separately using severe fluid flow conditions, *i.e.* air and water flows over CNF-coatings with a linear velocity of 100 m/s for 5 min and 2 m/s for 1 hour, respectively. Samples with CNFs were positioned and fixed in plastic tubing in such a way that the air/water flows were guided through/over the CNF-coating. After exposure to the fluid flows, the samples were removed from the tubing, and the weight of the samples was determined: the difference between the mass of the samples before and after the flowing air/water experiments is the loss of CNFs, and is used to qualify the mechanical attachment of the fibers to the substrates. These fluid flows (m/s-range) are much higher (six orders of magnitude) than typical fluids flows in microfluidic devices ($\mu\text{l/min}$ -range; in our case this equals 10^{-6} m/s range), such as microreactors in which the CNF-coatings will be used as catalyst support.

2.3 Results and discussion

2.3.1 Nickel/titanium

Since a nickel film of 25 nm thickness deposited on fused silica without an adhesion layer did not have an acceptable adhesion, the use of an adhesion layer was necessary (in fact, severe peeling of the as-deposited nickel layer occurred). Indeed, when 10 nm Ti was used no peeling of the as-deposited 25 nm Ni/10 nm Ti film was observed. CNF-synthesis experiments were performed on this metal configuration. Although CNFs

were formed, the CNF-coating was completely detached from the substrate and fragmented extensively. SEM images (*Fig. 2.3a-2.3b*) of the CNF-layer fragments show extensive fiber formation with an entangled morphology. Ni-particles at the tips of the fibers indicate tip-type growth of fibers [17].

The use of a significantly thicker Ti layer, 200 nm, resulted in a ‘CNF carpet’: a CNF-layer formed on the 25 nm Ni/200 nm Ti film and no fragmentation of the CNF coating occurred, but the whole stack is detached from the substrate (*i.e.* CNF-layer + metal films). SEM images of a CNF carpet revealed extensive growth of tip-type CNFs on one side of the carpet, whereas the other side appeared to be shiny (*Fig. 2.3b*). EDX analysis of this ‘shiny’ side of the carpet indicated a very high concentration of Ti (*Fig. 2.3c*). Although these CNF carpets are mechanically rather stable (the carpets do not fragment during the CNF-synthesis), the adhesion to the fused silica substrate is insufficient/poor. Details of these CNF carpets are presented elsewhere [34].

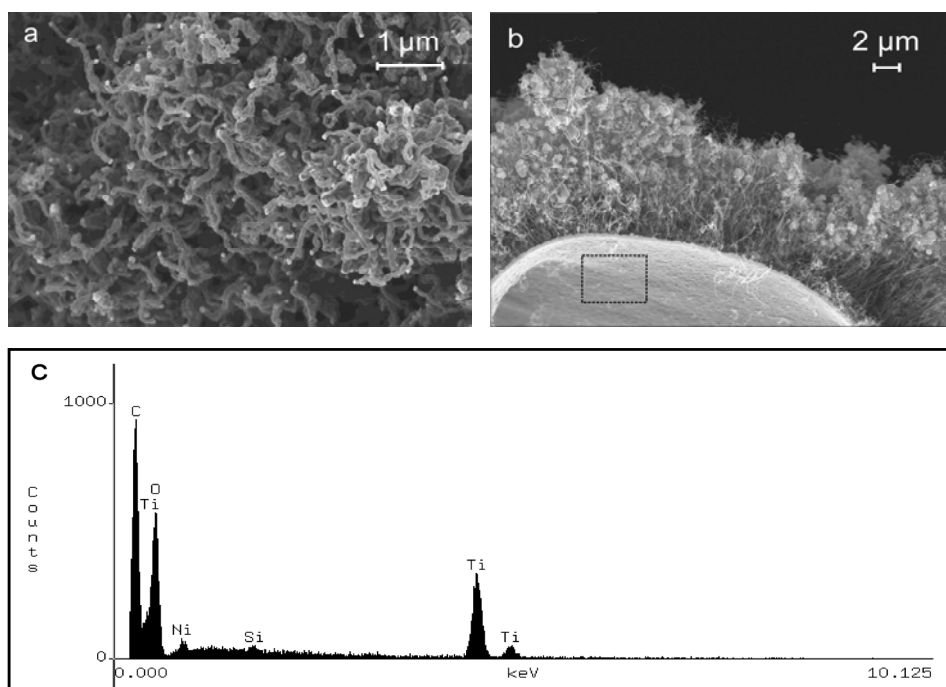


Figure 2.3: SEM image of: (a) fragments of the CNF-layer synthesized on 25 nm Ni/10 nm Ti, and (b) CNF-carpet synthesized on 25 nm Ni/200 nm Ti, and (c) EDX spectrum of the area marked in SEM image.

In order to understand the formation of CNF carpets, SEM imaging and XPS analyses were carried out at two stages prior to the CNF-synthesis process. SEM images show that the as-deposited 25 nm Ni/200 nm Ti film is reasonably uniform and dense (with some larger clusters) (Fig. 2.4a), while after reduction the surface morphology changes into a discontinuous film, indicating a re-organization of the metal components (Fig. 2.4b).

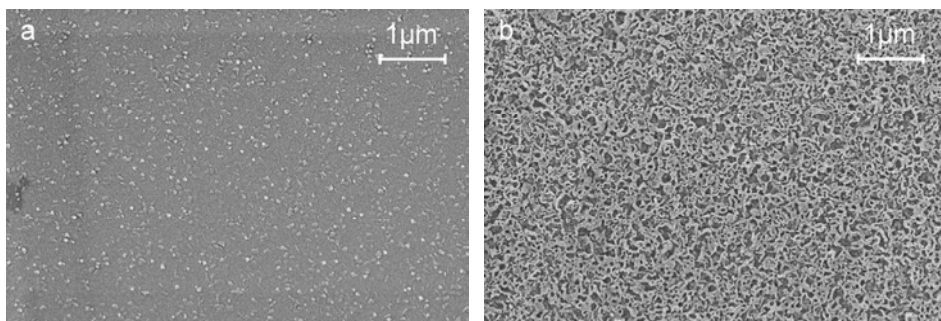


Figure 2.4: SEM images of 25 nm Ni/200 nm Ti: (a) as-deposited, and (b) after reduction.

XPS analyses revealed that the as-deposited samples have almost exclusively Ni on the surface, while after the reduction step mostly Ti is detected at the surface of the sample (Table 2.2).

Table 2.2: Surface elemental concentrations of Ni and Ti for an as-deposited and a reduced 25 nm Ni/200 nm Ti thin film. Oxygen and carbon were other elements observed in balance concentrations.

Elements	Atomic concentrations [%]	
	<i>As-deposited</i>	<i>Reduced</i>
Ni	10	2
Ti	0.1	21.4

Thus, during the high temperature treatment in hydrogen extensive segregation of Ti to the surface occurs. The data shown in this work is in agreement with Sieber *et al.* [35], who reported inter-diffusion of titanium and nickel, as well as formation of mixed phases during the reduction of Ni/Ti thin films in hydrogen atmospheres. In our case,

this results in poor adhesion of the tip-type mode grown CNF-coatings on fused silica substrates during/after CNF-synthesis for two reasons: (i) high temperatures used cause the distinct Ti adhesion layer to be relocated on top of the nickel layer to a large extent, thereby losing its adhesive function, and (ii) CNF-growth on the Ni/fused silica interface enhances the detachment of the CNF carpet.

It has to be mentioned here that for Ni/Ti thin films deposited on silicon substrates, the C-TCVD method (590 °C; growth time 18 min. using CH₄) resulted in well-adhesive vertically aligned multi-wall carbon nanotubes (MWCNTs) [36]. The root-grown MWCNTs on Ni/Ti/Si were firmly adhered due to the formation of Ti-Ni-C alloy, which is absent in case of Ni/Ti/SiO₂. For Co/Ti thin films Hsu *et al.* found similar differences in the CNT growth-mode as found by us and reported by Chuang *et al.* (*i.e.* tip-type growth on Ni/Ti/SiO₂ vs. root growth on Ni/Ti/Si): using the microwave PECVD method, cobalt (Co) catalytic particles were driven up on the tips of CNTs in case of Co/Ti/SiO₂/Si, and pinned down on the substrate in case of Co/Ti/Si [37]. Thus, interlayer reactions and/or alloying seems to have a significant influence on the growth mode of carbon nanostructures, as well as the adhesion of these structures to the substrate.

In conclusion, Ti is not a suitable adhesion layer for Ni when this Ni/Ti thin-film deposited on a SiO₂ surface is subjected to high temperatures (> 500 °C), which is the case for the investigated C-TCVD CNF-synthesis process.

2.3.2 Nickel/titanium–tungsten

SEM images of as-deposited and reduced 25 nm Ni/10 nm Ti-W samples are shown in *Fig. 2.5(a)* and *(b)*, respectively. It can be seen that the as-deposited film is smooth, in the reduced film and small grains are visible that are homogeneously distributed on the surface. This is in contrast with the reduced 25 nm Ni/200 nm Ti film, where significant restructuring was observed. XPS analysis also confirmed that there were hardly any compositional changes at the metal surface and Ni remained the main element at the surface before and after reduction (*Table 2.3*).

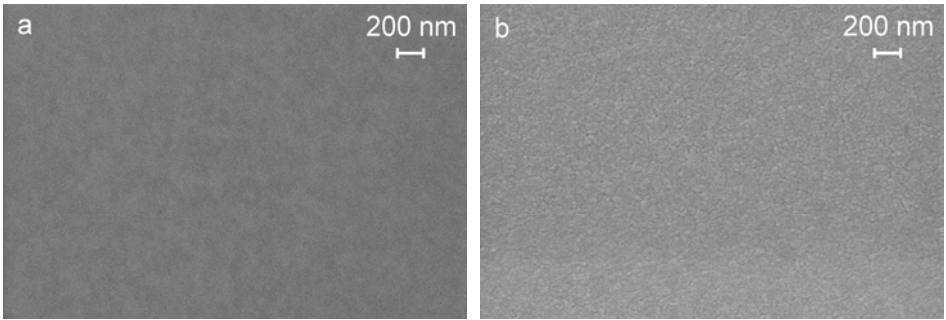


Figure 2.5: SEM images of 25 nm Ni/10 nm Ti-W: (a) as deposited, and (b) after reduction.

Table 2.3: Surface elemental concentrations of Ni, Ti and W for an as-deposited and a reduced 25 nm Ni/10 nm Ti-W thin films. Oxygen and carbon were other elements observed in balance concentrations.

Elements	Atomic concentrations [%]	
	<i>As-deposited</i>	<i>Reduced</i>
Ni	33	28
Ti	0.3	0.5
W	3.0	6.0

The presence of W seems to prevent migration of Ti to the surface during reduction of Ni/Ti-W films. In detail, Ti-W is a good adhesion material for Ni/Ti-W films because Ti-W preserves its adhesive function and the as-deposited Ni/Ti-W-configuration is not affected by the reduction at 500 °C. The C-TCVD CNF-synthesis procedure resulted in well-attached, entangled CNF-fiber coatings on Ni/Ti-W thin films (*Fig. 2.6a*). The average CNF-coating thickness is ~3.5 μm . The SEM image (*Fig. 2.6b*) shows that the fibers constituting the layer have a diameter of 80-125 nm, and have a nickel particle at the top of the fibers. The specific surface area of a CNF-coating grown on 25nm Ni/10 nm Ti-W was found to be 32 m^2/g .

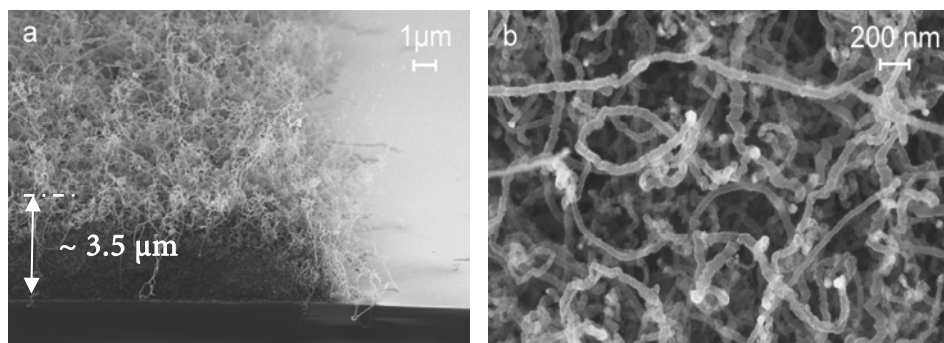


Figure 2.6: SEM images of a CNF-layer grown on 25 nm Ni/10 nm Ti-W: (a) cross-sectional view, and (b) surface view showing entangled morphology of tip-type fibers (Ni particles visible at the tips of the fibers).

Thus, Ti-W is a suitable adhesion material for Ni thin films that are exposed to 700 °C: Ti-W fulfills its function as adhesion layer at this temperature. As a consequence CNF-coatings that are well-attached to fused silica can be synthesized on Ni/Ti-W thin-films. In fact, for increasing synthesis times the thickness of the CNF-layers on Ni/Ti-W films increases, whereas the growth time does not influence the diameters of the fibers significantly [34].

To our best knowledge, this is the first time that Ti-W is used attempted as an adhesion layer on fused silica substrates to synthesize CNFs using Ni as growth catalyst. There are only a few papers which report the use of Ti-W as an adhesion or an anti-diffusion layer between the Ni catalyst and silicon. Merkulov *et al.*[38] and Caughman *et al.* [39] have synthesized CNFs with a very high degree of alignment using dc-plasma enhanced chemical vapor deposition (dc-PECVD) and inductively coupled plasma-enhanced chemical vapor deposition (both at 700 °C, and with C_2H_2/NH_3 or C_2H_2/H_2 , respectively). Since their intension was to produce carbon-based nanostructures for field emission device applications, which desires vertically aligned CNFs or CNTs, they opt for plasma-based synthesis techniques. These techniques produce highly aligned carbon nanostructures in preferred orientation, *i.e.* according to the direction of the electric field. However, the application of CNFs as catalyst support requires different properties of CNF coatings, such as a high degree of fiber entanglement. Entanglement of fibers increases the rigidity of CNF-based catalyst supports, and leads to higher specific surface areas compared to vertically aligned fiber layers (under similar growth conditions) due

to longer lengths of entangled fibers. This is of prime importance for the application of CNFs as efficient catalyst support in terms of better dispersion of active phase.

2.3.3 Nickel/tantalum

The use of tantalum as adhesion layer for nickel films resulted in the synthesis of CNF-coatings with excellent attachment to the fused silica substrate. *Figure 2.7a* shows images of a CNF-layer grown on 25 nm Ni/10 nm Ta. The CNF-coating is $\sim 3.6 \mu\text{m}$ thick, and composed of tip-type fibers with diameters ranging between 20-50 nm.

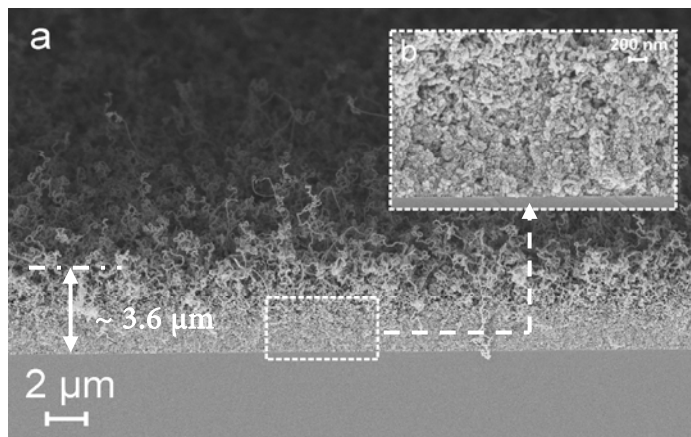


Figure 2.7: SEM image of a CNF-layer grown on 25 nm Ni/10 nm Ta: (a) cross-sectional view, and (b) cross-sectional view showing dense layer near the interface of the CNF layer and the substrate.

The specific surface area of these CNF-coatings is $87 \text{ m}^2/\text{g}$, the average pore diameter 40 nm (total void volume $0.2 \text{ cm}^3/\text{g}$), and there is nearly no microporosity (*i.e.* pores $< 2 \text{ nm}$) (note that porosity means the space between entangled fibers, the individual fiber is considered as nonporous). The mean diameter of the fibers can be calculated from the surface area, density of CNF and assuming cylindrical shape. Fiber diameters obtained from such calculations are $\sim 40 \text{ nm}$, which is within the range of values measured from HR-SEM (20-50 nm range). Thus, for a nearly identical CNF-layer thickness the specific surface area of the layer grown on Ni/Ta is *ca.* 2.7 times higher than for a CNF-coating grown on Ni/Ti-W, which is due to the smaller diameter of the fibers of the CNF-coating on Ni/Ta. Interestingly, CNFs grown on Ni/Ti-W have

a larger diameter (80-125 nm) than those grown on Ni/Ta (20 -50 nm). It is believed this difference in diameter is due to different sizes of Ni-crystallites formed during reduction. Although it is yet not clear why this happens, this phenomenon gives a possibility to control CNF diameters by choosing an appropriate adhesion metal under the Ni thin-film.

The Raman spectrum of a CNF-layer grown on 25 nm Ni/10 nm Ta is shown in *Fig. 2.8*. Two clear bands are visible, centered on 1340 cm^{-1} and 1570 cm^{-1} . It is known that the Raman spectrum of single-crystal graphite, as well as of highly oriented pyrolytic graphite have a single band at 1582 cm^{-1} (G-band), which is addressed as graphite mode. Less ordered carbon materials also have a band at about 1335 cm^{-1} , which is a defect-induced Raman band named the defect mode (D-band) [40, 41]. The ratio (R) of the relative intensity of the D-band and G-band ($R = I_D/I_G$) can be used to assess the degree of graphitization and the alignment of the graphite planes [21]. The R -value for the CNF layer synthesized on Ni/Ta is 1.33, which indicates the presence of interstitial defects or quasi-crystalline nature of the CNF [42].

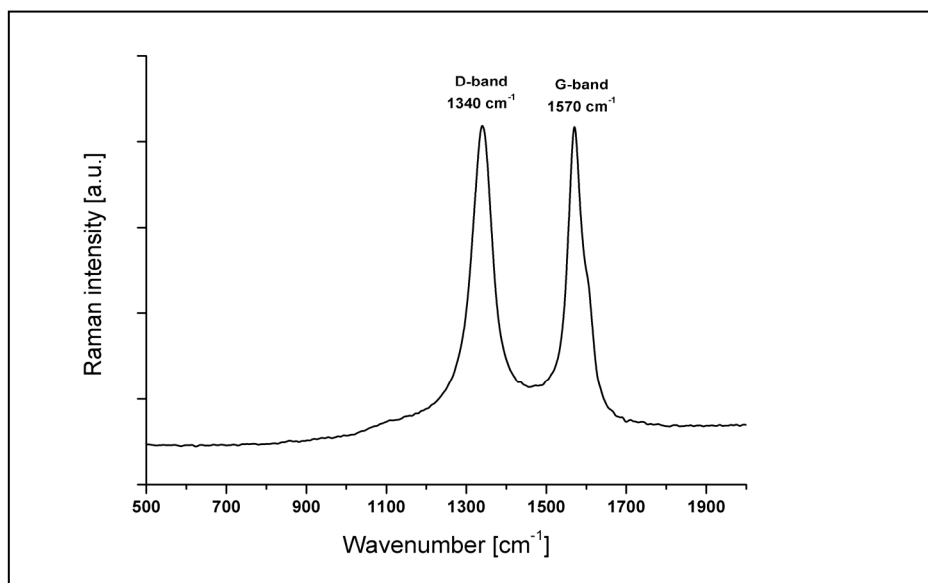


Figure 2.8: Raman spectrum of a CNF-layer synthesized on 25 nm Ni/10 nm Ta.

The TEM images shown in *Fig. 2.9* confirm the Raman data on the quasi-crystallinity of the CNF. *Figure 2.9a* shows the tip-type growth of the CNF with a Ni

particle at tip of fiber and *Fig. 2.9b* illustrates stacking of graphene sheets showing formation of platelet type CNFs.

The attachment of CNF-layers grown on 25 nm Ni/10 nm Ta to the fused silica substrate was evaluated by applying fluid flows, typical for catalytic applications, to the samples. CNF-layers exposed to an air flow showed a weight loss of 6%, whereas no further weight loss was found when exposed to a water flow. These experiments indicate a good adhesion of the CNF-coating to fused silica substrates: clearly, tantalum is an excellent adhesion layer for CNFs grown on Ni/Ta thin-films. It has to be mentioned that SEM images show that a dense(r) C-layer is present in the CNF-coating near the substrate surface (*Fig. 2.7b*). Although the exact nature of this sub-layer is not clear, it is believed this sub-layer might act as anchoring points for grown fibers, similar as for fibers synthesized on nickel foams [23].

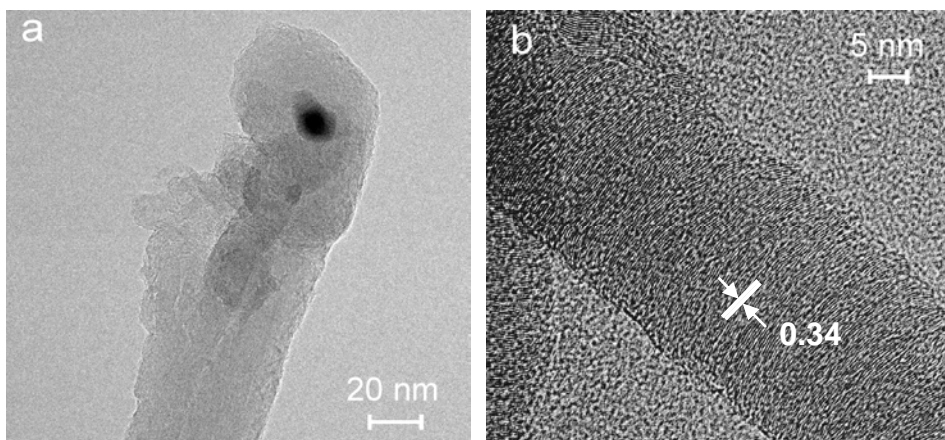


Figure 2.9: TEM images of a CNF-layer grown on 25 nm Ni/10 nm Ta: (a) nickel particle at the tip of a fiber, and (b) close-up of a fiber showing semi-crystalline graphene planes and interstitial defects.

The use of Ta as an adhesion layer has been reported by Lee *et al.* [43], who investigated the influence of different adhesion metal layers on the growth of carbon nanostructures. Cassell *et al.* [44] and Ng *et al.* [45] have also reported CNF synthesis using combinations of various growth metal catalysts and adhesion metals, including Ni/Ta. Although these groups synthesized carbon nanostructures on silicon substrates, we observed similar morphological features of CNFs on fused silica (*i.e.* high density CNF growth with entangled or random morphology) as the synthesis methods of Ng *et*

al. (C-TCVD at 750 °C using C_2H_2/Ar) and Lee *et al.* (hot filament-CVD at 700 °C using CH_4/H_2). Although these groups discuss the outcome of CNF synthesis in general terms, information on the influence of different adhesion layers on the properties of CNF coating is incomplete. By using various characterization techniques we have systematically highlighted the variation in CNF morphology corresponding to the choice of adhesion layer, and the properties of the coatings when to be used as catalyst support.

In order to use CNF-layers as efficient, rigid catalyst supports, it is essential to anchor catalytic sites to the fibers constituting the CNF-layer, such as metal particles of palladium (Pd) or platinum (Pt). This is possible: in previous work Pd metal particles were deposited on CNF synthesized on Ni foam material *via* adsorption of a Pd precursor in toluene [46]. *Figure 2.10* shows a SEM image of a CNF-layer with Pd-particles attached to the fibers.

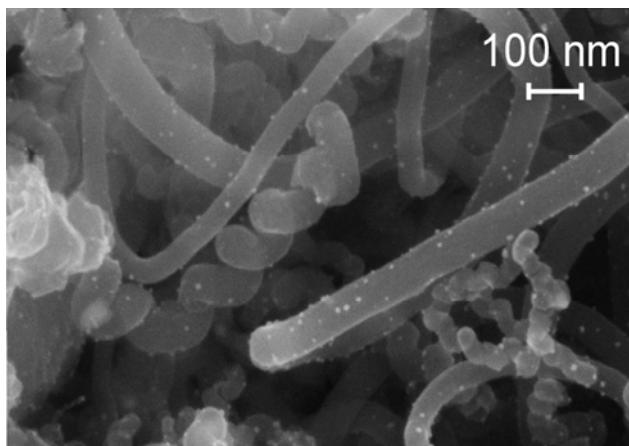


Figure 2.10: SEM image of catalytic Pd-particles anchored on CNFs [46].

2.4 Conclusions

In this work the synthesis of carbon nanofibers on fused silica substrates coated with nickel based thin-films using thermal catalytic chemical vapor deposition of ethylene (700 °C, 1h growth time) is investigated, for three different adhesion layers under the nickel layer. Although CNFs could be synthesized on 25 nm nickel with a titanium adhesion layer (10-200 nm), titanium is not a good adhesion material. The use of a 10 nm thick adhesion layer of titanium-tungsten or tantalum resulted in the formation of

well-attached CNF-layers. The carbon nanofibers in these layers were entangled, quasi-crystalline phased, tip-type growth mode. Moreover, for both metal layer configurations the thickness of the CNF-coating was $\sim 3.5 \mu\text{m}$, whereas the diameter of the fibers was smaller in case of Ta (20-50 nm) compared to Ti-W (80-125 nm), which most likely is related to the grain size of the nickel nanoparticles formed during the reduction treatment prior to the CNF synthesis step. The presented results on the adhesion and properties of CNF-coating synthesized on nickel based thin-films on fused silica yields important knowledge for the fabrication of CNF-based catalyst support layers to be used in microreactors for multiphase reactions.

Acknowledgements

This work was performed with the financial support from MicroNed program, under cluster-II of Smart Microchannel technology (SMACT) and work package II-G-2 and 3 (Smart Micro Reactors). The authors gratefully acknowledge Dr. M. Smithers for SEM and TEM analysis, G.A.M. Kip for XPS analysis, J.A.M. Vrieling for BET measurements, Dr. B. Mojet and M. van der Haven (Bruker Optics B.V., Delft) for Raman spectroscopic analysis, and Ing. B. Geerdink for technical support.

References

- [1] S. Iijima, *Nature* 354 (1991) 56-58.
- [2] M. Bockrath, D.H. Cobden, P.L. McEuen, N.G. Chopra, A. Zettl, A. Thess, R.E. Smalley, *Science* 275 (1997) 1922-1925.
- [3] M.M.J. Treacy, T.W. Ebbesen, J.M. Gibson, *Nature* 381 (1996) 678-680.
- [4] M.F. Yu, O. Lourie, M.J. Dyer, K. Moloni, T.F. Kelly, R.S. Ruoff, *Science* 287 (2000) 637-640.
- [5] S.J. Tans, M.H. Devoret, H.J. Dai, A. Thess, R.E. Smalley, L.J. Geerligs, C. Dekker, *Nature* 386 (1997) 474-477.
- [6] S.S. Fan, M.G. Chapline, N.R. Franklin, T.W. Tombler, A.M. Cassell, H.J. Dai, *Science* 283 (1999) 512-514.
- [7] S.M. Jung, J. Hahn, H.Y. Jung, J.S. Suh, *Nano Lett.* 6 (2006) 1569-1573.
- [8] E. Hammel, X. Tang, M. Trampert, T. Schmitt, K. Mauthner, A. Eder, P. Potschke, *Carbon* 42 (2004) 1153-1158.
- [9] A.C. Dillon, K.M. Jones, T.A. Bekkedahl, C.H. Kiang, D.S. Bethune, M.J. Heben, *Nature* 386 (1997) 377-379.

- [10] C. Liu, Y.Y. Fan, M. Liu, H.T. Cong, H.M. Cheng, M.S. Dresselhaus, *Science* 286 (1999) 1127-1129.
- [11] W.J. Huang, S. Taylor, K.F. Fu, Y. Lin, D.H. Zhang, T.W. Hanks, A.M. Rao, Y.P. Sun, *Nano Lett.* 2 (2002) 311-314.
- [12] J. Kong, N.R. Franklin, C.W. Zhou, M.G. Chapline, S. Peng, K.J. Cho, H.J. Dai, *Science* 287 (2000) 622-625.
- [13] A.M. Fennimore, T.D. Yuzvinsky, W.Q. Han, M.S. Fuhrer, J. Cumings, A. Zettl, *Nature* 424 (2003) 408-410.
- [14] S.J. Tans, A.R.M. Verschueren, C. Dekker, *Nature* 393 (1998) 49-52.
- [15] C. Wang, M. Waje, X. Wang, J.M. Tang, R.C. Haddon, Y.S. Yan, *Nano Lett.* 4 (2004) 345-348.
- [16] D. Villers, S.H. Sun, A.M. Serventi, J.P. Dodelet, S. Desilets, *J. Phys. Chem. B* 110 (2006) 25916-25925.
- [17] P. Serp, M. Corrias, P. Kalck, *Appl. Catal. A* 253 (2003) 337-358.
- [18] C. Pham-Huu, N. Keller, L.J. Charbonniere, R. Ziessle, M.J. Ledoux, *Chem. Commun.* (2000) 1871-1872.
- [19] M.J. Ledoux, C. Pham-Huu, *Catal. Today* 102 (2005) 2-14.
- [20] A.V. Melechko, V.I. Merkulov, T.E. McKnight, M.A. Guillorn, K.L. Klein, D.H. Lowndes, M.L. Simpson, *J. Appl. Phys.* 97 (2005) - 041301.
- [21] J.K. Chinthaginjala, K. Seshan, L. Lefferts, *Ind. Eng. Chem. Res.* 46 (2007) 3968-3978.
- [22] K.P. De Jong, J.W. Geus, *Catal. Rev. - Sci. Eng.* 42 (2000) 481-510.
- [23] J.K. Chinthaginjala, D.B. Thakur, K. Seshan, L. Lefferts, *Carbon* 46 (2008) 1638-1647.
- [24] L.I. Maissel, R. Glang, P.P. Budenstein, *J. Electrochem. Soc.* 118 (1971) 114C-115C.
- [25] I. Kondo, T. Yoneyama, O. Takenaka, A. Kinbara, *J. Vac. Sci. Technol. A* 10 (1992) 3456-3459.
- [26] R.M. Tiggelaar, R.G.P. Sanders, A.W. Groenland, J.G.E. Gardeniers, *Sens. Actuators A* 152 (2009), 39-47.
- [27] R.M. Tiggelaar, J.W. Berenschot, J.H. de Boer, R.G.P. Sanders, J.G.E. Gardeniers, R.E. Oosterbroek, A. van den Berg, M.C. Elwenspoek, *Lab Chip* 5 (2005) 326-336.
- [28] T. Maeder, L. Sagalowicz, P. Mural, *Jpn. J. Appl. Phys.* 37 (1998) 2007-2012.
- [29] C.J. Lee, T.J. Lee, J. Park, *Chem. Phys. Lett.* 340 (2001) 413-418.

- [30] V.I. Merkulov, A.V. Melechko, M.A. Guillorn, M.L. Simpson, D.H. Lowndes, J.H. Whealton, R.J. Raridon, *Appl. Phys. Lett.* 80 (2002) 4816-4818.
- [31] R.T.K. Baker, J.R. Alonzo, J.A. Dumesic, D.J.C. Yates, *J. Catal.* 77 (1982) 74-84.
- [32] H. Hiura, T.W. Ebbesen, K. Tanigaki, H. Takahashi, *Chem. Phys. Lett.* 202 (1993) 509-512.
- [33] M.A. Pimenta, G. Dresselhaus, M.S. Dresselhaus, L.G. Cancado, A. Jorio, R. Saito, *Phys. Chem. Chem. Phys.* 9 (2007) 1276-1291.
- [34] D.B. Thakur, R.M. Tiggelaar, K. Seshan, J.G.E. Gardeniers, L. Lefferts, *Adv. Sci. Technol.* 54 (2008) 231-236.
- [35] I. Sieber, H. Lange, K. Schade, *Physica Status Solidi A* 126 (1991) 171-179.
- [36] C.C. Chuang, W.L. Liu, W.J. Chen, J.H. Huang, *Surf. Coat. Technol.* 202 (2008) 2121-2125.
- [37] C.M. Hsu, C.H. Lin, H.J. Lai, C.T. Kuo, *Thin Solid Films* 471 (2005) 140-144.
- [38] V.I. Merkulov, A.V. Melechko, M.A. Guillorn, M.L. Simpson, D.H. Lowndes, J.H. Whealton, R.J. Raridon, *Appl. Phys. Lett.* 80 (2002) 4816-4818.
- [39] J.B.O. Cuaughman, L.R. Baylor, M.A. Guillorn, V.I. Merkulov, D.H. Lowndes, L.F. Allard, *Appl. Phys. Lett.* 83 (2003) 1207-1209.
- [40] M. Endo, K. Nishimura, Y.A. Kim, K. Hakamada, T. Matushita, M.S. Dresselhaus, G. Dresselhaus, *J. Mater. Res.* 14 (1999) 4474-4477.
- [41] C. Kim, S.H. Park, J.K. Cho, D.Y. Lee, T.J. Park, W.J. Lee, K.S. Yang, *J. Raman Spectrosc.* 35 (2004) 928-933.
- [42] A.C. Ferrari, J. Robertson, *Phys. Rev. B* 61 (2000) 14095-14107.
- [43] K.M. Lee, H.J. Han, S.H. Choi, K.H. Park, S. Oh, S. Lee, K.H. Koh, *J. Vac. Sci. Technol. B* 21 (2003) 623-626.
- [44] A.M. Cassell, Q. Ye, B.A. Cruden, J. Li, P.C. Sarrazin, H.T. Ng, J. Han, M. Meyyappan, *Nanotechnol.* 15 (2004) 9-15.
- [45] H.T. Ng, B. Chen, J.E. Koehne, A.M. Cassell, J. Li, J. Han, M. Meyyappan, *J. Phys. Chem. B* 107 (2003) 8484-8489.
- [46] N.A. Jarrah, *Microstructured Catalyst Support Based on Carbon Nano-Fibers (CNFs)*, PhD thesis, University of Twente, Enschede, The Netherlands, 2004.

Chapter 3

Carbon Nanofiber Layers to be used in Silicon based Microreactors: Influence of Growth Parameters on Carbon Nanofiber Morphology

Abstract

Carbon nanofiber (CNF) layers have been synthesized on flat fused silica and silicon substrates, as well as inside flow channels of silicon-technology based microreactors by thermal catalytic chemical vapor deposition of ethylene using nickel thin-film catalyst. These CNF layers are to be used as structured catalyst support. The influence of the ethylene concentration and addition of hydrogen to the carbon-containing gas on the morphology of CNF layers was studied. Very low amount of CNFs were produced at low ethylene concentrations (<25%) due to the restricted supply of carbon species. Addition of hydrogen during the CNF growth resulted in significant enhancement of the CNF-yield, producing thicker layers of CNFs and CNFs with smaller diameters. Channels containing silicon micropillars covered with these CNFs have a significantly enhanced surface-to-volume ratio compared to bare microreactor channels (3-4 orders of magnitude). Deposition of well distributed platinum nanoparticles was carried out on these CNF layers, exemplifying their functionality as structured catalyst support to be used in microreactors.

3.1 Introduction

Currently, there is a growing interest in the design and use of microscale reactors as efficient systems for the synthesis of specific, low volume, high value fine and specialty chemicals such as pharmaceuticals and additives. Microreactors are small-scale fluidic systems comprising fluid channels with lengths in the millimeter-to-centimeter range and cross-sectional dimensions in the range sub-micrometer to sub-millimeter [1, 2]. Due to these small dimensions microreactors have high surface-to-volume ratios (in the order $10^4 \text{ m}^2/\text{m}^3$) that result in improved heat and mass transfer characteristics, which are critical for carrying out chemical reactions efficiently [1-4]. Enhanced heat transfer rates prevent thermal runaway during reactions (*i.e.* safer operation), and improved mass transfer rates (*i.e.* small diffusion distances) avoid issues as concentration gradients and secondary reactions resulting in by products/waste [5]. Various industries can directly benefit from the use of microreactor technology: an example is the fine chemicals industry which often involves multiphase reactions (gas-liquid-solid), where the solid phase is mostly a catalyst. These catalytic reactions, however, pose a substantial challenge in achieving efficient contact and mass transfer between different phases [6-8].

The integration of a solid catalytic phase (heterogeneous catalyst) in microreactors is a challenging task. Conventionally, it is achieved in two ways, *i.e.* (i) by using a micro packed-bed of powdered catalyst [9-11], or (ii) by using a thin layer of catalyst coated on the inner wall of a microchannel [12-14]. However, a powdered catalyst packed-bed might result in high pressure drops along the length of reaction-channel, whereas a thin catalyst coating usually fails to utilize the entire volume of the reactor channel effectively. Most of these problems can be overcome by introducing nanoscale structural features in the microchannels. For microsystems various possibilities have been explored, such as use of porous anodic alumina layers [15, 16], walls coated with porous materials such as zeolites [17, 18], and black or porous silicon [19, 20]. An exciting option in this regard is the use of rigid, porous and orderly arranged catalyst supports based on carbon nanostructures, such as carbon nanofibers, onto which a metallic catalytic active phase (*e.g.* platinum (Pt) or palladium (Pd) nanoparticles) can be deposited.

Theory

Since the landmark paper by Iijima in 1991 [21], carbon nanostructured materials such as carbon nanofibers (CNFs) and carbon nanotubes (CNTs) have received a tremendous interest. This is due to their exceptional mechanical, electrical, physical and chemical characteristics [22-25], which makes them attractive for variety of applications. Applications of CNFs and CNTs include emitters for field emission displays (FED) [26], composite reinforcing materials [27], hydrogen storage [28], bio- and chemical sensors [29, 30], nano- and microelectronic devices [31, 32], and as a catalytic support electrodes for fuel cells [33, 34].

Carbon nanostructures offer numerous advantages as catalyst supports for chemical reactions *viz.*, (i) corrosion resistance to acid or base medium, (ii) high length (μm)-to-diameter (nm) ratio and high surface area, (iii) absence of micro porosity, (iv) possibility to tune the surface chemistry, and (v) easy recovery of precious metal catalysts supported on them by simply burning the carbon skeleton [35-37]. A range of structured materials including monoliths [38], foams [37, 39-41], filters [42], glass and carbon fibers [43, 44] and cloths [45] have been used for the synthesis of CNF layers. The small dimensions of carbon nanostructures and the above mentioned advantages as catalyst support motivate integration of CNFs and/or CNTs as structured catalyst support layers in miniaturized reaction systems *i.e.* microreactors.

The synthesis of carbon nanostructures can be achieved *via* arc discharge [46], laser ablation [47] and chemical vapor deposition (CVD) methods (*e.g.* catalytic thermal CVD and plasma enhanced CVD) [48-50]. The catalytic thermal chemical vapor deposition (C-TCVD) method is a versatile technique and a relatively cheap method for large scale applications [51-53], and therefore most often used for CNF synthesis. The C-TCVD method utilizes decomposition of carbon-containing gases on catalytically active components such as transition metals such as nickel (Ni), cobalt (Co) and iron (Fe) or alloys of these materials (due to their ability to dissolve carbon /or form metal carbides) [49]. Hydrocarbon gases such as methane (CH_4), acetylene (C_2H_2), ethylene (C_2H_4), ethane (C_2H_6), or other C-sources as carbon monoxide (CO) or synthesis gas ($\text{CO}+\text{H}_2$) can be used to obtain CNF growth on these metal catalysts at temperatures between 400 and 1000 °C [51].

There are, however, critical issues which have to be addressed in order to obtain microreactors of which the flow channels are filled with an efficient CNF-based catalyst support, *i.e.* a layer of entangled CNFs ‘jungle’ as shown in *Fig. 3.1* [54]. These are, (i) deposition of well adhered metal catalyst layer (*e.g.* Ni [12, 49]) required for the

synthesis of CNFs, (ii) good attachment of the synthesized CNF layer to the microchannel, (iii) obtaining controlled CNF growth, (iv) efficient utilization of the microchannel volume to obtain a high surface area for active metal deposition, and (v) preparing CNF based catalyst layer by depositing stable and well dispersed active metal particles.

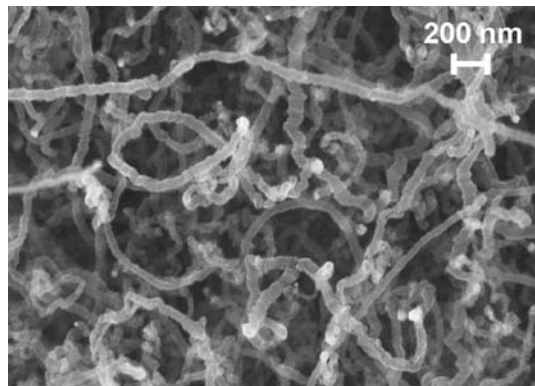


Figure 3.1: High-resolution SEM image of entangled ('jungle') carbon nanofibers [54].

In previous chapter, issues concerning the preparation of stable metallic layers for CNF-synthesis (*i.e.* Ni based thin-films) on fused silica substrates as well as improvement of the attachment of CNF-coatings were addressed [54, 55]. It was demonstrated that presence of a metal adhesion layer is necessary for the stability of the deposited Ni thin-film on the substrate, and the choice of a proper adhesion material (*i.e.* Ti-W and Ta) not only improves the attachment of synthesized CNF-coating, but also helps to tune morphological properties such as the diameter of CNFs.

In this chapter, new results are presented to probe the influence of some of the crucial CNF growth parameters on their growth as well as the resulting morphology. Furthermore, an approach to efficiently utilize the microchannel volume for reaction is shown, *i.e.* micromachined channels filled with arrays of pillars covered with a CNF-coating, as shown in *Fig. 3.2*.

The growth parameters investigated in this work are the hydrocarbon gas concentration and the addition of hydrogen during CNF-synthesis. A systematic approach has been followed to obtain knowledge on CNF growth *via* the use of a flat substrate-based model system mimicking the channel surfaces, which is then translated towards structured microchannels into which CNFs have to be anchored as catalyst

support. CNF layers were functionalized as catalytic support by depositing an active metal, such as Pt, by pulsed laser deposition.

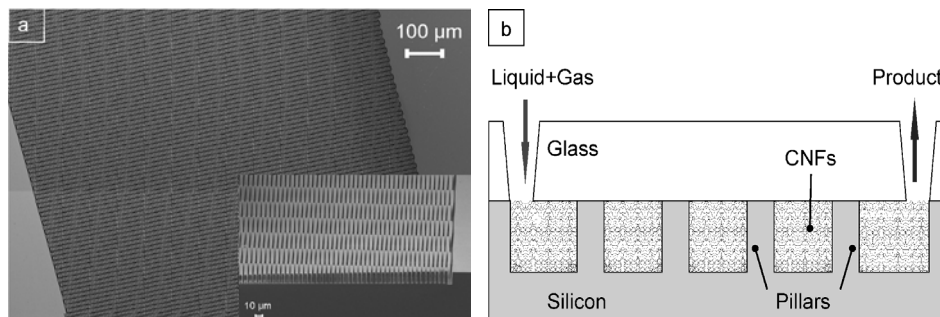


Figure 3.2: (a) SEM image of array of micromachined silicon pillars, (b) schematic cross-section of pillared microchannel with CNFs that act as catalyst support (not on scale).

3.2 Experimental

3.2.1 Preparation of nickel based thin-films on flat fused silica and silicon substrates

Ni-based thin films for the synthesis of CNFs were deposited on fused silica substrates (Corning, UV Grade 7980F; diameter 100 mm, thickness $500 \pm 25 \mu\text{m}$, roughness as-fabricated $<1 \text{ nm}$) and oxidized silicon substrates (standard p-type silicon substrates ($<100>$ -oriented, p-type, resistivity 5-10 Ωcm , 100 mm diameter, thickness 525 μm , single side polished; Okmetic, Finland - $\sim 250 \text{ nm SiO}_2$ using steam oxidation).

Post to nitric acid cleaning sequence and lithography, deposition of metals was done *via* evaporation (Ni/Ta) and sputtering (Ni/Ti-W). Experimental details of these procedures can be found elsewhere [54]. The thickness of the deposited adhesion layer was 10 nm, with on top 25 nm nickel. Finally, the substrates with the thin metal films were diced into samples of $1 \text{ cm} \times 1 \text{ cm}$, with a centered $8 \text{ mm} \times 8 \text{ mm}$ area of metal thin-film.

3.2.2 Fabrication of microchannels containing ordered arrays of pillars

Microchannels of $30 \times 1 \text{ mm}$ containing ordered arrays of elongated hexagonal pillars were defined in standard p-type silicon substrates ($<100>$ -oriented, p-type, resistivity 5-

10 Ωcm , 100 mm diameter, thickness 525 μm , single side polished; Okmetic, Finland). Prior to processing, the substrates were cleaned by immersion in fuming 100% nitric acid and boiling 69% nitric acid followed by quick dump rinsing in de-mineralized water and dry spinning. With standard UV-lithography microchannels with pillars (pillar specifications: length 15 μm , width 3 μm , and spacing 3 μm) were defined in photoresist, which was postbaked for 30 min at 120 $^{\circ}\text{C}$ (in air) after development. The photoresist acted as a masklayer during deep reactive ion etching (DRIE; Adixen AMS 100DE) of silicon with a Bosch process, *i.e.* a cyclic process which uses sulfur hexafluoride for etching of silicon and octafluorocyclo-butane for sidewall passivation. The height of the pillars (thus the depth of the channel) was ~ 20 μm . Post to etching the mask was stripped with an oxygen plasma and immersion in 100% nitric acid, followed by rinsing and drying. Fluorocarbons resulting from the DRIE process were removed by a wet oxidization step, followed by immersion in 1% hydrofluoric acid, rinsing in DI-water and drying. A second wet oxidation step (45 min, 1000 $^{\circ}\text{C}$) was used to deposit a ~ 250 nm thick SiO_2 layer on the etched microchannel. A thin-film of Ni/Ta (25 nm / 10 nm) was deposited on the micropillars using electron-beam evaporation (Balzers BAK600 system) in combination with a home-built stainless-steel shadowmask, using identical settings as for evaporation of Ni/Ta films on flat substrates. Finally, the substrates were diced into samples of 40×3 mm.

3.2.3 CNF layer synthesis

3.2.3.1 Reduction pretreatment

Prior to CNF synthesis the nickel-based thin-film samples, both flat substrates and microchannels with arrays of pillars, were first cleaned ultrasonically in acetone (5 min, Branson 200 ultrasonic cleaner) to remove organic contaminants, followed by washing with flowing deionized water (25 $^{\circ}\text{C}$) and dried with pressurized technical air. Subsequently, the samples were reduced in a mixture of 20 vol.% H_2 in N_2 (99.999%, INDUGAS) with total flow rate of 50 ml/min, while increasing the temperature to 500 $^{\circ}\text{C}$ (ramp up 5 $^{\circ}\text{C}/\text{min}$) and maintained at 500 $^{\circ}\text{C}$ for 2 h. This pretreatment is essential for the dewetting of the Ni thin film to produce nanoparticles which act as nucleation sites for CNF growth. After cooling down to room temperature, the samples were transferred to the CNF synthesis set-up for carrying out CNF synthesis.

3.2.3.2 CNF growth

CNF synthesis was performed in a quartz reactor heated by a vertical furnace and horizontal furnace for flat substrates and microreactor chips, respectively. The use of different furnaces was simply for the better handling of samples with different sizes. Flat fused silica samples with Ni-based thin-films were heated in N_2 in vertical furnace from room temperature to 700 °C at a rate of 5 °C/min, and at 700 °C exposed to a reactive gas mixture of C_2H_4 in N_2 (99.95%, PRAXAIR) and/or H_2 at a total flow rate of 100 ml/min. The reaction time at this temperature was one hour, after which the samples were cooled down in N_2 to room temperature. Two different sets of experiments were carried out to probe the influence of growth parameters on CNF growth and their morphology: (i) variation of ethylene concentration (5-15-25-30 vol.%) balanced with N_2 at 100 ml/min total flow rate, and (ii) H_2 addition during CNF growth (6.25-12.5-25 vol.%), using 25 vol.% C_2H_4 balanced with N_2 at 100 ml/min total flow rate. These hydrogen concentrations were chosen to obtain three different H_2/C_2H_4 ratios, *viz.* 1:4, 1:2 and 1:1. The amount of carbon deposited on each sample was determined by measuring the increase in weight.

CNFs were synthesized inside microchannels with arrays of pillars by positioning samples on a quartz boat in a horizontal quartz reactor heated by an outer furnace. The samples were heated in N_2 from room temperature to 635 °C at a rate of 5 °C/min, and at 635 °C exposed to a reactive gas mixture of C_2H_4 in N_2 (99.95%, PRAXAIR) and H_2 (0 and 6.25 vol.%) at a total flow rate of 100 ml/min. The reaction time was one hour or 2 h, after which the samples were cooled down in N_2 to room temperature.

3.2.4 Active metal deposition on CNF layers

Platinum (Pt) film was deposited by pulsed-laser deposition (PLD) using a KrF excimer laser beam with a wavelength of 248 nm. The spot size of the laser beam was 1.95 mm², with an energy density of 4.5 J/cm². A Pt target with a density of 21.45 g/cm³ (99.99%) was used. The distance between the platinum target and CNF-coated samples was 42 mm. The deposition rate was 0.04 nm/pulse, and the film thickness achieved on a fiber body was about 2.5 nm, which corresponds to ~3.5 wt. % loading of Pt (based on weight of deposited CNF layer). The deposition was carried out at room temperature in Ar atmosphere at a pressure of 0.01 mbar. The Pt film was further annealed at 500 °C for 2 h in N_2 atmosphere for thermal disintegration of the film to generate well dispersed nanoparticles.

3.2.5 Characterization

The morphology of the synthesized CNF-coatings was investigated by scanning electron microscopy (HRSEM; LEO 1550). Cross-sectional SEM analysis was performed on samples after cleaving manually with pliers. In case of CNF layers synthesized inside pillared microchannels, ultrasonication in water (5 min, Branson 200) was used to verify the attachment of CNF layers, followed by drying and SEM-inspection.

3.3 Results and discussion

Incorporation of a metal adhesion layer ensures good adhesion of the Ni thin-film to the fused silica substrate. Previously, it is shown that the use of Ta or Ti-W underneath Ni resulted in well-attached CNF-coatings, even under intense fluid flow conditions (*i.e.* flow in the m/s range). Moreover, the type of adhesion material influences the diameter of the fibers constituting this coating: Ta yields fibers with smaller diameter than Ti-W [54]. When synthesized in microchannels, control of the morphology of CNFs - *i.e.* average diameter of CNFs and CNF layer thickness - is important to be able to optimally fill the volume of the microchannels (efficient catalyst support), for example the spacing between pillars (see *Fig. 3.2b*).

It is known from literature that a variety of growth parameters can influence the morphology of CNFs. Important parameters are the growth catalyst, synthesis temperature, type of C-source gas and its concentration, gas velocity and partial pressures, growth duration and addition of hydrogen during CNF growth [53, 56-60]. Overall, the most crucial parameters in CNF synthesis are the concentration and flow rate of the C-source, the concentration of hydrogen, and the synthesis temperature [53]. In this work the influence ethylene concentration and addition of hydrogen on the C-TCVD CNF growth process is studied.

3.3.1 Influence of growth parameters on CNF synthesis

3.3.1.1 Ethylene concentration

Fused silica samples with a metal thin-film of Ni/Ti-W were exposed to the C-TCVD process. The ethylene concentration in the reacting mixture was varied from 5 vol.% to 30 vol.%. *Figure 3.3* shows top-view SEM images of the samples for increasing C₂H₄ concentrations, and *table 3.1* presents the amount of deposited carbon deposited as well as the average CNF diameters CNFs for different concentrations of C₂H₄. The SEM

images clearly show a change in the CNF morphology as a function of the C_2H_4 concentration. For 5 vol.% C_2H_4 nearly no CNF growth is observed (*Fig. 3.3a*): only a small amount of carbon is deposited with a scattered growth of CNF resembling structures. For 15 vol.% C_2H_4 a small amount of CNFs is found with an average diameter of 150 nm (*Fig. 3.3b*). In case of 25 and 30 vol.% C_2H_4 rather large amounts of uniform layers of entangled CNFs are seen (*Fig. 3.3c* and *3.3d*). The amount of deposited carbon increased with increasing C_2H_4 concentration, but seems to level off at high C_2H_4 concentrations. Cross-sectional SEM-images (not shown here) revealed the presence of a ‘dense’ C-layer at the metal interface (*i.e.* underneath the open, entangled jungle CNF layer).

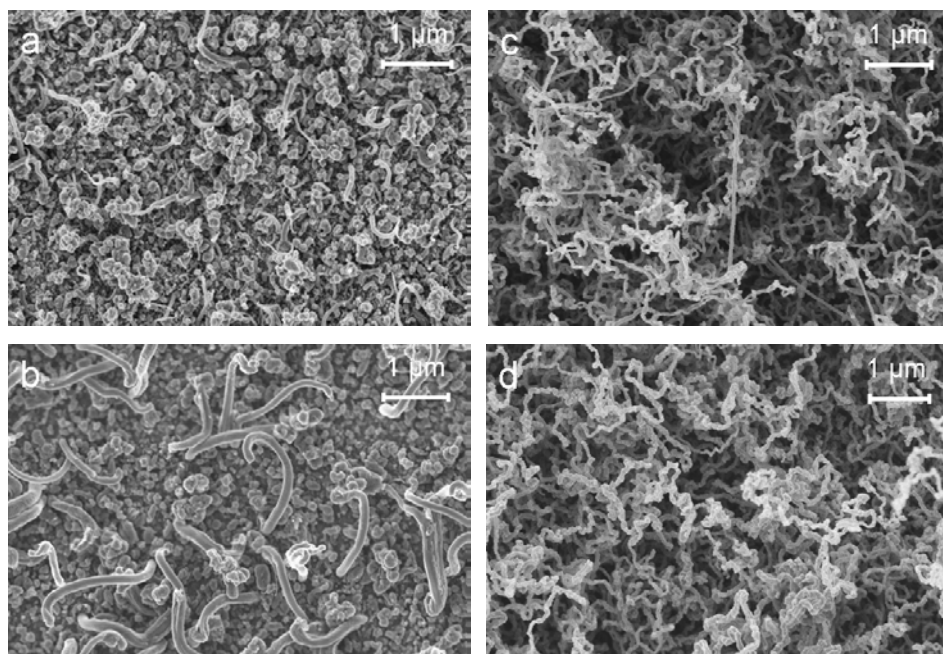


Figure 3.3: Top-view SEM images illustrating CNF morphology for different C_2H_4 concentrations (total flow rate of 100 ml/min; fused silica samples with 25 nm Ni and 10 nm Ti-W): (a) 5 vol.%, (b) 15 vol.%, (c) 25 vol.%, and (d) 30 vol.%.

In *Fig. 3.4* the thicknesses of this ‘dense’ C-layer as well as the CNF layer are plotted as a function of the C_2H_4 concentration. For increasing ethylene concentrations the thickness of both layers increases, and only for C_2H_4 concentrations exceeding 15

vol.% significant CNF-growth is visible (for lower concentrations only deposition of carbonaceous species).

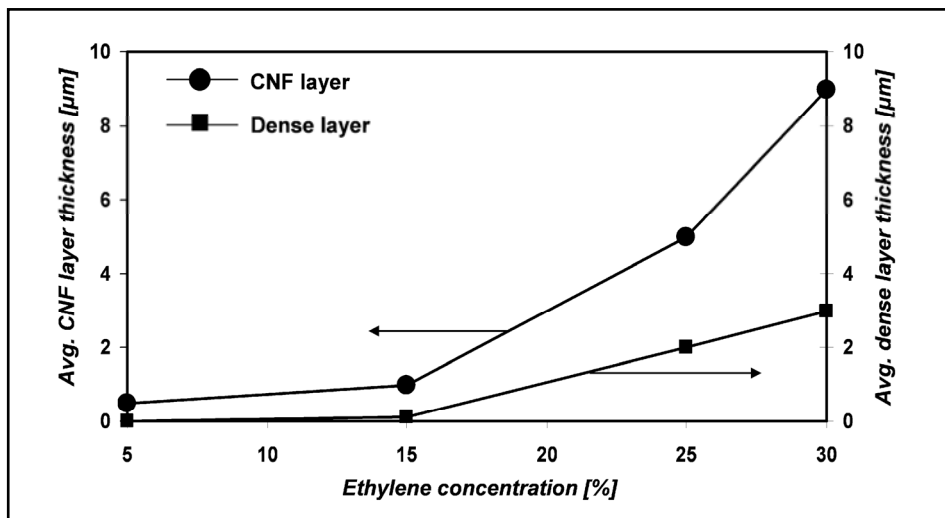


Figure 3.4: Influence of the ethylene concentration on the average thicknesses of the CNF layer and the 'dense' C-layer between the CNF layer and the substrate.

From literature it is known that the concentration of the C-source gas influences both the CNF growth rate and the rate of deactivation [56]. At lower concentrations insufficient supply of C-species restricts deposition of carbon and hence the CNF growth rate, whereas at very high concentrations the rate of deposition of carbon on the nickel particles is becoming so high that carbon consumption *via* CNF growth is not able to keep up. As a consequence, excess carbon on the nickel surface leads to encapsulation of the nickel particle, deactivating the particle for CNF growth. Data in *Fig. 3.3* and *3.4* and *table 3.1* shows that such a deactivation effect is not yet prominent for the conditions used in this study and CNF deposition comply increase with increase in ethylene concentration. However, since the C-layer underneath the CNF-layer is at most microporous (*i.e.* poresize < 2 nm), this material cannot be classified as 'open' catalyst support (in contrast to entangled CNF layers). Therefore, the thickness of this C-layer should not be too large (*i.e.* < 2 μm), which motivates why to use 25 vol.% C_2H_4 for further experiments.

Table 3.1: Amounts of deposited carbon and average diameter of CNFs for different ethylene concentrations (total flow rate = 100 ml/min; X vol. % C₂H₄ balanced with N₂)

C ₂ H ₄ concentration [X vol.% balanced with N ₂]	C-deposition μg C / μg Ni	Avg. CNF diameter ^a [nm]
5	1.4	52
15	4.3	150
25	12.9	100
30	15.7	71

^a Avg. of ~50 fibers from HR-SEM images

3.3.1.2 Addition of hydrogen during CNF growth

Ni/Ti-W thin-film samples exposed to the C-TCVD synthesis process during which H₂ was added to the reacting mixture contained significantly thicker CNF layers. This is clearly visible from SEM images (*Fig. 3.5*). From the cross-sections it can also be seen that the overall morphology of the CNF layer has changed: underneath the ‘open’ entangled jungle of CNFs a dense(r) but amorphous C-layer can be distinguished, of which the porosity is (much) lower than of the CNF layer. Furthermore, near the metal surface a dense but rather ordered C-layer is visible, with a nearly vertical alignment of the carbon material. The morphology of this material is very similar to tungsten oxide nanowires synthesized on W-based thin-films with a similar C-TCVD process [61], as a consequence of which it is assumed that the structured layer visible near the metal interface is composed of tungsten-based species.

Figure 3.6 shows the thicknesses of the CNF-coating and the dense C-layer (summation of the amorphous and ordered sublayers) as a function of the hydrogen concentration, and *table 3.2* contains the amounts of deposited carbon and average CNF diameter. It is well known that addition of hydrogen during CNF-synthesis affects the carbon yield, as well as the morphology of produced carbon nanostructures [62-64]. Hydrogen is usually added to slow down the hydrocarbon decomposition, and to achieve better control on carbon formation by rehydrogenating the reactive carbon species in the gas phase as well as reduction of the formation of undesired carbon deposits from the pyrolysis of the carbon feedstock [57]. Due to a lower deactivation

rate it also results in higher yields of carbon, resulting in the formation of longer fibers. Data on the amount of deposited carbon (*table 3.2*) and *Fig. 3.6* are in agreement with this theory. However, the fact that thick dense C-layers are formed with hydrogen concentrations above 6.25 vol.% (*i.e.* $> 12 \mu\text{m}$) makes CNF-coatings synthesized with high H_2 -concentrations unattractive as structured, open catalyst support in the case of Ni/Ti-W thin film samples.

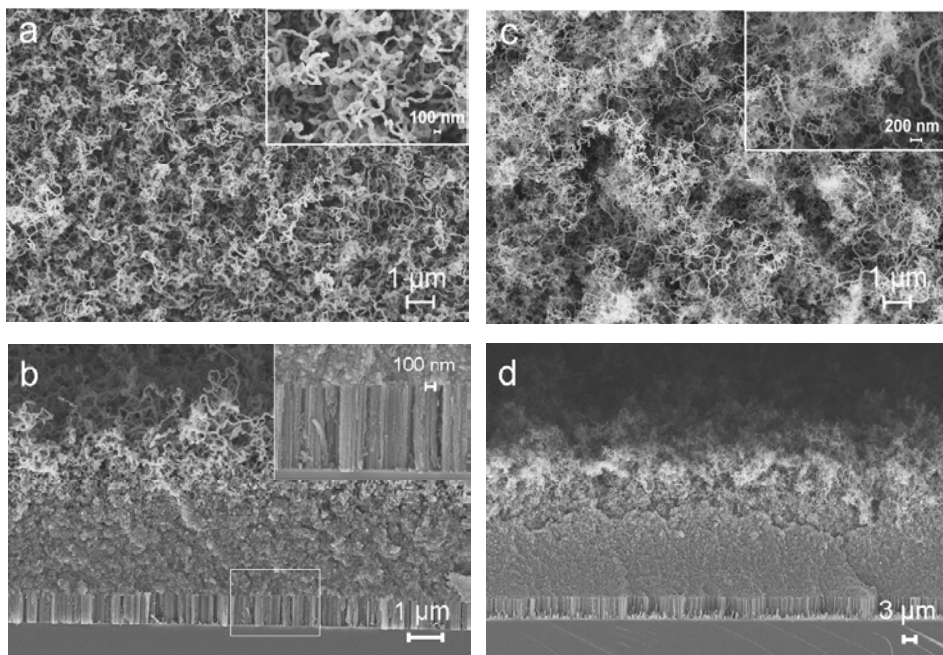


Figure 3.5: HR-SEM images illustrating CNF layer morphology for different H_2 concentrations (total flow rate of 100 ml/min; fused silica samples with 25 nm Ni and 10 nm Ti-W): (a) top-view of CNF layer grown with addition of 6.25 vol.% H_2 ($\text{H}_2:\text{C}_2\text{H}_4 = 1:4 \text{ v/v}$); Inset: higher magnification image of CNFs, (b) cross-sectional view of this CNF layer (inset: CNF layer with vertical alignment), (c) top-view of CNF layer grown with addition of 25 vol.% H_2 ($\text{H}_2:\text{C}_2\text{H}_4 = 1:1 \text{ v/v}$); Inset: higher magnification image of CNFs, and (d) cross-sectional view of this CNF layer.

The diameters of fibers constituting the CNF layers decrease with increasing hydrogen content. Park *et al.* have suggested that presence of hydrogen in the reactant responsible for inducing reconstruction/fragmentation of the Ni-particles, *i.e.* the generation of a set of smaller particles with faces that favor the precipitation of carbon in

the form of graphite: for increasing hydrogen concentrations in the reactant gas, the associated metal particles tend to become progressively more faceted. During this reconstruction process, the metal particles also undergo a wetting-and-spreading action on graphite at temperatures above 600 °C, *i.e.* incorporation of particles in the fibers. This reconstruction process, thus the formation of smaller metal particles, is responsible for the reduction of the average fiber diameter with increasing hydrogen content [62]. In this work a decrease in carbon yield was found for 25 vol.% H₂ (*table 3.2*), which is in agreement with literature [63, 65, 66]. This stresses the fact that there is an optimal hydrogen concentration for achieving the maximum growth of CNFs: for Ni/Ti-W thin-films this is 6.25 vol.% H₂ in 25 vol.% C₂H₄.

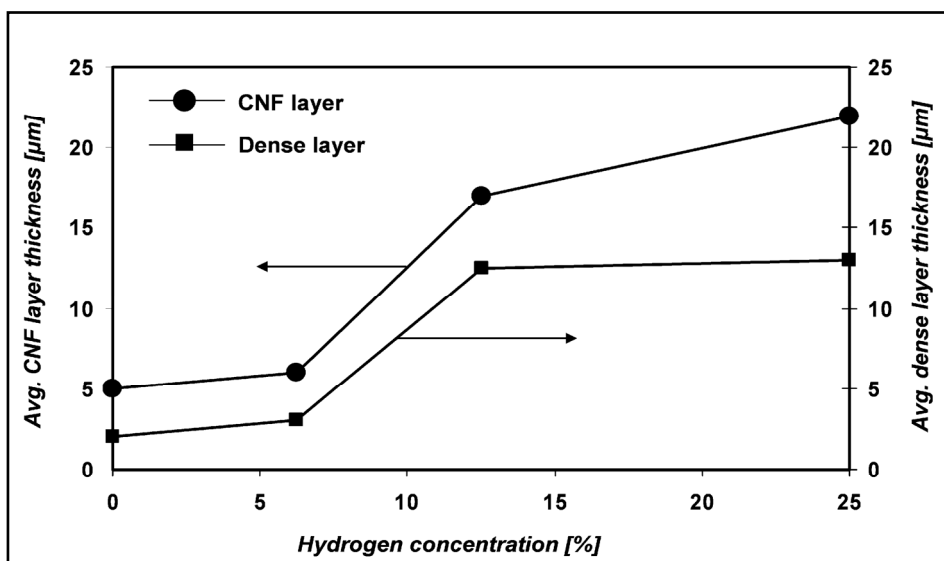


Figure 3.6: Influence of the addition of hydrogen to ethylene on the average thicknesses of the CNF layer and ‘dense’ C-layer(s) between the CNF layer and the substrate (total flow rate of 100 ml/min; fused silica samples with 25 nm Ni and 10 nm Ti-W).

The presence of (a) dense C-layer(s) between a layer of entangled CNFs and the fused silica substrate is undesired in case of catalyst support applications, and can be avoided by using Ta as adhesion layer instead of Ti-W. On fused silica with Ni/Ta no dense C-layers were found for any of the investigated C-TCVD settings as used for Ni/Ti-W (*Fig. 3.7*) [54]. Moreover, CNFs synthesized on Ni/Ta have smaller diameters than CNFs on Ni/Ti-W (for similar synthesis conditions), resulting in higher surface-

areas, which is beneficial for the amount of catalytically active species to be anchored to the CNF-based catalyst support. However, the stability of thus synthesized layer was found similar to the similar when tested for typical fluid flow conditions as described in chapter 2 of this thesis.

Table 3.2: Amounts of deposited carbon and average diameter of CNFs for different hydrogen concentrations (total flow rate = 100 ml/min; X vol. % H_2 in 25 vol. % C_2H_4 balanced with N_2)

H₂ concentration [X vol.% in 25 vol. % C_2H_4 balanced with N_2]	C-deposition $\mu g\ C / \mu g\ Ni$	Avg. CNF diameter ^a [nm]
0 ^b	12.9 ^b	100 ^b
6.25	35.0	47
12.5	65.0	32
25	59.3	17

^a Avg. of ~50 fibers from HR-SEM images

^b Tabulated for comparison (no hydrogen added during CNF growth)

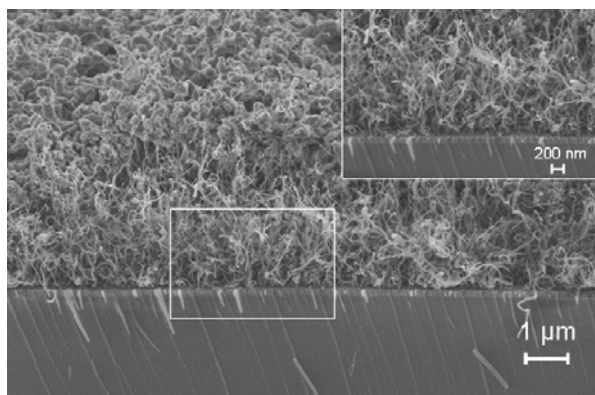


Figure 3.7: HR-SEM image showing the morphology of a CNF layer grown on 25 nm Ni and 10 nm Ta on fused silica. Synthesis conditions: 25 vol.% C_2H_4 balanced with N_2 at 700 °C for 1h, total flow rate 100 ml/min (inset: underneath the CNF layer no dense C-layer(s) are present).

3.3.1.3 CNF layer synthesis on silicon based flat substrates

Samples with Ni/Ta deposited on oxidized silicon were exposed to the C-TCVD synthesis process. The ‘optimal’ CNF growth settings as described in 3.3.1.1. and 3.3.1.2. were used, *i.e.* 25 vol.% C_2H_4 and at most 6.25 vol.% H_2 . Fig. 3.8a and 3.8b show SEM images of a CNF layer grown without hydrogen, and Fig. 3.8c and 3.8d, a CNF layer synthesized with H_2 added to the reaction mixture.

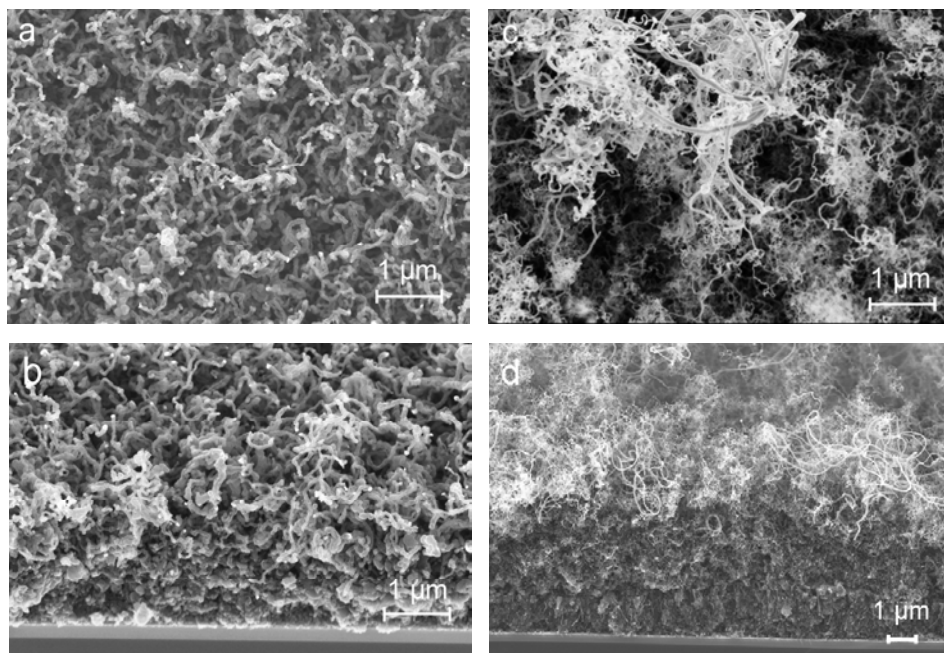


Figure 3.8: HR-SEM images illustrating the morphology of a CNF layer grown on 25 nm Ni and 10 nm Ta on oxidized silicon (total flow rate 100 ml/min): CNF layer synthesized without addition of hydrogen to 25 vol.% C_2H_4 (a) top-view, (b) cross-sectional; CNF layer synthesized with 6.25 vol.% H_2 added to 25 vol.% C_2H_4 ($H_2:C_2H_4=1:4$ v/v) (c) top-view, (d) cross-sectional view.

There is no noticeable difference in the morphology of CNFs compared to CNFs grown on fused silica, *i.e.* the diameters and CNF layer thicknesses are similar. Moreover, the presence or absence of hydrogen during synthesis affects the CNF layers in an identical way. Chinthaginjala *et al.* [66] recently published results describing the influence of hydrogen addition on the formation of thin CNF layers on Ni foam

material. Although in their case the amount of nickel available for CNF growth is different compared to thin films used in this work, they have similar observations concerning the change in CNF morphology (*i.e.* their diameter and CNF layer thickness) when hydrogen is present during the growth of CNFs. They indicated that carbon deposition is reduced by adding hydrogen (*i.e.* H_2 suppresses the encapsulation of Ni particles with carbon (which leads to deactivation), thereby obtaining thicker CNF layers), which is in agreement with our results. In addition, they not only observed the formation of thinner fibers on addition of hydrogen to the reaction mixture (which in excellent agreement with our observations), but also concluded this based on BET-measurements: for increasing concentrations of hydrogen the BET-area increased, which is due to increasing amounts of thin fibers. Thus, hydrogen improves the balance between graphene precipitation and carbon deposition in small Ni particles, limiting their encapsulation and extending formation of thin CNFs.

The similar results of CNF growth morphology obtained in case of fused silica and oxidized silicon flat substrates show that the morphology of CNF-layers on Ni/Ta does not depend on the type of the substrate, which implies that morphological data of CNF-synthesis on flat substrates will be (nearly) similar to morphological properties of CNF-coatings grown on microchannels filled with oxidized silicon pillars.

3.3.2 Carbon nanofiber based catalyst supports in microreactors

3.3.2.1 Microchannels with high specific surface areas

As mentioned earlier microreactors offer high surface-to-volume ratios ($\geq 10^4 \text{ m}^2/\text{m}^3$) which make them attractive for not only performing reactions that require better heat and mass transfer characteristics, but also for processes that require better interphase contact such as gas-liquid-solid reactions. In general, the surface-to-volume ratio is defined as the ratio of surface area [m^2] (where for example catalyst can be anchored) of a system and its internal (void) volume [m^3] (*i.e.* the amount of volume accessible to liquids/gases). For example, when a change is made from a 30m^3 stirred vessel to 1L laboratory reactor, this ratio increases a factor 30. If these macrosystems are changed into a microchannel having fluidic channels with a diameter of $30 \mu\text{m}$, this ratio rises by a factor of 3000 [67]. The specific surface area available for catalyst deposition inside microreactors can be further improved by washcoatings or a layer of porous material [15, 16, 68, 69]. For example, Urbiztondo *et al.* have reported in their work on the development of microstructured zeolite films as highly accessible catalytic coatings for

microreactors, that such coatings can exhibit values of the external surface-to-volume ratio in the 400,000–700,000 m²/m³ range depending on the preparation conditions. Roumanie *et al.* [68] have shown that use of arrays of micropillars in microchannels results in a 13 fold increase of specific wall area. In our case of flow channels filled with hexagonal solid pillars (*Fig. 3.2a*), the surface-to-volume ratio is *ca.* 10⁵ m²/m³. Nevertheless, the use of a microporous catalyst support layer (such as an alumina washcoat) might cause internal mass transfer problems in microsystems, particularly for reactions involving liquid-solid mass transfer [41]. However, when these pillars are covered with carbon nanofibers, in such a way that the spacing between the pillars is completely filled with ‘open’ CNFs, remarkable surface-to-volume ratios, up to 10⁸ m²/m³. This value is in good agreement with the values estimated by Popp and Schneider [70], who demonstrated the use of a monolithic porous carbon nanotube structure as a chemical reactor that exhibited a surface-to-volume ratio of 5·10⁶ to 2·10⁷ m²/m³. Such large surface-to-volume ratios provide a considerably higher catalytic activity per unit volume of the channels (assuming homogeneous distribution of catalytic material on the rigid, open CNF-based catalyst support), without facing any internal diffusion limitations for reactant molecules, or hydrodynamic problems for fluid flow, which is essential for performing gas-liquid-solid reactions in an efficient way.

In this work CNF-based catalyst supports are grown in microchannels with arrays of elongated hexagonal silicon pillars containing a thin-film of Ni/Ta, using the optimal CNF-synthesis parameters described in section 3.3.1.

3.3.2.2 Synthesis of CNFs in microchannels containing arrays of micropillars

Flow channels in silicon containing arrays of oxidized silicon micropillars covered with a thin-film of Ni/Ta were exposed to the C-TCVD CNF synthesis process. *Figures 3.9a* and *3.9b* show cross-sectional SEM images of micropillars prior and post to a CNF growth procedure using 25 vol.% C₂H₄ for 1 hour. The entangled morphology of the CNFs is visible, however, the thickness of the CNF layer is not uniform across the height of the pillars. This non-uniformity can be prevented (to a large extent) by adding hydrogen to the reaction mixture, combined with a longer growth time. In *Fig. 3.9c* and *3.9d*, SEM images are shown for a growth procedure using 25 vol.% C₂H₄ with 6.25 vol.% H₂ and a growth time of 2 h. The thickness of the CNF layer is uniform over the height of the pillars. Furthermore, the addition of hydrogen and lengthened growth time

resulted in (nearly) complete filling of the pillar spacing, and the CNF layer maintained its open structure.

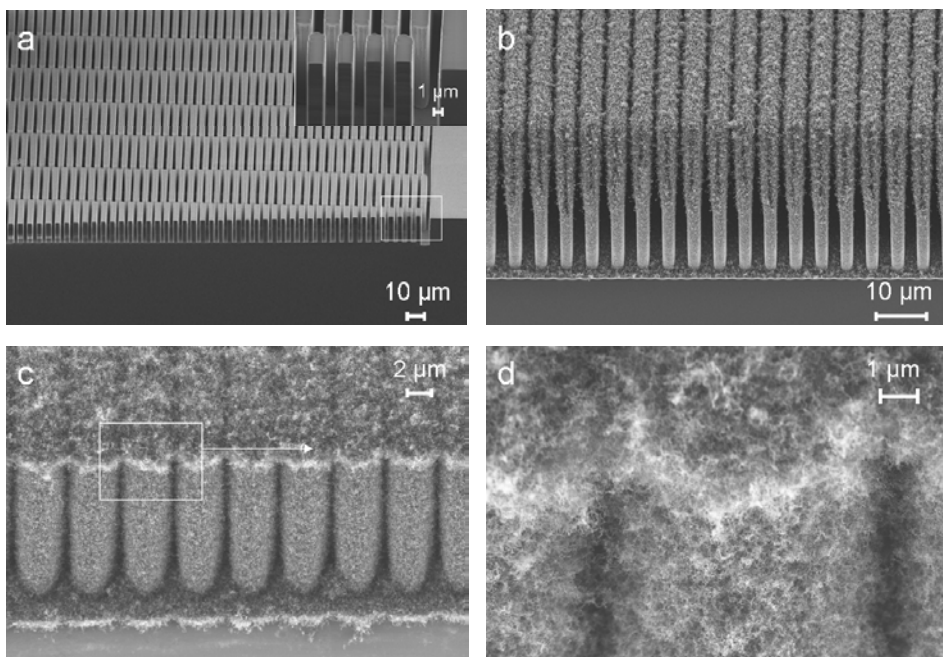


Figure 3.9: Cross-sectional SEM images showing arrays of micromachined silicon pillars (a) prior to CNF-synthesis, (b) post to CNF-synthesis without hydrogen (25 vol.% C_2H_4 for 1 hour), (c) post to CNF-synthesis with 6.25 vol.% H_2 added to C_2H_4 (growth time 2 hour): the CNF layer fills the complete pillar spacing, and (d) the grown CNF-coating exhibits the open structure of entangled CNFs.

The thickness non-uniformity of the CNF layer across the height of the micropillars (as seen in *Fig. 3.9b*) is a consequence of two issues. Firstly, the (rather) mono-directional origin of the used metal deposition technique plays a role. Like any other PVD-deposition technique, electron-beam evaporation is subject to the ‘cosine effect’ [71], which means that more material is deposited on planes facing the vapor flux (*i.e.* planes perpendicular to the flux), than on inclined planes (*i.e.* planes non-perpendicular to the flux). In fact, due to this effect a metal film deposited on the sidewall of a trench exhibits a thickness gradient: near the top of the trench the layer is thicker than on the sidewalls in deeper areas of the trench, as well as on the bottom of

the trench [72]. For Ni deposited in a microchannel filled with arrays of pillars this implies that the metal layer thickness on top of the pillars will be thicker than the layers at the bottom of the trench and at the sidewalls of the pillars. Moreover, the metal film at the sidewalls of the pillars will have a thickness gradient: the thickness will reduce towards deeper areas of the channel. Since the thickness of the Ni-layer can affect the growth rate of CNFs this will result in a CNF layer thickness non-uniformity on the pillar sidewalls.

Secondly, gradients in the hydrocarbon gas across the depth of the microchannel due to close packing of the micropillars can negatively affect the CNF growth rate at deeper areas of the channel. For high-aspect ratio arrays, *i.e.* high pillars with small spacing, gas diffusion limitations can become an issue during CNF growth, similar to gas diffusion problems that occur during deep reactive ion etching of narrow, deep trenches [73].

The presented non-uniformity of the CNF-layer on the pillar sidewalls (*Fig. 3.9b*) can be reduced/avoided by increasing the pillar spacing, reduction of the pillar height/channel depth, or by using deposition technique other than conventional PVD-techniques (*i.e.* more multi-directional methods). However, for the pillar array configuration used in this work, the CNF-thickness uniformity can also be significantly improved by adding hydrogen to the hydrocarbon source (as shown in *Fig. 3.9c* and *3.9d*).

3.3.3 Deposition of catalytic active metal sites on CNF layers

In order to use CNF-layers as efficient, rigid catalyst supports, it is essential to anchor catalytic sites to the fiber bodies, such as metal particles of platinum (Pt). In this work pulsed laser deposition (PLD) is used to deposit a Pt thin-film on CNFs synthesized on silicon based substrates. Post to PLD the samples were annealed at 500 °C in nitrogen for 2 h to generate Pt nanoparticles. *Figure 3.10* shows high-resolution SEM images of a CNF-layer with Pt-particles attached to the fibers: well-distributed Pt-particles with a size distribution from 5 to 10 nm are visible as white dots (indicated by arrows).

For the application of CNFs as a structured catalyst support in the aqueous phase, modification (and control) of the surface hydrophobicity of the fibers is crucial. It is important to increase the hydrophilicity of the fibers, which can be obtained by oxidation of the surface of the fibers (*e.g.* by immersion in HNO₃), in order to increase the amount of oxygen containing groups such as carboxylic acid functional groups [74]. The presence of these groups also helps to obtain a higher degree of dispersion of the

active phase, particularly when the catalyst preparation will be performed *via* conventional aqueous phase catalyst preparation methods, such as impregnation and/or homogeneous deposition precipitation. A study of the use of these catalyst preparation methods for CNF-based supports is the subject of next chapter 4.

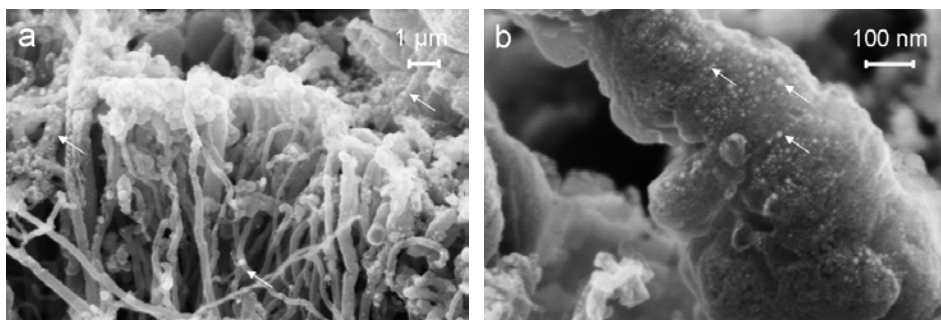


Figure 3.10: HR-SEM images of Pt particles deposited onto CNFs: (a) the particles are uniformly distributed of along the thickness of the CNF layer, and (b) well dispersed Pt catalyst particles (5-10 nm) cover each fiber (Pt particles are white spots, and are indicated by arrows).

3.4 Conclusions and Outlook

In this work the synthesis and characterization of carbon nanofiber (CNF) layers on fused silica and oxidized silicon substrates using nickel-based thin-films (i.e. Ni/Ti-W and Ni/Ta) is described. By means of high-resolution SEM imaging the influence of various growth parameters on the morphology of catalytic thermal chemical vapour deposited CNF-coatings is studied.

It was found that the most important parameters are the variation in ethylene concentration and addition of hydrogen to the reactant mixture. In case of Ni/Ti-W and Ni/Ta thin-films (25 nm Ni, 10 nm Ti-W or Ta) on flat fused silica or oxidized silicon substrates, open, entangled ‘jungle’ CNF layers were found for ethylene concentrations ≥ 25 vol.%. Moreover, addition of hydrogen to ethylene significantly enhances the rate of formation of CNFs, and reduces the average diameter of the fibers. When Ti-W is used as adhesion material for Ni, the concentrations of ethylene and hydrogen should not exceed 25 vol.% and 6.25 vol.%, respectively, in order to avoid the existence of a thick ‘dense’ C-layers between the substrate and the ‘open’ CNF layer. However, for similar synthesis conditions this C-layer is absent when Ta is used as adhesion material.

CNF layers are to be used as a structured catalyst support in microreactors. The 'optimal' C-TCVD conditions (25 vol.% C₂H₄ with 6.25 vol.% H₂ and a Ni/Ta thin-film) resulted in a good thickness uniformity of CNFs synthesized on the sidewalls of oxidized silicon micropillar arrays. The CNF layers filled the complete space between the pillars, which is important for performing gas-liquid-solid reactions. Catalytic metal particles were successfully pulsed laser deposited on such rigid, open-structure CNF-coatings, and the particles were homogeneously dispersed over the complete CNF layer. Despite the visually 'open, entangled jungle' character of the CNF layer and the homogeneous distribution of the nanoparticles across its thickness, prior to use of functionalized CNFs in microreactors issues such as mass transfer need to be verified experimentally. These aspects will be investigated for liquid phase reactions with Pd and/or Ru anchored to the CNF-layer.

Acknowledgements

This work was performed with the financial support from MicroNed program, under cluster-II of Smart Microchannel technology (SMACT) and work package II-G-2 and 3 (Smart Micro Reactors). The authors gratefully acknowledge Dr. M. Smithers for SEM analysis, and Ing. B. Geerdink for technical support. Drs. Minh Duc Nguyen (Inorganic Materials Science group, University of Twente, Enschede, The Netherlands) is acknowledged for performing pulsed laser deposition experiments.

References

- [1] W. Ehrfeld, V. Hessel, H. Lowe, *Microreactors - New Technology for Modern Chemistry*, 1st ed., Wiley-VCH, Weinheim, 2000.
- [2] G. Kolb, V. Hessel, Chem. Eng. J. 98 (2004) 1-38.
- [3] H. Lowe, W. Ehrfeld, Electrochim. Acta 44 (1999) 3679-3689.
- [4] V. Hessel, A. Renken, J.C. Schouten, J. Yoshida (Eds.) *Micro Process Engineering - A Comprehensive Handbook*, WILEY-VCH, 2009.
- [5] L. Kiwi-Minsker, A. Renken, Catal. Today 110 (2005) 2-14.
- [6] J. Kobayashi, Y. Mori, K. Okamoto, R. Akiyama, M. Ueno, T. Kitamori, S. Kobayashi, Science 304 (2004) 1305-1308.
- [7] J. Kobayashi, Y. Mori, S. Kobayashi, Chem.-Asian J. 1 (2006) 22-35.
- [8] V. Hessel, A. Renken, J.C. Schouten, J. Yoshida (Eds.) *Micro Process Engineering - A Comprehensive Handbook*, WILEY-VCH, 2009.

- [9] S.K. Ajmera, C. Delattre, M.A. Schmidt, K.F. Jensen, *Stud. Surf. Sci. Catal.* 145 (2003) 97-102.
- [10] C.D. Baertsch, M.A. Schmidt, K.F. Jensen, *Chem. Commun.*, (2004) 2610-2611.
- [11] K. Shah, R.S. Besser, *AIChE Annu. Meet., Conf. Proc.*, Cincinnati, OH, United States, Oct. 30-Nov. 4, 2005, 36b/31-36b/38.
- [12] V. Meille, *Appl. Catal. A* 315 (2006) 1-17.
- [13] K. Haas-Santo, O. Gorke, P. Pfeifer, K. Schubert, *Chimia* 56 (2002) 605-610.
- [14] K. Haas-Santo, M. Fichtner, K. Schubert, *Appl. Catal. A* 220 (2001) 79-92.
- [15] J.C. Ganley, E.G. Seebauer, R.I. Masel, *AIChE J.* 50 (2004) 829-834.
- [16] S.R. Deshmukh, A.B. Mhadeshwar, D.G. Vlachos, *Ind. Eng. Chem. Res.* 43 (2004) 2986-2999.
- [17] V. Sebastian, O. de la Iglesia, R. Mallada, L. Casado, G. Kolb, V. Hessel, J. Santamaria, *Microporous Mesoporous Mater.* 115 (2008) 147-155.
- [18] V. Valtchev, S. Mintova, M. Tsapatsis (Eds.) *Ordered Porous Solids*, Amsterdam, 2009.
- [19] M. Rournanie, C. Delattre, F. Mittler, G. Marchand, V. Meille, C. de Bellefon, C. Pijolat, G. Tournier, P. Pouteau, *Chem. Eng. J.* 135 (2008) S317-S326.
- [20] M.W. Losey, R.J. Jackman, S.L. Firebaugh, M.A. Schmidt, K.F. Jensen, J. *Microelectromech. Sys.* 11 (2002) 709-717.
- [21] S. Iijima, *Nature* 354 (1991) 56-58.
- [22] M. Bockrath, D.H. Cobden, P.L. McEuen, N.G. Chopra, A. Zettl, A. Thess, R.E. Smalley, *Science* 275 (1997) 1922-1925.
- [23] M.M.J. Treacy, T.W. Ebbesen, J.M. Gibson, *Nature* 381 (1996) 678-680.
- [24] M.F. Yu, O. Lourie, M.J. Dyer, K. Moloni, T.F. Kelly, R.S. Ruoff, *Science* 287 (2000) 637-640.
- [25] S.J. Tans, M.H. Devoret, H.J. Dai, A. Thess, R.E. Smalley, L.J. Geerligs, C. Dekker, *Nature* 386 (1997) 474-477.
- [26] S.S. Fan, M.G. Chapline, N.R. Franklin, T.W. Tombler, A.M. Cassell, H.J. Dai, *Science* 283 (1999) 512-514.
- [27] E. Hammel, X. Tang, M. Trampert, T. Schmitt, K. Mauthner, A. Eder, P. Potschke, *Carbon* 42 (2004) 1153-1158.
- [28] A.C. Dillon, K.M. Jones, T.A. Bekkedahl, C.H. Kiang, D.S. Bethune, M.J. Heben, *Nature* 386 (1997) 377-379.
- [29] W.J. Huang, S. Taylor, K.F. Fu, Y. Lin, D.H. Zhang, T.W. Hanks, A.M. Rao, Y.P. Sun, *Nano Lett.* 2 (2002) 311-314.

- [30] J. Kong, N.R. Franklin, C.W. Zhou, M.G. Chapline, S. Peng, K.J. Cho, H.J. Dai, *Science* 287 (2000) 622-625.
- [31] A.M. Fennimore, T.D. Yuzvinsky, W.Q. Han, M.S. Fuhrer, J. Cumings, A. Zettl, *Nature* 424 (2003) 408-410.
- [32] S.J. Tans, A.R.M. Verschueren, C. Dekker, *Nature* 393 (1998) 49-52.
- [33] C. Wang, M. Waje, X. Wang, J.M. Tang, R.C. Haddon, Y.S. Yan, *Nano Lett.* 4 (2004) 345-348.
- [34] D. Villers, S.H. Sun, A.M. Serventi, J.P. Dodelet, S. Desilets, *J. Phys. Chem. B* 110 (2006) 25916-25925.
- [35] C. Pham-Huu, N. Keller, L.J. Charbonniere, R. Ziessle, M.J. Ledoux, *Chem. Commun.* (2000) 1871-1872.
- [36] P. Serp, M. Corrias, P. Kalck, *Appl. Catal. A* 253 (2003) 337-358.
- [37] M.J. Ledoux, C. Pham-Huu, *Catal. Today* 102 (2005) 2-14.
- [38] N. Jarrah, J.G. van Ommen, L. Lefferts, *Catal. Today* 79 (2003) 29-33.
- [39] N.A. Jarrah, F.H. Li, J.G. van Ommen, L. Lefferts, *J. Mater. Chem.* 15 (2005) 1946-1953.
- [40] A. Cordier, E. Flahaut, C. Viazzi, C. Laurent, A. Peigney, *J. Mater. Chem.* 15 (2005) 4041-4050.
- [41] P.W.A.M. Wenmakers, J. van der Schaaf, B.F.M. Kuster, J.C. Schouten, *J. Mater. Chem.* 18 (2008) 2426-2436.
- [42] P. Tribolet, L. Kiwi-Minsker, *Catal. Today* 102 (2005) 15-22.
- [43] Z.R. Ismagilov, N.V. Shikina, V.N. Kruchinin, N.A. Rudina, V.A. Ushakov, N.T. Vasenin, H.J. Veringa, *Catal. Today* 102-103 (2005) 85-93.
- [44] S.S. Tzeng, K.H. Hung, T.H. Ko, *Carbon* 44 (2006) 859-865.
- [45] M. Cantoro, V.B. Golovko, S. Hofmann, D.R. Williams, C. Ducati, J. Geng, B.O. Boskovic, B. Kleinsorge, D.A. Jefferson, A.C. Ferrari, B.F.G. Johnson, J. Robertson, *Diamond Relat. Mater.* 14 (2005) 733-738.
- [46] T.W. Ebbesen, P.M. Ajayan, *Nature* 358 (1992) 220-222.
- [47] A. Thess, R. Lee, P. Nikolaev, H.J. Dai, P. Petit, J. Robert, C.H. Xu, Y.H. Lee, S.G. Kim, A.G. Rinzler, D.T. Colbert, G.E. Scuseria, D. Tomanek, J.E. Fischer, R.E. Smalley, *Science* 273 (1996) 483-487.
- [48] V. Ivanov, J.B. Nagy, P. Lambin, A. Lucas, X.B. Zhang, X.F. Zhang, D. Bernaerts, G. Vantendelo, S. Amelinckx, J. Vanlanduyt, *Chem. Phys. Lett.* 223 (1994) 329-335.

- [49] A.V. Melechko, V.I. Merkulov, T.E. McKnight, M.A. Guillorn, K.L. Klein, D.H. Lowndes, M.L. Simpson, J. Appl. Phys. 97 (2005) - 041301.
- [50] C.S. Cojocaru, A. Senger, F. Le Normand, J. Nanosci. Nanotechnol. 6 (2006) 1331-1338.
- [51] K.P. De Jong, J.W. Geus, Catal. Rev.-Sci. Eng. 42 (2000) 481-510.
- [52] M.L. Toebes, Y.H. Zhang, J. Hajek, T.A. Nijhuis, J.H. Bitter, A.J. van Dillen, D.Y. Murzin, D.C. Koningsberger, K.P. de Jong, J. Catal. 226 (2004) 215-225.
- [53] Z.X. Yu, D. Chen, B. Totdal, T.J. Zhao, Y.C. Dai, W.K. Yuan, A. Holmen, Appl. Catal. A 279 (2005) 223-233.
- [54] D.B. Thakur, R.M. Tiggelaar, J.G.E. Gardeniers, L. Lefferts, K. Seshan, Surf. Coat. Technol. 203 (2009) 3435-3441.
- [55] D.B. Thakur, R.M. Tiggelaar, J.G.E. Gardeniers, K. Seshan, L. Lefferts, Adv. Sci. Technol. 54 (2008) 231-236.
- [56] I. Kvande, D. Chen, Z. Yu, M. Ronning, A. Holmen, J. Catal. 256 (2008) 204-214.
- [57] H.S. Nalwa (Ed.) *Encyclopedia of Nanoscience and Nanotechnology*, American Scientific Publishers, 2004.
- [58] J.L. Chen, Y.D. Li, Y.M. Ma, Y.N. Qin, L. Chang, Carbon 39 (2001) 1467-1475.
- [59] H. Zhang, G.P. Cao, Z.Y. Wang, Y.S. Yang, Z.J. Shi, Z.N. Gu, J. Phys. Chem. C 112 (2008) 12706-12709.
- [60] I. Kvande, G. Oye, N. Hammer, M. Ronning, S. Raaen, A. Holmen, J. Sjoblom, D. Chen, Carbon 46 (2008) 759-765.
- [61] A. Agiral, A.W. Groenland, J.K. Chinthaginjala, K. Seshan, L. Lefferts, J.G.E.H. Gardeniers, J. Phys. D: Appl. Phys. 41 (2008) - 194009.
- [62] C. Park, R.T.K. Baker, J. Catal. 179 (1998) 361-374.
- [63] C. Pham-Huu, N. Keller, V.V. Roddatis, G. Mestl, R. Schlogl, M.J. Ledoux, Phys. Chem. Chem. Phys. 4 (2002) 514-521.
- [64] Z.X. Yu, D. Chen, B. Totdal, A. Holmen, Mater. Chem. .Phys. 92 (2005) 71-81.
- [65] C. Park, R.T.K. Baker, J. Catal. 190 (2000) 104-117.
- [66] J.K. Chinthaginjala, L. Lefferts, Carbon, 47 (2009) 3175-3183.
- [67] O. Worz, K.P. Jackel, T. Richter, A. Wolf, Chem. Eng. Technol. 24 (2001) 138-142.
- [68] M. Roumanie, V. Meille, C. Pijolat, G. Tournier, C. de Bellefon, P. Pouteau, C. Delattre, Catal. Today 110 (2005) 164-170.

- [69] M.A. Urbiztondo, E. Valera, T. Trifonov, R. Alcubilla, S. Irusta, M.P. Pina, A. Rodriguez, J. Santamaria, *J. Catal.* 250 (2007) 190-194.
- [70] A. Popp, J.J. Schneider, *Angew. Chem., Int. Ed.* 47 (2008) 8958-8960.
- [71] A.J. Hart, B.O. Boskovic, A.T.H. Chuang, V.B. Golovko, J. Robertson, B.F.G. Johnson, A.H. Slocum, *Nanotechnol.* 17 (2006) 1397-1403.
- [72] T.S. Cale, G.B. Raupp, T.H. Gandy, *J. Appl. Phys.* 68 (1990) 3645-3652.
- [73] M.J. de Boer, J.G.E. Gardeniers, H.V. Jansen, E. Smulders, M.J. Gilde, G. Roelofs, J.N. Sasserath, M. Elwenspoek, *J. Microelectromech. Sys.* 11 (2002) 385-401.
- [74] T.G. Ros, A.J. van Dillen, J.W. Geus, D.C. Koningsberger, *Chem.-Eur. J.* 8 (2002) 1151-1162.

Chapter 4

Ruthenium Catalyst on CNF Support Layers for Si-based Structured Microreactors, Part I: Preparation and Characterization

Abstract

The preparation and characterization of ruthenium catalytic nanoparticles on carbon nanofiber (CNF) support layers via homogeneous deposition precipitation (HDP) and pulsed laser deposition (PLD) is presented. Prior to ruthenium deposition the CNF layers were functionalized via liquid phase oxidation treatment using nitric acid at 90 °C. This acid treatment not only effectively removed accessible CNF-growth catalyst, but also resulted in the formation of oxygen containing functional groups on the external surface of CNFs. A variety of characterization techniques, viz. TEM, XRD, XRF, XPS, and point-of-zero-charge (PZC) measurements were used to analyze the influence of the oxidation pretreatment on physico-chemical properties of CNF layers qualitatively and quantitatively. HDP yielded a very sharp size distribution (~85% of the particles had a diameter of 1.0-1.5 nm), whereas PLD had a less narrow distribution (the diameter of ~75% of the particles was 1-3 nm). Both methods yielded a ruthenium loading of 2.3 ± 0.1 wt.%, and in particular HDP showed uniform anchoring of particles throughout the thickness of the CNF layer. Using optimal conditions, the space in a silicon-based microreactor channel was efficiently filled with open, entangled CNF layer, which were used as anchor points for Ru using HDP and PLD.

4.1 Introduction

Microreactors have achieved a great deal of attention in recent years [1, 2]. They are miniaturized continuous flow reaction systems or reaction vessels with typical channel or chamber widths in the range of 10–500 μm [1]. Smaller diffusion distances in microreactors result in enhanced mass transfer rates and allow reactions to be carried out more efficiently. Microreactors also have high surface area-to-volume ratios ($\sim 10^4 \text{ m}^2/\text{m}^3$) that lead to improved heat transfer rates, and hence safer operation conditions, *e.g.*, avoidance of thermal runaways in case of highly exothermic reactions [2, 3]. These benefits are advantageous for the production of, for example, fine and/or specialty chemicals, which often involves multiphase reactions (fluid-solid) where the solid phase is mostly a catalyst. However, the integration of a solid catalytic phase (heterogeneous catalyst) in multiphase microreactors is a challenging task.

There are two ways which are explored previously for incorporating a solid phase catalyst inside the microreactor channels: *(i)* by using a micro-packed bed of powdered catalyst, and *(ii)* by using a thin layer of catalyst coated on the inner wall of a microchannel [2-8]. In the first case, high pressure drop(s) across the packed bed and diffusion limitations might arise, whereas in the latter case the thin catalyst coating usually fails to efficiently utilize the entire volume of the reactor channel. Most of these problems can be overcome by introducing nano- and/or microscale structural features in the microchannels. An attractive option is the use of carbon nanostructures onto which catalyst clusters are deposited, *e.g.* Ru, Pd or Pt metal particles.

Since the landmark paper by Iijima in 1991 [9], carbon nanostructured materials such as carbon nanofibers (CNFs) and carbon nanotubes (CNTs) have generated tremendous interest due to their exceptional mechanical, electrical, physical and chemical characteristics [10-13]. One promising application is the use of carbon nanostructures as catalyst support. They offer numerous advantages over conventional supports, *viz.* *(i)* corrosion resistance to acid or base medium, *(ii)* sufficiently high surface areas and absence of micro porosity, and *(iii)* easy recovery of precious metal catalysts supported on them by simply burning the carbon skeleton [14-16], moreover it has also been claimed that performance of CNF supported catalyst can be influenced by adsorption of reactants on the CNF support. For example, for the liquid phase hydrogenation of cinnamaldehyde over Pt/CNF catalyst it was demonstrated that catalytic action of Pt is influenced by the amount of cinnamaldehyde adsorbed on the support in the vicinity of Pt particles [17, 18].

The synthesis of carbon nanostructures can be achieved *via* a variety of techniques, of which details are reported elsewhere [17-26]. The catalytic thermal chemical vapor deposition (C-TCVD) method uses metals (*e.g.* Ni, Co, Fe) to catalyze CNF-growth from “C” containing gases (*e.g.* C_xH_y and CO) [19]. C-TCVD is a versatile technique and a relatively cheap method for large scale applications [19, 20, 21, 27]. *Figure 1.5* in chapter 1 exemplified the advantages of integrating a layer of carbon nanostructures in a microreactor channel as an alternative to a washcoated layer. A CNF layer has easier accessibility of active sites for reactant molecules due to its open structure, as a consequence of which diffusion problems are avoided [22, 23].

There are, however, critical issues in incorporating CNF layer as catalyst support in microreactors. The most important issues are the attachment of the CNF layer to the microreactor channel walls, and the deposition of stable and well dispersed active metal particles on the CNF layer. We have shown previously that a vapor deposited nickel layer can be stabilized with an adhesion layer of tantalum. In presence of C_2H_4 around 635-700 °C well attached CNF layers can be formed on fused silica and oxidized silicon substrates [24-26]. These CNF layers, typically with thickness of 10-20 μm and fiber diameters in the range 20-70 nm, are suitable for incorporation in microchannels [26].

In this work, we address the issue of anchoring catalyst clusters, *i.e.* ruthenium nanoparticles, on CNF layer by means of homogeneous deposition precipitation (HDP) and pulsed laser deposition (PLD). Deposition experiments and analysis are performed on oxidized silicon samples as well as with silicon-based microchannels containing ordered arrays of cylinders. The latter are to be used as microreactors for aqueous phase catalytic reduction applications.

4.2 Experimental

4.2.1 Fabrication of flat samples and microchannels with arrays of cylinders

Flat samples of 10 mm \times 10 mm and microchannels were prepared from standard silicon substrates (<100>-oriented, p-type, resistivity 5-10 Ωcm , 100 mm diameter, thickness 525 μm , single side polished; Okmetic, Finland). Channels of 30 mm \times 1 mm contained ordered arrays of cylinders arranged on an equilateral triangular grid. Prior to processing, the silicon substrates were cleaned by immersion in fuming 100% nitric acid (10 min) and boiling 69% nitric acid (15 min), followed by quick dump rinsing in demineralized water and dry spinning. In case of microchannels standard UV-lithography was used to define the pattern in 1.7 μm thick photoresist, which was postbaked for 30

min at 120 °C (in air) after development. The photoresist acted as a masklayer during deep reactive ion etching (DRIE; Adixen AMS 100SE) of silicon with a Bosch process, *i.e.* a cyclic process which uses sulfur hexafluoride for etching of silicon and octa-fluorocyclobutane for sidewall passivation [28]. An etchtime of *ca.* 13.5 min was required for 40-45 μm high cylinders (outer diameter 20 μm , inner diameter 10 μm ; pillar spacing 20 or 50 μm). Post to etching the mask was stripped with an oxygen plasma and immersion in 100% nitric acid, followed by rinsing and drying. Fluorocarbons resulting from the DRIE process were removed by a wet oxidation step (30 min, 800 °C), followed by immersion in 1% hydrofluoric acid (1 min), rinsing in DI-water and drying. A second wet oxidation step (45 min, 1000 °C) was used to deposit a ~ 250 nm thick SiO_2 layer on the etched microchannel. This latter oxidation step was also used for the preparation of flat samples.

Thin films of nickel/tantalum (25nm/10nm) were deposited on the oxidized substrates using electron-beam evaporation (Balzers BAK600 system). In case of substrates with etched microchannels a home-built stainless-steel shadow mask was used to deposit Ni/Ta in the channels. The purity of the Ni target material was 99.99%, and >99.95% for Ta. Evaporation rates (at pressures below 10^{-7} mbar) were in the range 1-5 $\text{\AA}/\text{s}$ for Ta and 10-15 $\text{\AA}/\text{s}$ for Ni. The thicknesses of evaporated films were controlled using an in situ thickness monitor [25]. Finally, the substrates were diced into samples of 10 mm \times 10 mm (flat samples) or 35 mm \times 5 mm (microchannel samples) (Disco DAD-321 dicing machine).

4.2.2 CNF layer synthesis

Prior to CNF synthesis the samples were cleaned ultrasonically in acetone (5 min, Branson 200 ultrasonic cleaner) to remove organic contaminants, followed by washing with flowing deionized water (25°C) and dried with pressurized technical air. Subsequently, the samples were reduced in a mixture of 20 vol.% H_2 in N_2 (99.999%, INDUGAS) with total flow rate of 50 ml/min, while increasing the temperature to 650 °C (ramp up 5°C/min) and maintained at 650 °C for 1 h. This pretreatment is essential to produce Ni nanoparticles which act as nucleation sites for CNF growth. After reduction the samples were cooled in N_2 from 650 to 635 °C (5°C/min), and exposed for 1h to a gas mixture of C_2H_4 (and H_2 in case of CNF-growth in microchannels) in N_2 (99.95%, PRAXAIR; total flow rate 100 ml/min), followed by cooling down to room temperature in N_2 . The amount of carbon deposited on each sample was determined by measuring the increase in weight.

4.2.3 Oxidation of CNF layers and ruthenium deposition

Samples with CNF layers were refluxed in concentrated (65 wt.%) as well as diluted (10 wt.%) nitric acid at 90 °C for different time intervals (*i.e.* 30, 60, 90 and 120 min). After the reflux the samples were washed thoroughly with de-mineralized water and dried at 110 °C for 2 hours.

Two methods were used to incorporate ruthenium in the CNF layers: HDP and PLD. In the case of HDP, oxidized CNFs were exposed to a $\text{RuNO}(\text{NO}_3)_3 \cdot n\text{H}_2\text{O}$ solution (Ru 32.16% w/w, Alfa Aesar; 0.022 g/l). The pH of the solution was adjusted to 1 by adding droplets of HNO_3 (65 wt.%, Merck) and a N_2 flow was used to expel CO_2 from the solution. The pH value of the solution was monitored during the whole process. The solution with immersed substrates was heated to 75 °C and urea (1.75g, 99.5%, Sigma-Aldrich) was added. Afterwards, the samples were washed thoroughly with de-mineralized water, dried at 110 °C and reduced at 500 °C in a mixture of 20% H_2/N_2 gases (50 ml/min) for 90 minutes. In case of PLD, oxidized CNFs were exposed to a Ru flux at room temperature. The target size was 0.25 cm², the target-substrate distance 45 mm, the spot size of the laser beam 1 mm², and the energy density 5 J/cm². After deposition the samples were calcined at 500 °C for 90 minutes under a 20% H_2/N_2 stream (total flow 50 ml/min, heating rate 5 °C/min, cooling rate 10 °C/min).

4.2.4 Characterization of CNF layers

CNF layers synthesized were analyzed by a variety of techniques. The morphology of the CNF layer and the particle size of Ru were investigated by scanning electron microscopy (SEM; LEO 1550) and transmission electron microscopy (TEM; Philips CM300ST-FEG equipped with Gatan Ultrascan 1000 CCD camera), respectively. X-ray diffraction (XRD; Philips PW1830) and Raman spectroscopy (Senterra, Bruker Optik GmbH) were used to analyze the structure/ crystallinity of CNFs. X-ray fluorescence spectrometry (XRF; Philips PW1480) was used to determine the nickel and ruthenium contents in/on CNFs, and X-ray photoelectron spectroscopy (XPS; Quantera SXM Physical Electronics) to obtain information on the surface composition of CNFs. PZC measurements were performed according to the procedure described by Mullet *et al.* [29]. In case of PLD, the presence of Ru on CNF layers was evidenced *via* energy-dispersive X-ray spectroscopy (EDX) coupled with TEM.

4.3 Results and Discussion

4.3.1 Synthesis of carbon nanofibers

In order to synthesize CNFs, the as-deposited nickel-based thin film needs to be dewetted (*i.e.* formation of nanoparticles), which is usually done *via* a pretreatment in hydrogen [20, 30, 31]. In previous work we have described in detail the pretreatment of nickel-based thin films, and subsequent synthesis of well-attached CNFs on oxidized silicon using a Ni/Ta (Ni/Ta:25 nm/10 nm) film and C-TCVD of C_2H_4 [25, 26]. *Figure 4.1* shows typical CNF-synthesis results [26]. The top view SEM-image reveals a highly entangled morphology, and that the fibers are ‘tip-type’ grown (nickel particles are visible on the tips). The diameter of the fibers ranges from 20 nm to 80 nm. The cross-sectional view shows that the CNF layer is $\sim 2\text{--}3\text{ }\mu\text{m}$ thick and has an open structure. Near the substrate surface a denser C-layer is visible. Although the exact composition and origin are not clear yet, this layer benefits the stability and adhesion of the CNF layer to the substrate [25, 32], which allows them to be used as support for catalyst under reactant flow typical for microsystems [25].

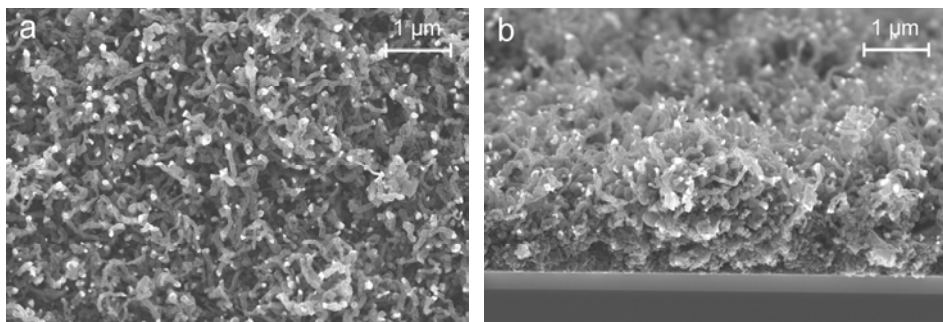


Figure 4.1: SEM images illustrating (a) top-view and (b) cross-sectional view of the synthesized CNF layer on silicon based flat substrates using C-TCVD of ethylene [26].

4.3.2 Oxidation treatment of CNF layers

Carbon nanofibers are graphitic in nature and thus hydrophobic. This limits the choice of methods to deposit/anchor catalyst material on them. Moreover, their intrinsic hydrophobic nature can also influence the performance of CNF-supported catalysts in aqueous phase reactions. In order to deposit Ru with the HDP method, it is essential that the surface of CNFs is hydrophilic: an oxidative treatment can be applied to introduce polarity on the CNF surface [19]. Oxidation with nitric acid is the most

common method, and results in the formation of oxygen-containing groups on the CNF surface (*e.g.* -COOH, -CHO, -OH, -CO) that make the surfaces polar and hydrophilic [15, 33, 34]. These functional surface groups can be used to enhance the chemical interaction of the surfaces of CNFs, leading to anchoring of catalyst precursor complexes during the deposition of an active phase [35]. The CNF layers were oxidized with concentrated nitric acid (65 wt. % HNO_3) at 90 °C for different time intervals (*e.g.* 30, 60, 90 and 120 minutes).

A qualitative analysis of the functional groups formed on CNF surface was performed by following the PZC of CNF layers. PZC was estimated by measuring initial pH (pH_0) and final pH (pH_1 ; after introducing CNF into solution) of the solution. The PZC value is identified as the pH at which a surface has no net charge, *i.e.* when ΔpH ($= \text{pH}_1 - \text{pH}_0$) is zero. *Figure 4.2* shows that the PZC value for pristine CNFs is 6.22, and 4.87 for oxidized CNFs 4.87 after a nitric acid treatment of 90 minutes.

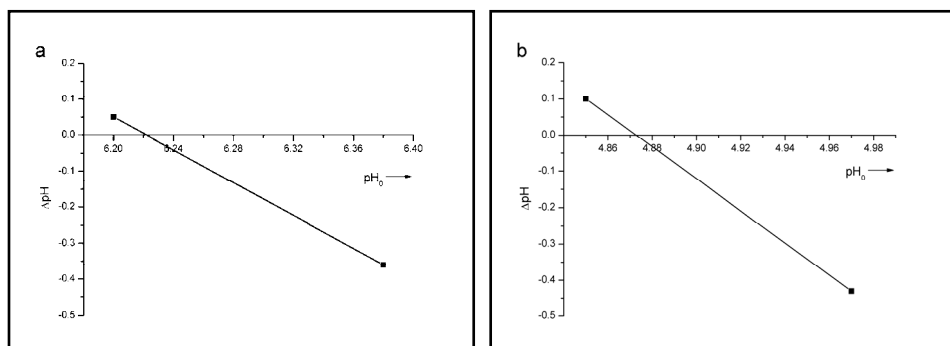


Figure 4.2: PZC measurements of (a) pristine CNF layers, and (b) oxidized CNFs (90 min. in 65 wt.% HNO_3 at 90 °C).

XPS was also used to analyze the surface chemistry of oxidized CNFs. *Figure 4.3* shows the fitting curves of the deconvoluted O1s peak of oxidized CNF layers, which are assigned to: (i) to carbonyl oxygen in esters and anhydrides (530.96–530.98 eV), (ii) to oxygen in hydroxyl or ethers (532.26–532.28 eV), (iii) to oxygen in carboxyl groups (533.66–533.68 eV), and (iv) to adsorbed water (534.96–534.98 eV) [36]. In *table 4.1*, the results of curve fitting are given for two different oxidation times for different nitric acid concentrations. Acidic groups such as carboxyl and hydroxyl groups are the dominant oxygen-containing groups on the surfaces of oxidized CNFs, which is the reason for the reduction of PZC value after oxidation treatment.

Oxidation with nitric acid has an additional advantage. Nickel is a commonly used catalyst for a variety of reactions, such as hydrogenation and steam reforming. Since the Ru-functionalized CNFs in this work are intended to be used for the catalytic reduction of bromate, nickel remaining from the CNF-growth process might influence this reaction. However, nitric acid can leach out nickel, such that this material does not interfere with subsequent catalytic experiments: thus HNO_3 treatment ‘purifies’ the CNFs.

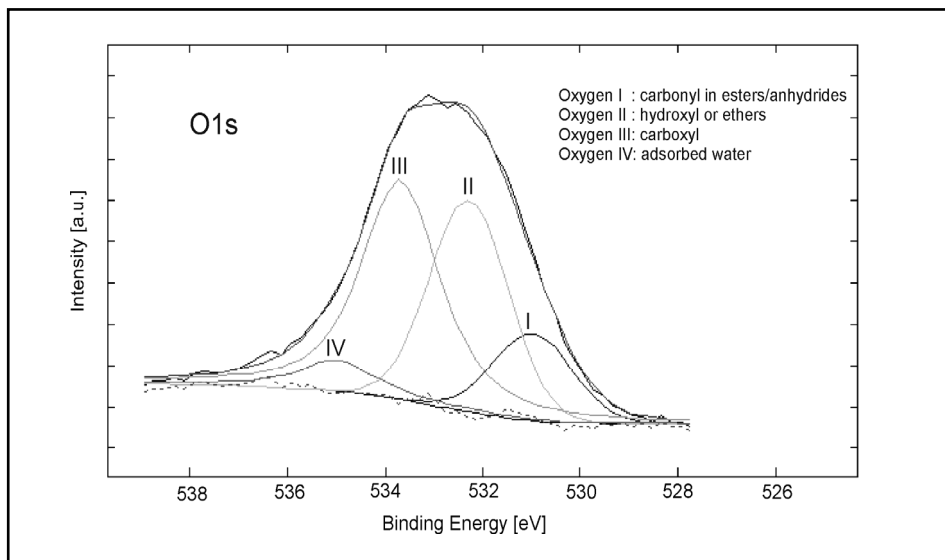


Figure 4.3: XPS spectrum of oxidized CNFs (90 min in 65 wt.% HNO_3 at 90 °C): deconvoluted O1s peak

XRF spectrometry was used to determine the nickel content in pristine and oxidized CNF layers. Figure 4.4 shows the amount of nickel present in CNF layers after various oxidation times. After 30 minutes the nickel content is decreased significantly (~75 % of the initial amount is dissolved). Longer treatment times further reduce the nickel content, but after 90 minutes the amount of nickel remains at a fixed value and the O/C atomic ratio reaches a stable value of ~0.04. Moreover, there is only a marginal difference between the use of concentrated (65 wt.%) and diluted (10 wt.%) nitric acid.

Table 4.1: Binding energies (B. E.) of various oxygen participating into the O1s peak of oxidized CNF layers (90 min in 65 wt.% and 10 wt.% HNO_3 at 90 °C), and corresponding O/C ratios.

Nitric acid Concentration	Oxidation time	O1s			O/C atom ratio
		B. E. (eV)	O-type	% Area	
65 wt.%	90 minutes	530.98	Carbonyl	13.83	0.0415
		532.28	Hydroxyl or ethers	33.31	
		533.68	Carboxyl	45.94	
		534.98	Adsorbed H_2O	6.92	
	120 minutes	530.96	Carbonyl	13.59	0.0411
		532.26	Hydroxyl or ethers	33.49	
		533.66	Carboxyl	43.31	
		534.96	Adsorbed H_2O	9.61	
10 wt.%	90 minutes	530.98	Carbonyl	13.79	0.0386
		532.28	Hydroxyl or ethers	33.19	
		533.68	Carboxyl	45.62	
		534.98	Adsorbed H_2O	7.40	
	120 minutes	530.96	Carbonyl	13.48	0.0392
		532.26	Hydroxyl or ethers	33.37	
		533.66	Carboxyl	43.20	
		534.96	Adsorbed H_2O	10.95	

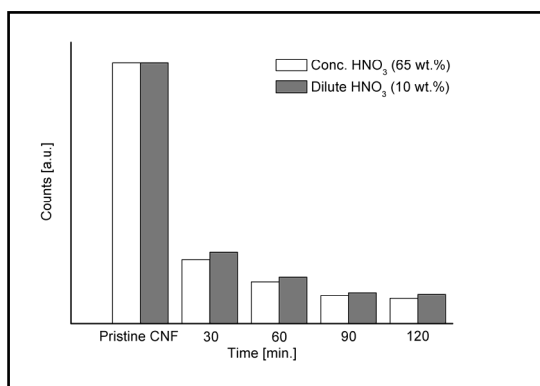


Figure 4.4: Influence of duration of oxidation treatment on the amount of nickel present in CNF layers

TEM analysis of samples after 90 min oxidation (*Fig. 4.5*) revealed the presence of encapsulated nickel particles (solid circle) at CNF-tips and along its length, as well as a location where a nickel particle apparently was dissolved (dotted circle). Since fully-encapsulated nickel particles cannot be dissolved by the acid, XRF will give a stable non-zero signal after long oxidation times. Encapsulated Ni is also not expected to interfere in catalytic measurements. Pristine and oxidized CNF layers were also subjected to XRD, to analyze the effect of the oxidation treatment on the graphitic structure. From diffraction patterns it followed that the 2θ -peak at 44.36° (attributed to Ni) of pristine Ni loaded CNFs undergoes considerable changes in terms of intensity: after oxidation it was difficult to identify this peak. In contrast, the sharpness and intensity of the 2θ -peak of graphite (26.42°) did not alter after oxidation.

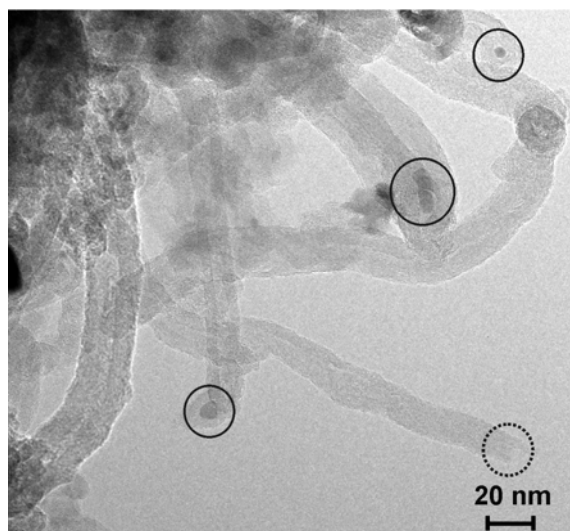


Figure 4.5: TEM image of oxidized CNFs (90 min in 65 wt.% HNO_3 at 90°C).

SEM-images (*Fig. 4.6a-c*) indicate only a subtle change in the morphology of CNF layers after treatment with concentrated HNO_3 . Thinner carbon nanofibers seem to be affected by concentrated nitric acid (*Fig. 4.6b*): their structure is destroyed, thereby slightly altering the morphological appearance. Since this only happens with very small diameter fibers, there is no measurable weight loss found of samples prior and post to the oxidation treatment. In their review on the use of CNFs and CNTs for catalytic applications, Serp *et al.* [15] highlight the role of various oxidation treatments for the functionalization of these materials. Factors that can affect the degree of

functionalization and morphology of CNFs during liquid phase oxidation are discussed, of which the most important are: (i) the oxidizing agent, (ii) the temperature of the agent, and (iii) the treatment time. The use of diluted HNO_3 (10 wt.%) revealed that these CNF layers indeed show a better preservation of the morphological structure of pristine CNFs: Fig. 4.6c shows that the structural features remain unaffected during oxidation with 10 wt.% nitric acid (in contrast to the use of concentrated HNO_3). The BET surface area was estimated around $136 \text{ m}^2/\text{g}$ after oxidation with 10 wt.% nitric acid, which is similar to the surface area value of $132 \text{ m}^2/\text{g}$ for pristine CNFs. This is in contrast to the relatively lower value of $115 \text{ m}^2/\text{g}$ for CNFs treated with 65 wt.% nitric acid and caused by the loss of thin CNFs.

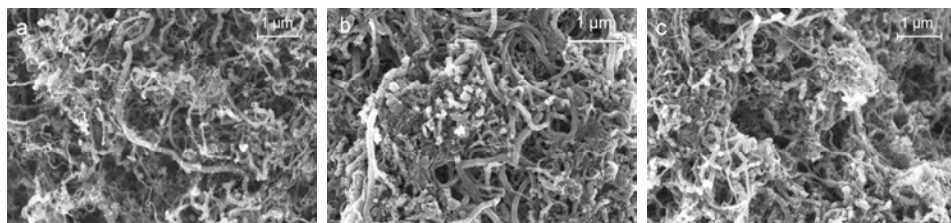


Figure 4.6: High resolution SEM images of (a) pristine CNF layer, (b) oxidized CNF layer in concentrated HNO_3 (90 min in 65 wt.% HNO_3 at 90°C), (c) oxidized CNF layers in diluted HNO_3 (90 min in 10 wt.% HNO_3 at 90°C)

The nickel removal rate is not influenced by the nitric acid concentration (see Fig. 4.4). Raman spectroscopy showed that the degree of crystallinity of oxidized CNFs did not depend on the nitric acid concentration: the ratio I_D/I_G was 1.34 (I_D and I_G are the intensities of the D-band and G-band, respectively), which is consistent with a previously reported value of 1.33 [25]. The observed change in morphology in case of oxidation with concentrated nitric acid without affecting the crystallinity of CNFs is in agreement with works reported by Ros *et al.* and Toebe *et al.* [35, 37]. In their works on surface oxidation of CNFs using HNO_3 or H_2SO_4 , both indicate that the morphology of CNFs can alter due to liquid phase oxidation treatments without sacrificing the graphitic nature of CNFs. From XPS analysis (Table 4.1), it was found that neither the O/C ratio on the surfaces of CNFs was influenced by the nitric acid concentration. This observation is in line with the work of Serp *et al.* [15], who proved that $80\text{--}90^\circ\text{C}$ is adequate to generate oxygen-containing groups on fibers, and that the acid concentration is not a critical factor [38–40].

From PZC-measurements, XPS, XRF, TEM, SEM and XRD the following issues can be concluded regarding the oxidative treatment of CNFs, resulting in hydrophilic CNFs. There is a loss in nickel content after oxidation due to dissolution of non-encapsulated particles at fiber tips, but fully-encapsulated particles in the fiber bodies and/or tips remain unaffected. Whereas concentrated nitric acid influences the morphology of the CNF layers, the use diluted nitric acid (10 wt.%) avoids this because in the latter solution small diameter fibers are not destroyed. Nevertheless, the crystallinity of oxidized CNFs is not influenced by the acid concentration, neither the surface chemistry of the fibers. The dominant oxygen-containing groups on the fibers are carboxyl and hydroxyl groups. Hence the layer of entangled CNFs synthesized on flat substrates can be functionalized by oxidation treatment with nitric acid without affecting the anchoring of the layers on the surface and preserving the mechanical stability. Based on these findings the CNF layers oxidized using 10 wt.% HNO_3 will be utilized further.

4.3.3 Deposition of ruthenium on oxidized CNFs *via* HDP

Supported noble metal catalysts are often prepared *via* techniques such as impregnation or ion-exchange in the aqueous phase. Impregnation is the most commonly used method to deposit metals on CNFs, such as Pt or Pd [15]. However, the desired active phase distribution, loading and/or dispersion can not always be achieved with this technique [41]. Homogeneous deposition precipitation helps to overcome the above problems and has been employed effectively for synthesizing CNF-supported metal catalysts [42]. In this work, ruthenium incorporation by HDP using an aqueous solution of ruthenium nitrosyl nitrate is performed.

Figure 4.7 shows the variation in pH during the HDP process. After introducing the samples in a Ru precursor solution (pH \sim 3.2), during deposition precipitation the presence of an oxidized CNF layer clearly influences the precipitation process: the slope of the curve of the precipitation on an oxidized CNF layer is smaller than the slope of the curve of precipitation without a CNF layer. This can be explained by the neutralization of acidic groups on the surfaces of CNFs by OH^- ions produced from urea, see *Eq. (4.1)*; this effect is more pronounced in the initial stages (*i.e.* till the pH reaches \sim 5). The amount of deposited Ru reaches its maximum when the pH approaches 7.0. Around 2.2-2.4 wt.% of Ru could be loaded with this HDP procedure.

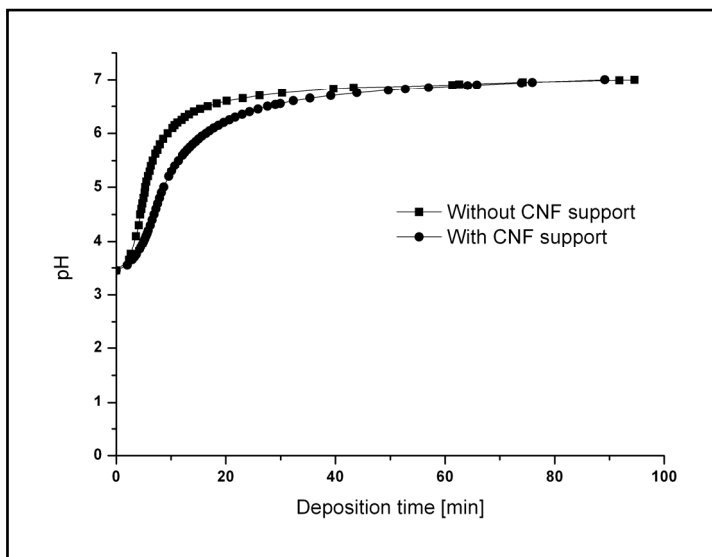
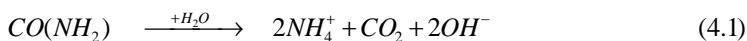
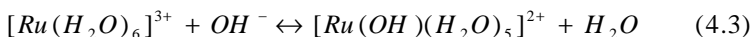
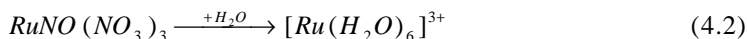


Figure 4.7: The pH as function of the deposition time in the presence and absence of an oxidized CNF layer

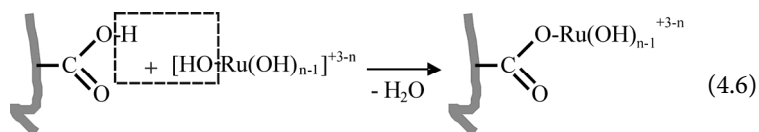
For HDP a metal precursor and urea are dissolved in water and homogeneously distributed. Upon heating to 70-90 °C, urea decomposes to produce OH^- locally *Eq. (4.1)*.



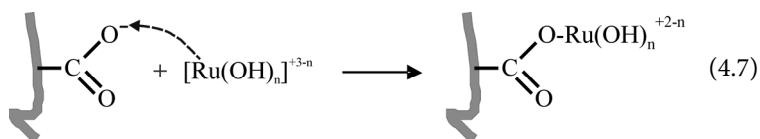
OH^- hydrolyzes metal salts and precipitates as metal hydroxide species. It has been shown earlier that of all known Ru precursors $\text{RuNO}(\text{NO}_3)_3 \cdot n\text{H}_2\text{O}$ yields the smallest particle size on CNF layers *via* HDP [42]. The hydrolysis of the metal cation and the reaction with the precipitation agent are *Eq. (4.2) – (4.5)*:



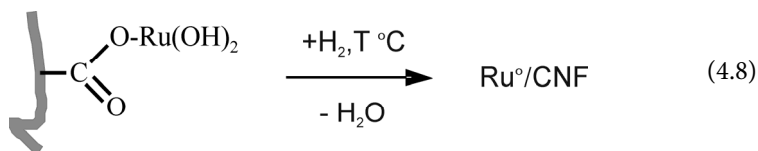
Interactions between $[\text{Ru}(\text{OH})_n]^{n-1}$ precursor species and oxidized CNFs are schematically shown below. As the pH of solution progressively change from ~ 3.2 to 7.0 , variation of reactions pathways can occur during the HDP. If the pH is below the PZC of the oxidized CNFs (*i.e.* $\text{pH} < 4.87$) then situation depicted in Eq. (4.6) occurs. For example, in the case of a carboxylic acid group, deprotonation occurs and the Ru precursor is anchored to the carboxylic acid.



When the pH is above the PZC of oxidized CNFs, the reaction is as in Eq. (4.7):



Further reactions that take place during drying and/or reduction are given in Eq. (4.8):



After drying the samples at 110°C and reduction in hydrogen at 500°C (reasonably higher temperature than reported in literature for obtaining reduced Ru metal [42]), Ru nanoparticles were well dispersed over the surface of entangled CNFs. However, Ru in fresh Ru/CNF catalyst still consists of oxidized Ru species, *i.e.* RuO_2 . Even though the catalyst was prereduced at 500°C , exposure to air at ambient oxidizes Ru, in agreement with literature [43]. This has also been confirmed using XPS analysis (not shown here). TEM was used to determine the average size of Ru particles deposited on CNF (Fig. 4.8a): a narrow particle size distribution was found (see the histogram depicting particle size distribution in Fig. 4.8a alongside TEM image), estimating the diameter of about 150 particles in total. It was observed that around $\sim 87\%$ of the particles had a diameter in the range $1.0 - 1.5\text{ nm}$ ($\sim 10\%$ $1.5 - 2.0\text{ nm}$, $\sim 3\%$ $> 2.0\text{ nm}$). When samples with Ru deposited CNF layers were exposed to high(er) reduction temperatures, *i.e.* 800°C , sintering of Ru nanoparticles occurred, which resulted in the

formation of larger particles (diameter of ~ 8 nm) throughout the thickness of the CNF layer (Fig. 4.8b and 4.8c). The presence of Ru particles near the interface with the substrate indeed evidences that the oxidized CNF layer exhibits highly porous structure: the aqueous precursor solution penetrated during HDP experiment into the deepest areas of the CNF layer, resulting in a good distribution of Ru nanoparticles throughout the thickness of the CNF layer.

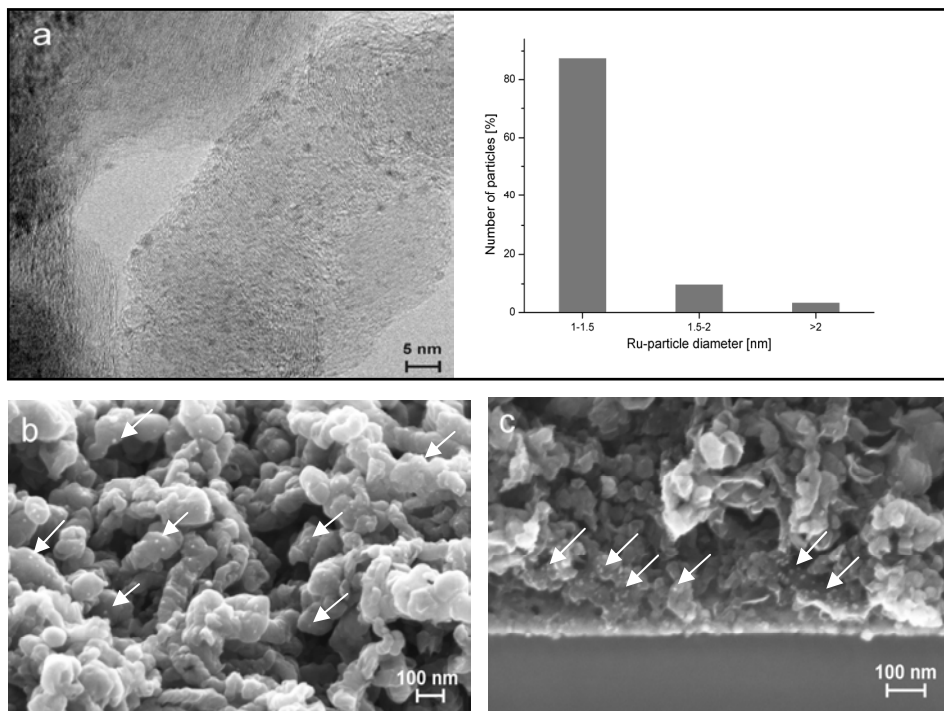


Figure 4.8: (a) TEM image of oxidized CNFs alongside a particle size distribution histogram after Ru deposition using HDP: well distributed nanoparticles are visible on the fibers; cross-sectional SEM images of (b) top area and (c) bottom area of a CNF layer: arrows indicate Ru nanoparticles after sintering at 800 °C.

Other alternatives for deposition of metal particles in microsystems are chemical and physical vapor deposition methods [44, 45].

4.3.4 Deposition of ruthenium on oxidized CNFs *via* PLD

In order to deposit Ru *via* the PLD method, the same oxidized CNFs were used, since this oxidation treatment is essential for removing Ni. After deposition a continuous thin film mask of Ru metal with a thickness of *ca.* 2.7 nm was observed while probing with TEM/EDX (see EDX spectrum shown in *Fig. 4.9a*).

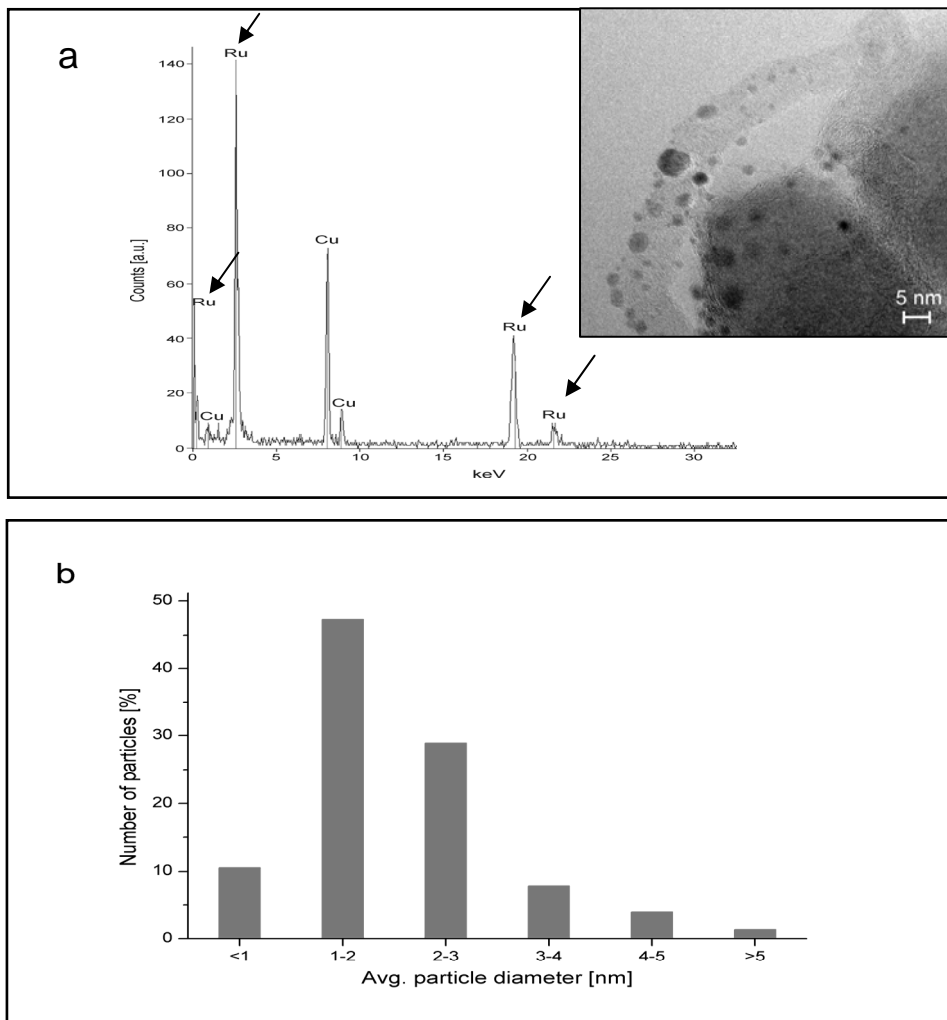


Figure 4.9: (a) TEM-EDX spectrum indicating presence of PLD deposited Ru thin film on CNFs; TEM image of CNFs showing well-distributed Ru nanoparticles after reduction of Ru thin film, (b) Ru particle size distribution after reduction of PLD layer

With XRF spectrometry a Ru loading of 2.3 wt.% was estimated. Hydrogen reduction at 500 °C (90 min) caused fragmentation of the film mask into nanoparticles (*Fig. 4.9a*). The size distribution (*Fig. 4.9b*) shows that the particle diameter is 1 to 5 nm. Compared to HDP, PLD method yields a less sharp particle size distribution and the average particle size is larger. However, it has to be mentioned that a major advantage of PLD is that it is possible with this method to perform multi-component deposition, maintaining required stoichiometry to obtain bi-metallic/oxidic catalytic materials [46, 47].

4.3.5 CNF supported Ru catalyst inside silicon-based microreactor channels

CNF layers were synthesized inside microchannels using the same experimental conditions as for flat substrates. SEM image (*Fig. 4.10a*) reveals similar morphology of the CNF layer for both microchannel and flat substrates. The thickness of CNF layer was in the same range as that of flat substrates (*i.e.* ~2-3 μm). In the case of microchannels the spacing between the cylinders is not completely filled (despite the uniform CNF-coverage of the channel bottom and cylinder sidewalls). In order to use the complete volume of the microchannel efficiently, the thickness of the CNF layer has to be enlarged. Complete filling of the spacings between cylinders in microchannels can be obtained by two ways, (1) reducing the cylinder spacing, and (2) adding hydrogen to the reactant gas during CNF growth. The latter results in thicker CNF layers while preserving the CNF morphology and fluid accessibility [26]. Accordingly, the spacing between the cylinders was reduced to 20 μm , and 25 vol.% hydrogen was added to ethylene. It is known that spacing between pillars down to 12 μm does not give rise to significant pressure drop issues for microchannels with 50 μm high pillars [48]. A growth time of 10 minutes resulted in a CNF layer of ~10 μm on each wall. *Figure 4.10b* and *c*, shows the results: with these settings the CNF layers cover the cylinder and filling completely the void space is obtained.

In order to functionalize CNF layers in the microchannels, the reactor chips were immersed in dilute nitric acid (10 wt.%) for 1.5 h (90 °C). The HDP method resulted in a good particle size distribution and a loading of 2.2 wt.%, which is in excellent agreement with results on flat samples (identical experimental settings were used). *Figure 4.10d* shows a high-resolution SEM image of a CNF with anchored Ru particles after reduction treatment: the particles are uniformly distributed on the fiber. Oxidized CNF layers in microchannels, also yielded similar Ru loading and particle size

distribution with PLD as obtained previously with flat substrates (*i.e.* *ca.* 2.3 wt.% and 1-5 nm, respectively).

Performance of such a microreactor, incorporating Ru on CNF layers and its advantages over a conventional supported ruthenium catalyst is presented in chapter 6. Catalytic reduction of bromate in aqueous solutions is studied and details discussed.

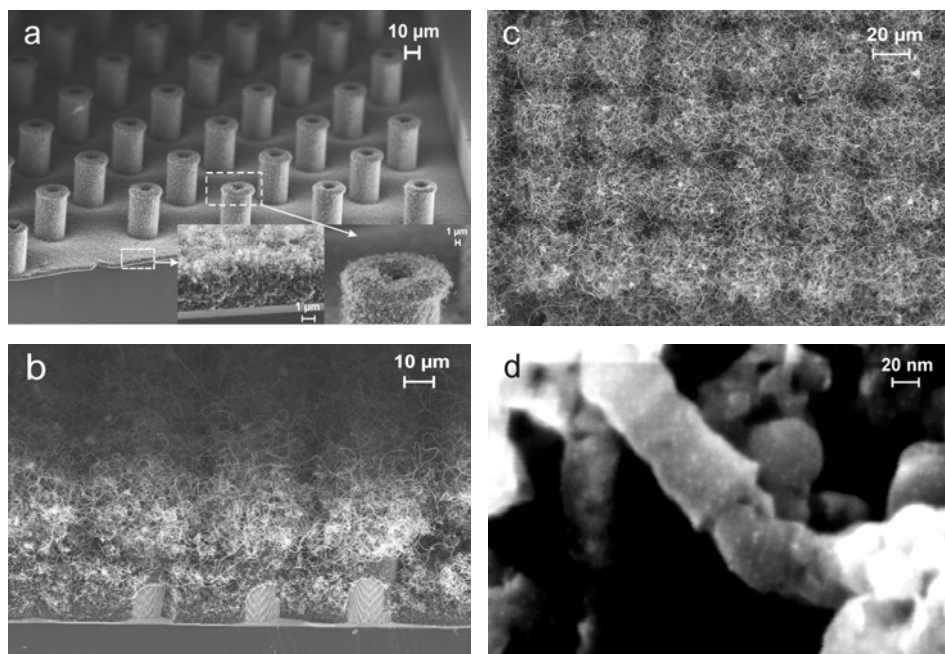


Figure 4.10: SEM images of oxidized CNF layer in microchannel with array of cylinders: (a) 50 μm spacing between cylinders and 1h C-TCVD at 635 $^{\circ}\text{C}$ with C_2H_4 , (b) 20 μm spacing between cylinders and 10 min C-TCVD at 635 $^{\circ}\text{C}$ with $\text{H}_2/\text{C}_2\text{H}_4$, (c) top-view of CNF layers uniformly covering the microchannel, (d) HR-SEM image of well distributed HDP deposited Ru nanoparticles on CNFs in microchannel (after reduction).

4.4 Conclusions

In this work of ruthenium catalytic nanoparticles on carbon nanofiber support layers are realized *via* homogeneous deposition precipitation and pulsed laser deposition. CNF layers are functionalized by oxidation with nitric acid to facilitate Ru deposition. Besides removal of exposed nickel (used for CNF-growth), acid treatment forms oxygen-containing groups on the surfaces of CNFs (mainly carboxyl and hydroxyl groups).

Ruthenium was anchored on oxidized CNF layers by means of HPD and PLD. Critical issues for a good dispersion of the particles and a sharp size distribution are the pH of the precursor solution (HDP) and the reduction treatment after deposition (PLD). Both optimized deposition methods resulted in a ruthenium loading of 2.3 ± 0.1 wt.% (HDP had a narrower particle size distribution). The presence of nanoparticles across the complete thickness of the CNF layers was found to be uniform when HDP was used to deposit Ru on CNF layers. Using the optimal CNF-growth settings such that the spacings between cylinders in a silicon-based microreactor channel were completely filled with an open, entangled jungle CNF layer, these CNF layers were successfully functionalized and well dispersed ruthenium clusters grown. A catalytic microreactor module containing Ru particles attached to carbon nanofibers which fill the entire reactor volume keeping the highly porous and/or open structure, is achieved.

Acknowledgements

This work was performed with the financial support from MicroNed program, under cluster-II of Smart Microchannel technology (SMACT) and work package II-G-2 and 3 (Smart Micro Reactors). The authors gratefully acknowledge Dr. M. Smithers for SEM and TEM analysis, J.A.M. Vrielink for XRF spectrometry, and B. Geerdink for technical support. Drs. Minh Duc Nguyen (Inorganic Materials Science group, University of Twente, Enschede, The Netherlands) is acknowledged for assisting in pulsed laser deposition experiments.

Appendix

Determination of Ru loading on CNF layers

X-ray fluorescence spectrometry (XRF) was used to determine the amount of Ru deposited on CNF layers. A systematic approach was utilized for this: firstly, Ru film was deposited on “fresh” Si substrate through a shadow-mask, which was clamped on top of the substrate to make the step-wise thin film deposition (with increasing number of laser pulses), secondly the thickness of Ru film was checked by using atomic force microscopy (AFM). The graph (*Fig. 4.11*) depicting the dependence of Ru-layer thickness on the number of pulses (or deposition time) indicated the linear dependence of Ru-layer thickness on the number of pulses. This implies that the deposition occurs consistently, resulting in a homogenous distribution of Ru over the whole area of sample.

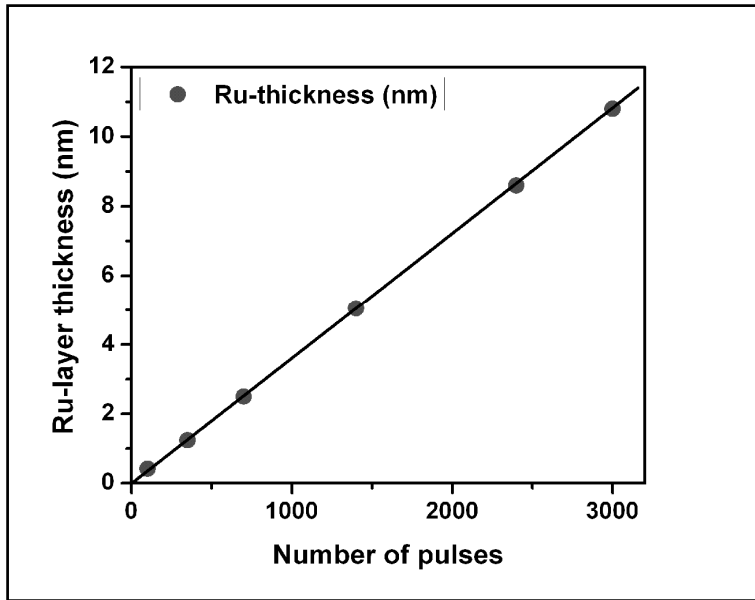


Figure 4.11: Thickness of Ru-layer versus number of deposition pulses

This deposition procedure assures the precise thickness of Ru deposited, which means the desired mass/loading of Ru can be accurately achieved which then can be calculated from the equation:

$$m_{Ru} = d \times A \times \delta \quad (4.9)$$

Where,

d = density of Ruthenium (*ca.* 12.45 g/cm³)

A = area of sample (*i.e.* 0.64 cm²/substrate)

δ = thickness of Ru-film (cm)

The Ru deposited silicon test samples were then analyzed with XRF. The intensity of Ru peak in XRF spectrum corresponds to a given amount of Ru. Also, the weight of Ru deposited on CNFs by PLD is known. Therefore, the values of intensity of Ru peaks obtained from XRF analysis of above samples were used to establish the correlation between the intensity and the weight of Ru deposited on sample (*Fig. 4.12*). This correlation then can be directly used to determine the amount of Ru deposited on CNFs not only by PLD based preparation but also by HDP based preparation procedure.

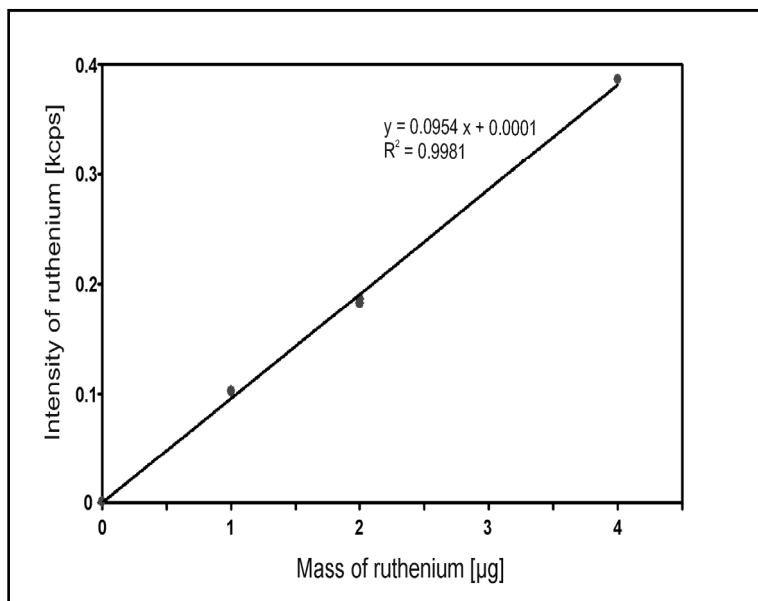


Figure 4.12: Graphical correlation between Ru loading deposited on CNF layers and intensity of counts of Ru determined by XRF analysis.

References

- [1] H. Lowe, W. Ehrfeld, *Electrochim. Acta* 44 (1999) 3679-3689.
- [2] K. Haas-Santo, M. Fichtner, K. Schubert, *Appl. Catal. A* 220 (2001) 79-92.
- [3] M.W. Losey, M.A. Schmidt, K.F. Jensen, *Ind. Eng. Chem. Res.* 40 (2001) 2555-2562.
- [4] K. Haas-Santo, O. Gorke, P. Pfeifer, K. Schubert, *Chimia* 56 (2002) 605-610.
- [5] V. Hessel, P. Angeli, A. Gavriilidis, H. Lowe, *Ind. Eng. Chem. Res.* 44 (2005) 9750-9769.
- [6] V. Meille, *Appl. Catal. A* 315 (2006) 1-17.
- [7] J. Kobayashi, Y. Mori, S. Kobayashi, *Chem.-Asian J.* 1 (2006) 22-35.
- [8] O. Muraza, E.V. Rebrov, M.H.J.M. de Croon, J.C. Schouten, *Microporous and Mesoporous Mater.* 124 (2009) 20-29.
- [9] S. Iijima, *Nature* 354 (1991) 56-58.
- [10] S.J. Tans, M.H. Devoret, H.J. Dai, A. Thess, R.E. Smalley, L.J. Geerligs, C. Dekker, *Nature* 386 (1997) 474-477.
- [11] M.M.J. Treacy, T.W. Ebbesen, J.M. Gibson, *Nature* 381 (1996) 678-680.

- [12] M. Bockrath, D.H. Cobden, P.L. McEuen, N.G. Chopra, A. Zettl, A. Thess, R.E. Smalley, *Science* 275 (1997) 1922-1925.
- [13] M.F. Yu, O. Lourie, M.J. Dyer, K. Moloni, T.F. Kelly, R.S. Ruoff, *Science* 287 (2000) 637-640.
- [14] C. Pham-Huu, N. Keller, L.J. Charbonniere, R. Ziessle, M.J. Ledoux, *Chem. Commun.* (2000) 1871-1872.
- [15] P. Serp, M. Corrias, P. Kalck, *Appl. Catal. A* 253 (2003) 337-358.
- [16] M.J. Ledoux, C. Pham-Huu, *Catal. Today* 102 (2005) 2-14.
- [17] M.L. Toebes, Y.H. Zhang, J. Hajek, T.A. Nijhuis, J.H. Bitter, A.J. van Dillen, D.Y. Murzin, D.C. Koningsberger, K.P. de Jong, *J. Catal.* 226 (2004) 215-225.
- [18] A.J. Plomp, H. Vuori, A.O.I. Krause, K.P. de Jong, J.H. Bitter, *Appl. Catal. A* 351 (2008) 9-15.
- [19] K.P. De Jong, J.W. Geus, *Catal. Rev. – Sci. Eng.* 42 (2000) 481-510.
- [20] L. Delzeit, B. Chen, A. Cassell, R. Stevens, C. Nguyen, M. Meyyappan, *Chem. Phys. Lett.* 348 (2001) 368-374.
- [21] Z.X. Yu, D. Chen, B. Totdal, T.J. Zhao, Y.C. Dai, W.K. Yuan, A. Holmen, *Appl. Catal. A* 279 (2005) 223-233.
- [22] J.K. Chinthaginjala, K. Seshan, L. Lefferts, *Ind. Eng. Chem. Res.* 46 (2007) 3968-3978.
- [23] P.W.A.M. Wenmakers, J. van der Schaaf, B.F.M. Kuster, J.C. Schouten, *J. Mater. Chem.* 18 (2008) 2426-2436.
- [24] D.B. Thakur, R.M. Tiggelaar, J.G.E. Gardeniers, K. Seshan, L. Lefferts, *Adv. Sci. Technol.* 54 (2008) 231-236.
- [25] D.B. Thakur, R.M. Tiggelaar, J.G.E. Gardeniers, L. Lefferts, K. Seshan, *Surf. Coat. Technol.* 203 (2009) 3435-3441.
- [26] D.B. Thakur, R.M. Tiggelaar, J.G.E. Gardeniers, L. Lefferts, K. Seshan, *Chem. Eng. J.* (2010) 899-908.
- [27] L. Delzeit, C.V. Nguyen, B. Chen, R. Stevens, A. Cassell, J. Han, M. Meyyappan, *J. Phys. Chem. B* 106 (2002) 5629-5635.
- [28] R.M. Tiggelaar, V. Verdool, H. Eghbali, G. Desmet, J.G.E. Gardeniers, *Lab Chip* 9 (2009) 456-463.
- [29] M. Mullet, P. Fievet, A. Szymczyk, A. Foissy, J.C. Reggiani, J. Pagetti, *Desalination* 121 (1999) 41-48.
- [30] A.V. Melechko, V.I. Merkulov, T.E. McKnight, M.A. Guillorn, K.L. Klein, D.H. Lowndes, M.L. Simpson, *J. Appl. Phys.* 97 (2005) - 041301.

- [31] K.B.K. Teo, C. Singh, M. Chhowalla, W.I. Milne (Eds.), *Catalytic Synthesis of Carbon Nanotubes and Nanofibers*, American Scientific Publishers, 2004.
- [32] J.K. Chinthaginjala, D.B. Thakur, K. Seshan, L. Lefferts, Carbon 46 (2008) 1638-1647.
- [33] K.L. Klein, A.V. Melechko, T.E. McKnight, S.T. Retterer, P.D. Rack, J.D. Fowlkes, D.C. Joy, M.L. Simpson, J. Appl. Phys. 103 (2008) - 061301.
- [34] A.J. Plomp, D.S. Su, K.P. de Jong, J.H. Bitter, J. Phys. Chem. C 113 (2009) 9865-9869.
- [35] T.G. Ros, A.J. van Dillen, J.W. Geus, D.C. Koningsberger, Chem. – Eur. J. 8 (2002) 1151-1162.
- [36] D. M. Nevskaia, R. M. Martin-Aranda, Catal. Lett. 87 (2003) 143-147.
- [37] M.L. Toebe, E.M.P. van Heeswijk, J.H. Bitter, A.J. van Dillen, K.P. de Jong, Carbon 42 (2004) 307-315.
- [38] C. Park, R.T.K. Baker, J. Phys. Chem. B 102 (1998) 5168-5177.
- [39] C. Park, R.T.K. Baker, J. Phys. Chem. B 103 (1999) 2453-2459.
- [40] C.H. Liang, Z.L. Li, J.S. Qiu, C. Li, J. Catal. 211 (2002) 278-282.
- [41] R.A. van Santen, P.W.N.M. van Leeuwen, J.A. Moulijn, B.A. Averill, *Catalysis: An Integrated Approach*, Second, Revised and Enlarged Edition, Elsevier Amsterdam, 1999.
- [42] M.L. Toebe, M.K. van der Lee, L.M. Tang, M.H.H. in 't Veld, J.H. Bitter, A.J. van Dillen, K.P. de Jong, J. Phys. Chem. B 108 (2004) 11611-11619.
- [43] H.G. Manyar, D. Weber, H. Daly, J.M. Thompson, D.W. Rooney, L.F. Gladden, E.H. Stitt, J.J. Delgado, S. Bernal, C. Hardacre, J. Catal. 265 (2009) 80-88.
- [44] R. Moene, M. Makkee, J.A. Moulijn, Chem. Eng. J. Biochem. Eng. J. 53 (1993) 13-24.
- [45] P. Serp, P. Kalck, R. Feurer, Chem. Rev. 102 (2002) 3085-3128.
- [46] G. Koster, *Artificially layered oxides by pulsed laser deposition*, PhD Thesis, University of Twente, Enschede, The Netherlands, 1999.
- [47] G. Rijnders, *The initial growth of complex oxides: study and manipulation*, PhD Thesis, University of Twente, Enschede, The Netherlands, 2001.
- [48] S.R.A. de Loos, J. van der Schaaf, R.M. Tiggelaar, T.A. Nijhuis, M.H.J.M. de Croon, J.C. Schouten, Microfluid. Nanofluid. 9 (2010) 131-144.

Chapter 5

Palladium Catalyst on Carbon Nanofiber Support Layers for Si-based Structured Microreactors: Catalytic Reduction of Nitrite Contaminants in Aqueous Phase

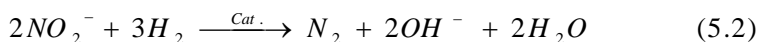
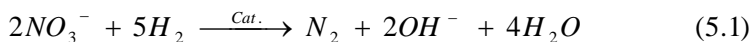
Abstract

Carbon nanofiber layers containing palladium particles were synthesized inside the channels of a silicon based microreactor. This module was used to study the kinetics of hydrogenation of nitrite ions in aqueous phase. Nitrite hydrogenation is known to be kinetically facile reaction, thus chosen to evaluate the performance and efficiency of the Pd containing CNF layers inside the microreactor module. Pd catalyst was prepared via dry impregnation using palladium acetylacetonate precursor solution in toluene. Relatively large Pd particles uniformly distributed across the CNF layers were obtained. The mass transfer properties, both external and internal, were probed. In the case of CNF layer thickness below $\sim 13\ \mu\text{m}$, hydrogenation was under kinetic control indicating absence of mass transfer limitations. Thus optimized CNF layers then can be applied for performing relevant aqueous phase reactions.

5.1 Introduction

There is continuous and strict demand to achieve high water purity levels for both industrial and domestic use [1]. The sources of these contaminants in water originate from excessive fertilization; industrial effluents [2]. Even though nitrate ions (NO_3^-) do not exhibit toxicity, their further transformation to nitrite (NO_2^-) by reduction process, however, can be detrimental for human health. It is known to be a cause of blue baby syndrome in addition to hypertension, and is a precursor for the carcinogenic nitroso amine [3-5]. European Commission directives have restricted the nitrate and nitrite concentration levels in drinking water to 50 mg/L and 0.5 mg/L, respectively [5]. Various physicochemical techniques such as ion exchange, reverse osmosis, and electrodialysis are available for removal of nitrate ions contamination from water. However, they only accumulate and are not able to convert these ions into less harmful products/materials. The biological process, on the other hand, is slow and complicated [5].

It is known from literature that most of the drawbacks of above mentioned conventional methods can be overcome *via* application of catalytic de-nitrification of nitrates and nitrites from aqueous solution using hydrogenation over noble-metal solid catalysts [6]. Recent work in our group on catalytic hydrogenation of nitrites (an intermediate in nitrate hydrogenation) to nitrogen by using nickel foam based thin layer Pd/CNF catalyst has shown promising results in terms of catalytic performance compared to the conventional catalyst, inside fixed bed reactor [7]. It is understood from literature that, nitrite reduction to nitrogen, *Eq. (5.2)*, is extremely fast and hence can easily induce internal concentration gradients due to mass transfer limitations [8-11].



Thus it can be ideal reaction system for testing the diffusion limitations along the CNF layers and hence suitability of them as catalyst support when synthesized inside microreactor channels. Thus tested CNF layers with optimized mass transport properties and exhibiting intrinsic catalytic activity can then be applied for heterogeneously carried out liquid phase reactions inside microreactors.

5.2 Experimental

5.2.1 Fabrication of microchannels with arrays of pillars

Microchannels were prepared from standard silicon substrates (<100>-oriented, p-type, resistivity 5-10 Ωcm , 100 mm diameter, thickness 525 μm , single side polished; Okmetic, Finland). Channels of 30 mm \times 1 mm contained ordered arrays of pillars. Prior to processing, the silicon substrates were cleaned by immersion in fuming 100% nitric acid (10 min) and boiling 69% nitric acid (15 min), followed by quick dump rinsing in de-mineralized water and dry spinning. A standard UV-lithography was used to define the pattern in 1.7 μm thick photoresist, which was postbaked for 30 min at 120 $^{\circ}\text{C}$ (in air) after development. The photoresist acted as a masklayer during 'deep reactive ion etching' (DRIE; Adixen AMS 100SE) of silicon with a Bosch process, *i.e.* a cyclic process which uses sulfur hexafluoride for etching of silicon and octa-fluorocyclobutane for sidewall passivation [12]. An etchtime of *ca.* 13.5 min was required for 40-45 μm high pillars (diameter 20 μm , pillar spacing 20 μm). Post to etching the mask was stripped with an oxygen plasma and immersion in 100% nitric acid, followed by rinsing and drying. Fluorocarbons resulting from the DRIE process were removed by a wet oxidization step (30 min, 800 $^{\circ}\text{C}$), followed by immersion in 1% hydrofluoric acid (1 min), rinsing in DI-water and drying. A second wet oxidation step (45 min, 1000 $^{\circ}\text{C}$) was used to deposit a \sim 250 nm thick SiO_2 layer on the etched microchannel.

Thin films of nickel/tantalum (25nm/10nm) were deposited on the oxidized substrates with etched microchannels using home-built stainless-steel shadow mask by electron-beam evaporation (Balzers BAK600 system). The purity of the Ni target material was 99.99%, and >99.95% for Ta. Evaporation rates (at pressures below 10^{-7} mbar) were in the range 1-5 $\text{\AA}/\text{s}$ for Ta and 10-15 $\text{\AA}/\text{s}$ for Ni. The thicknesses of evaporated films were controlled using an in situ thickness monitor [13]. Finally, the substrates were diced into samples of 35 mm \times 5 mm (microchannel samples) (Disco DAD-321 dicing machine).

5.2.2 CNF layer synthesis

Prior to CNF synthesis the samples were cleaned ultrasonically in acetone (5 min, Branson 200 ultrasonic cleaner) to remove organic contaminants, followed by washing with flowing deionized water (25 $^{\circ}\text{C}$) and dried with pressurized technical air. Subsequently, the samples were reduced in a mixture of 20 vol.% H_2 in N_2 (99.999%, INDUGAS) with total flow rate of 50 ml/min, while increasing the temperature to 650

°C (ramp up 5°C/min) and maintained at 650 °C for 1 h. This pretreatment is essential to produce Ni nanoparticles which act as nucleation sites for CNF growth. After reduction the samples were cooled in N₂ from 650 to 635 °C (5°C/min), and exposed to a gas mixture of 25 vol.% C₂H₄ and 25 vol.% H₂ in N₂ (99.95%, PRAXAIR; total flow rate 100 ml/min) followed by cooling down to room temperature in N₂. It was shown in *chapter 3*, that the thicknesses of CNF layers on substrates can be manipulated by varying, (i) feed composition, such as addition of hydrogen to reactant mixture, and (ii) growth time. The knowledge obtained from this exercise was applied to vary the thickness of the CNF layers in present study to investigate their mass transfer properties when synthesized inside microreactor channels. *Table 5.1* shows the properties of the materials used. The amount of carbon deposited on each sample was determined by measuring the increase in weight.

5.2.3 Preparation of Pd/CNF catalyst layers inside microreactor chips

Palladium deposition on oxidized CNF layers (*i.e.* with 10 wt.% HNO₃, as described in *chapter 4*) was performed *via* incipient phase impregnation using palladium acetylacetonate dissolved in toluene. The appropriate amount of Pd was deposited by injecting precursor solution *via* microsyringe from a 0.5 mL stock solution. Toluene was completely evaporated by placing the microreactor chips in vacuum oven at 50°C for 3 hrs, leaving behind the Pd precursor on CNF layers. The CNF supported Pd precursor was further calcined for 1 hour at 250°C (gas Flow: 100 mL/min of tech. air) with ramp of 5°C /min. Afterwards reduction was carried out at the same temperature for 2 hours under hydrogen atmosphere using 20 % H₂ in N₂ at total flow rate of 100 mL/min. The Pd/CNF microreactors were then cooled down to room temperature in nitrogen at a ramp of 10 °C /min.

5.2.4 Fluidic set-up and procedure

Catalytic hydrogenation of nitrite was performed in microreactor chips, containing Pd/CNF layer, and fixed in a homemade Teflon (PTFE) holder provided with inlet and outlet fluid flow connections (*Figure 5.1 a-d*). The module was placed in an oven (Binder GmbH) and the reaction temperature was maintained accurately at 25°C (± 0.5 °C). The Nitrite concentration in the aqueous reactant solution was always maintained at 40 mg/L (1087 µmol/L). The aqueous solution was pre-saturated with H₂ (Flow Rate: 100mL/min; 1bar).

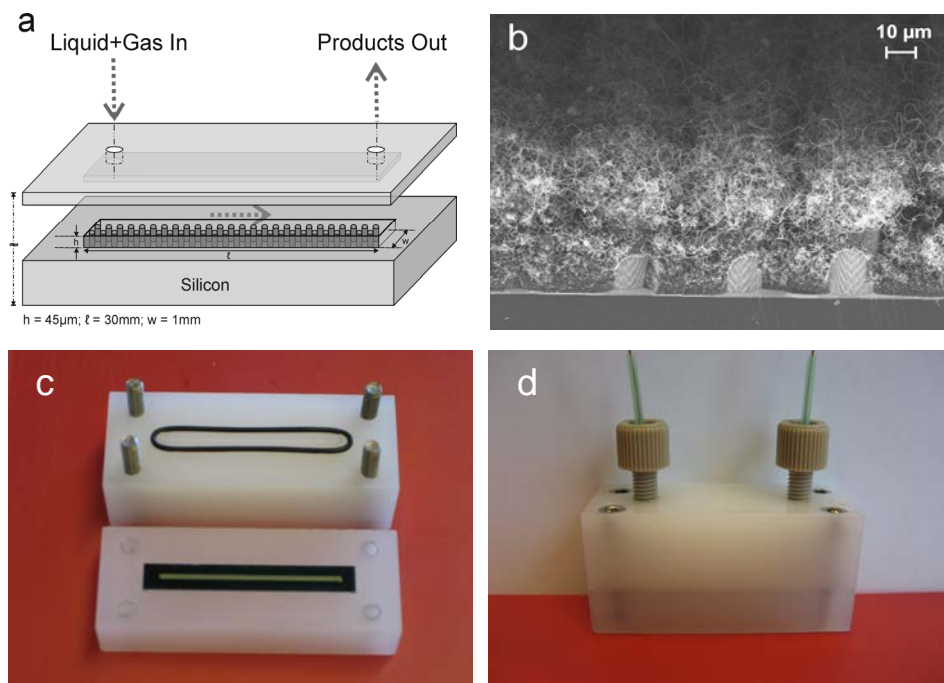


Figure 5.1: (a) Schematic representation of silicon-based microreactor with an array of micromachined cylindrical pillars, (b) Cross-sectional view of pillard microchannel with CNF layers uniformly covering the microchannel ($20\mu\text{m}$ spacing between pillards and 10 min C-TCVD at 635°C with $\text{H}_2/\text{C}_2\text{H}_4$), (c) microreactor channel positioned inside a Teflon (PTFE) holder provided with fluid flow connections, (d) the assembled microreactor holder with a channel with a Pd/CNF catalyst layer that is ready for use for the aqueous nitrite reduction reaction.

Aqueous nitrite solution saturated with hydrogen was pumped through the microreactor module with the HPLC pump (Dionex, Ultimate 3000) via flexible fused silica capillary tubing (Polymicro Technologies; outer diameter $360\mu\text{m}$, inner diameter $250\mu\text{m}$). the pressure drop measured across the module was less than 0.4 bar. The reactor bed volume was varied by connecting two identical reactor module in series (0.00165 cm^3 each). The linear velocity was estimated equal to 90.9 cm/min for a single module and 181.8 cm/min for two module in series at the flow rate of $50\mu\text{L/min}$ and $100\mu\text{L/min}$, respectively, maintaining the space velocity at 0.22 min^{-1} . The total amount of Pd catalyst used was varied between 0.08 to $0.28\mu\text{mol}$ when varying Pd loading from

3 to 10 wt.%. Nitrite and ammonium concentrations in the reactants and/or products were measured with Ion Chromatography (IC) (DIONEX, ICS 1000) system. Before starting the reaction measurements, the initial concentration was measured by sending the Nitrite solution directly to the IC system.

5.2.5 Characterization

X-ray fluorescence spectrometry (XRF) [Philips PW 1480] was used to determine the Pd loading on CNF layers. The Pd particle size distribution was determined using transmission electron microscopy (TEM) [Philips CM300ST-FEG quipped with Gatan Ultrascan 1000 CCD camera]. The average particle size estimated from TEM was based on the analysis *ca.* 20 images, estimating the diameter of about 150 particles in total, and this average size was used to calculate dispersion values assuming spherical shapes using the formula described by Scholten *et al.* [14],

$$D = 10^{21} \cdot \frac{6 \cdot M \cdot \rho_{site}}{d \cdot \rho_{metal} \cdot N} \quad (5.3)$$

where, D is dispersion ($Pd_{surface}/Pd_{total}$), M is the atomic mass (106.42 g/mol for Pd), ρ_{site} is the palladium surface site density (10.2 Pd atoms/nm²), d is particle size (nm), ρ_{metal} is the metal density (12.02 g/cm³ for Pd) and N is the Avogadro's constant. This estimates the correlation for the Pd catalysts,

$$D = \frac{0.9}{d (nm)} \quad (5.4)$$

Investigation of CNF layer morphology and qualitative study of Pd distribution across the CNF layer thickness was carried out using scanning electron microscopy (SEM) [LEO 1550] equipped with energy dispersive X-ray analysis (EDX) [Thermo Noran Vantage system]. Cross sectional analysis was facilitated simply by breaking the microreactor chips after Pd deposition on CNF layers, allowing an analysis with EDX at isolated spots in lateral direction.

5.3 Results and discussion

5.3.1 Characterizations of Pd/CNF layers in microreactor channels

Previously optimized growth settings were used to effectively fill microchannel volume with CNF layers. For example, *Fig. 5.2* (reproduced for clarity) shows the morphology of

entangled CNF layers with thicknesses of $\sim 13 \mu\text{m}$ (with $\sim 300 \mu\text{g}$ of carbon deposited over 10 min. of CNF growth time, see *Table 5.1* for details).

Table 5.1: *Properties of CNF deposits in the microreactor channels*

Time of growth [min.]	Average CNF layer thickness [μm]	Weight of carbon deposited [μg]	Pd [wt.%] ^a	Average Pd particle diameter Φ_p [nm] ^b	Dispersion [%] ^c
5	11	256	2.94	8	11.3
10	13	305	3.12	9	10.0
			5.10	7	12.9
			6.92	8	11.3
			10.15	7	12.9
15	17	460	3.04	7	12.9
40	20	536	2.88	8	11.3
60	21	598	3.08	7	12.9

^aDetermined from XRF, ^bDetermined from TEM, ^cEstimated using derivation of Scholten et al. [14]

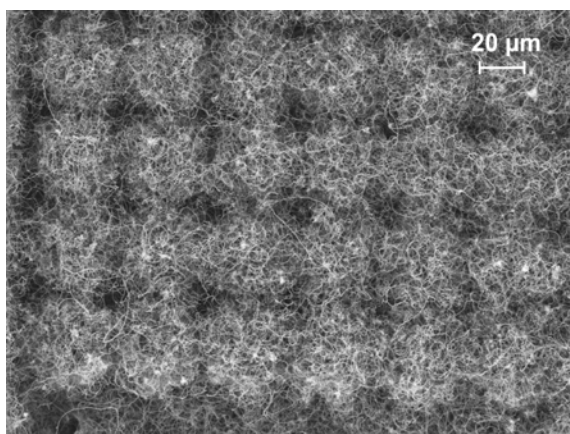


Figure 5.2: SEM images showing top view of microchannel with a CNF layer on the internals (with interpillar spacing of $20 \mu\text{m}$), and (b) cross sectional view: complete filling of the channel volume with CNFs (CNF growth conditions: 25% C_2H_4 and 25% H_2 in balance N_2 at 100 mL/min total flow rate, $T = 635^\circ\text{C}$, growth time = 10 min).

The Pd loading on CNF layers was varied between 3 to 10 wt.% with a $\sim 13\ \mu\text{m}$ thick CNF layer. Further CNF layers of different thicknesses loaded with *ca.* 3 wt.% palladium were also prepared. *Table 5.1* illustrates the Pd loading and corresponding dispersion values for all samples. In all samples the dispersion was below 15% and the average Pd particle size estimated to be $\sim 7\ \text{nm}$. *Figure 5.3* shows well distributed Pd particles on CNF layers.

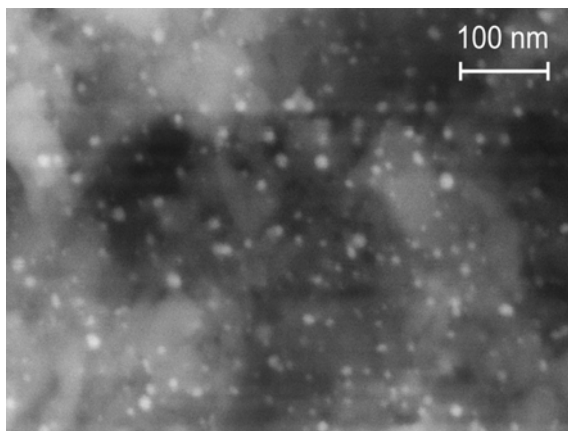


Figure 5.3: Secondary electron detector (SE) image obtained using SEM, shows well distributed Pd nanoparticles (visible as bright spots) deposited on CNF layers inside microreactor channels (Top-view).

Distribution of Pd within the CNF layer was also probed qualitatively using SEM-EDX analysis [7]. Figure 5.4a shows a typical cross-sectional view of Pd deposited CNF layer inside microreactor channel. EDX analysis was carried out at three different locations in lateral direction. The ratio of palladium to carbon is shown as a function of the position along CNF layer thickness in figure 5.4b. The Pd concentration is slightly higher in the top part (indicated by location '1') compared to the deeper part i.e. near the interface of CNF layer and microchannel surface (indicated by location '3').

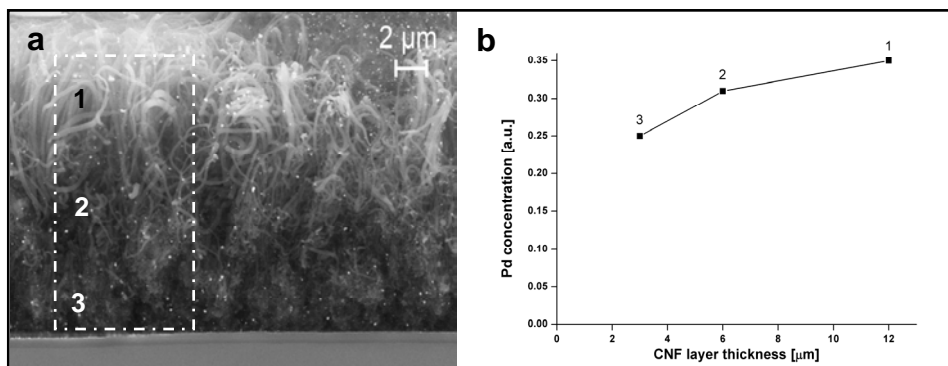


Figure 5.4: (a) Cross-sectional secondary electron detector (SE) image obtained using SEM highlighting lateral distribution of Pd across CNF layer with well distributed Pd particles (as probed by EDX analysis), (b) qualitative representation of Pd distribution across a ~13 μm thick and with ca. 3 wt.% Pd loaded CNF layer in a microchannel

5.3.2 Aqueous phase reduction of nitrite by Pd/CNF catalyst layers inside fixed space time by increasing the linear velocity of the nitrite solution stream, at the same time increasing the amount of Pd catalyst proportionally. This was achieved by two separate experiments, (i) with a single microreactor module consisting microchip with Pd/CNF layer at flow rate of 50 μL/min (linear velocity = 90.9 cm/min), and (ii) by adding second module in series to the first one with microchips having identical properties of Pd/CNF layers at flow rate of 100 μL/min (linear velocity = 181.8 cm/min). The series arrangement of two microreactor modules, with identical Pd/CNF catalyst layers, results in the proportional increase of Pd, maintaining a space velocity of 0.22 min⁻¹. Figure 5.5 shows the nitrite conversion as a function of the linear velocity of reactant solution. It can be observed that nitrite conversion remains constant in both the experiments, indicating absence of external mass transfer limitations at the selected linear velocity value *i.e.* 90.9 cm/min, for a single module. Hence, it would be appropriate to carry out further experiments with the same linear velocity using single microreactor module.

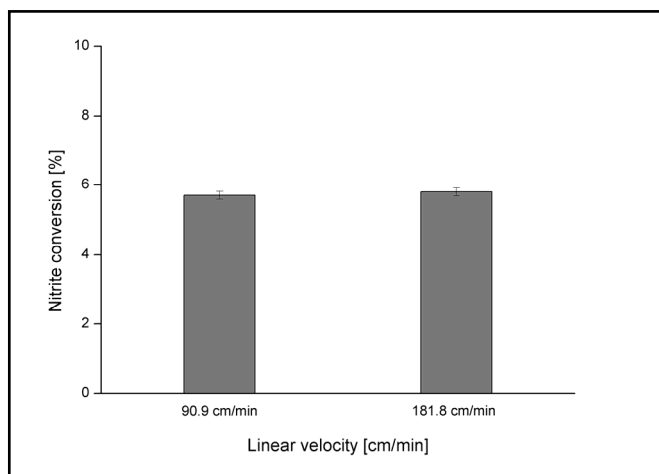


Figure 5.5: Nitrite conversion at fixed space time on a 13 μm thick CNF layer with ca. 3 wt.% Pd on CNF layers, at a space velocity of 0.22 min^{-1} .

The turn-over-frequency (TOF) of nitrite hydrogenation, *i.e.* rate of nitrite conversion per mole of surface palladium over CNF layers inside microreactor, remains stable till CNF layer thickness of $\sim 13 \mu\text{m}$ (see Fig. 5.6, 10 min growth time).

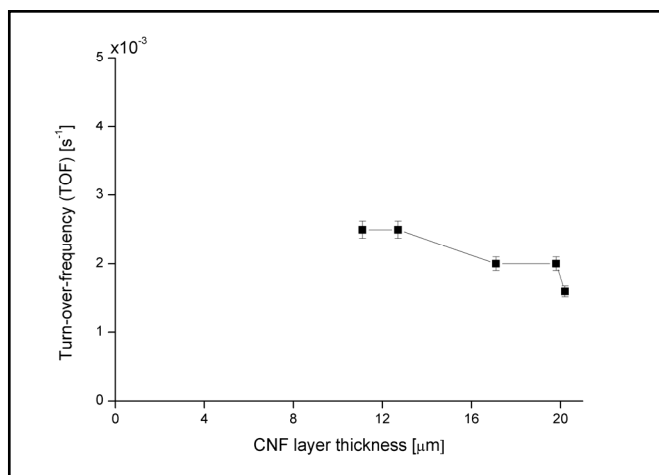


Figure 5.6: Rate of nitrite conversion per mole of surface palladium on CNF layers inside microreactor channels with thicknesses between 11 and 21 μm and Pd loading ca. 3 wt.%, measured at linear velocity of 90.9 cm/min and space velocities between 0.26 to 0.11 min^{-1} .

For larger thicknesses TOF decreases, indicating the presence of internal mass transfer limitations. The Pd loading was kept constant in these experiments at *ca.* 3 wt.% based on weight of deposited carbon, implying that the total amount of Pd varies proportionally with the CNF layer thickness. Further, when Pd loading is varied at constant CNF layer thickness of 13 μm , the TOF does not change (see Fig. 5.7). Thus, CNF layer thickness up to $\sim 13\ \mu\text{m}$ provide better accessibility of deposited Pd without any internal mass transfer limitations for reactant molecules. The TOF of $0.003\ \text{sec}^{-1}$ was determined under the present experimental conditions when measured for CNF layer thickness $< 13\ \mu\text{m}$. This is typically in the range reported for the reduction of nitrite on various Pd catalysts [7, 15]. Chinthaginjala *et al.* reported a higher value *i.e.* $0.02\ \text{sec}^{-1}$, with hairy foam based thin layer CNF catalysts [7] for the reduction of nitrite. The main difference between these studies is that in our case the CNFs were pre-oxidized in nitric acid to remove nickel (see chapter 4). Surface oxygen functionalities are known to influence catalytic activity of CNF supported metal particle. Toebe *et al.* [16] studying Ru/CNF showed that the degree of oxidation of the CNF can have tremendous influence on the catalytic activity. For example, oxidized CNF layers showed an order of magnitude lower TOF for the hydrogenation of cinnamaldehyde compared to a non-oxidized CNF supported catalyst. The exact reasons for this are not discussed [7, 16] and is not directly relevant for the current discussion.

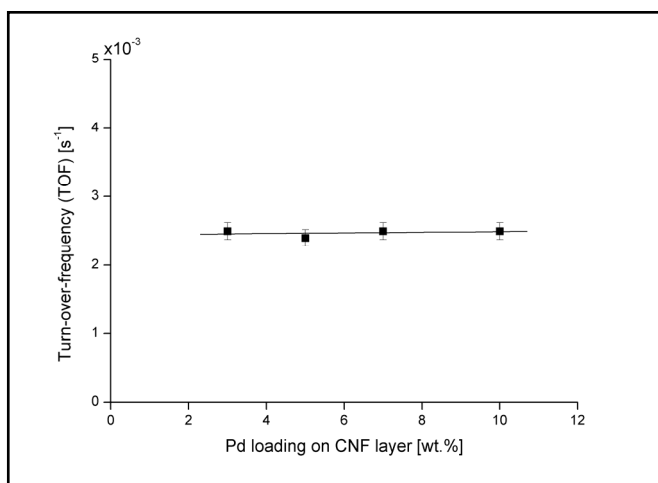


Figure 5.7: Rate of nitrite conversion per mole of surface palladium on CNF layers inside microreactor at Pd loading between 3 and 10 wt.% and a CNF layer thickness of 13 μm , measured at linear velocity of 90.9 cm/min and space velocity of $0.22\ \text{min}^{-1}$.

The results in *Fig. 5.6* and *Fig. 5.7* indicate that internal mass transfer limitations are indeed absent for CNF layers with thicknesses $<13\ \mu\text{m}$ and support the assumption that Pd is homogeneously distributed across CNF layer in microreactor channels in the context of intrinsic catalytic activity. Catalytic performance of thus tested Pd/CNF layers inside microreactors showed mostly $<30\%$ selectivity for N_2 and the selectivity for ammonia was normally greater than 70%, typically in the range reported for nitrite reduction using Pd/CNF catalyst [17].

5.4 Conclusions

Carbon nanofiber supported palladium (Pd) catalyst layers synthesized inside silicon based microreactors were used for studying the reduction of aqueous nitrite solution. Nitrite hydrogenation is known to be kinetically fast reaction, hence ideal for demonstrating performance of synthesized CNF layers inside microreactor systems. The catalyst layers were prepared *via* incipient organic impregnation method using palladium acetylacetonate precursor solution in toluene. A relatively large average particle size of Pd ($\sim 7\text{--}9\ \text{nm}$) was obtained with uniform distribution across the CNF layers. The mass transfer properties, both external and internal, were probed and the intrinsic rates of nitrite conversion (TOF) were found to be independent of the, (i) linear velocity higher than $90\ \text{cm/min}$ (flow rate of $50\ \mu\text{L/min}$ for the current microreactor module), and (ii) CNF layer thickness below $\sim 13\ \mu\text{m}$, indicating the absence of any mass transfer limitations. Thus optimized CNF layers then can be applied for performing relevant aqueous phase reactions, such as aqueous phase bromate reduction.

Acknowledgements

This work was performed with the financial support from MicroNed program, under cluster-II of Smart Microchannel technology (SMACT) and work package II-G-2 and 3 (Smart Micro Reactors). The authors gratefully acknowledge Dr. M. Smithers for SEM and TEM analysis, J.A.M. Vrieling for XRF, and B. Geerdink for technical support. The fruitful discussions with Dr. J.K. Chinthajinjala are gratefully acknowledged.

References

- [1] *WHO guidelines for drinking-water quality: second addendum, Vol. 1, Recommendations*, 3rd ed., Geneva (2008) 50-56.

- [2] F.J.J.G. Janssen, R.A. van Santen, *Environmental Catalysis*, Catalytic Science Series, Imperial College Press, 2001.
- [3] L.W. Canter, *Nitrates in ground water*, CRC Press, Boca Raton, Florida, 1996.
- [4] C.S. Bruning-Fann, J.B. Kaneene, *Vet. Hum. Toxicol.* 35 (1993) 521-538.
- [5] A. Kapoor, T. Viraraghavan, *J. Environ. Eng.* 123 (1997) 371-380.
- [6] K.D. Vorlop, T. Tacke, *Chem. Ing. Tech.* 61 (1989) 836-837.
- [7] J.K. Chinthaginjala, J.H. Bitter, L. Lefferts, *Appl. Catal. A* 383 (2010) 24-32.
- [8] S. Hörold, K.D. Vorlop, T. Tacke, M. Sell, *Catal. Today* 17 (1993) 21-30.
- [9] A. Pintar, G. Bercic, J. Levec, *AIChE* 44 (1998) 2280-2292.
- [10] A.J. Lecloux, *Catal. Today* 53 (1999) 23-34.
- [11] M.D. Arino, F. Pinna, G. Strukul, *Appl. Catal. B* 53 (2004) 161-168.
- [12] R.M. Tiggelaar, V. Verdood, H. Eghbali, G. Desmet, J.G.E. Gardeniers, *Lab Chip* 9 (2009) 456-463.
- [13] D.B. Thakur, R.M. Tiggelaar, J.G.E. Gardeniers, L. Lefferts, K. Seshan, *Surf. Coat. Technol.* 203 (2009) 3435-3441.
- [14] J.J.F. Scholten, A.P. Pijpers, A.M.L. Hustings, *Catal. Rev. - Sci. Eng.* 27 (1985) 151-206.
- [15] V. Höller, K. Rådevik, I. Yuranov, L. Kiwi-Minsker, A. Renken, *Appl. Catal. B* 32 (2001) 143-150.
- [16] M.L. Toebes, F.F. Prinsloo, J. H. Bitter, A.J. van Dillen, K.P. de Jong, *J. Catal.* 214 (2003) 78-87.
- [17] J.K. Chinthaginjala, *Hairy Foam: Thin layers of carbon nanofibers as catalyst support for liquid phase reactions*, PhD thesis, University of Twente, Enschede, The Netherlands (2010).

Chapter 6

Ruthenium Catalyst on CNF Support Layers for Si-based Structured Microreactors, Part II: Catalytic Reduction of Bromate Contaminants in Aqueous Phase

Abstract

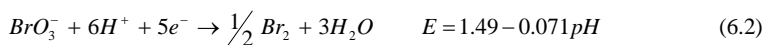
Carbon nanofiber supported ruthenium (Ru/CNF) catalyst layers prepared using homogeneous deposition precipitation method, inside a structured channel of silicon based microreactor are used to remove traces of aqueous bromate by heterogeneous redox catalysis. It is demonstrated that CNF based catalyst are highly active for bromate reduction, resulting in turn over frequencies (TOF) at least two times larger in comparison to the tested conventional powdered catalyst i.e. activated carbon (AC). This enhanced catalytic performance is due to improved mass transfer properties of entangled CNF layers with macroporous (open) structure, which offer low tortuosity and subsequently enhanced accessibility to all the Ru active sites in contrast to the poor accessibility of active sites in the case of AC support material.

Although promising catalytic activity of Ru/CNF catalyst was observed for bromate reduction, a continuing deactivation was observed during 5 h time on stream operation. A variety of characterization techniques including TEM, XPS, TPR, ICP probed that along with catalyst sintering, formation of catalytically inactive Ru(OH)_x phase on catalyst surface was an important reasons of this deactivation behavior. Use of higher alcohols proved to be beneficial for achieving sustainable activity of Ru/CNF catalyst for bromate reduction, however with reduced levels of overall activity. It is expected that hence developed highly porous open structured catalyst layers based on CNF support inside microreactor systems will provide a promising option particularly for liquid phase reactions to be carried out efficiently.

6.1 Introduction

As mentioned in chapter 5, high water purity levels in both industrial and domestic use have been strictly regulated and continuously monitored. As a consequence, presence of undesirable and possibly toxic disinfection components in water purification treatment processes will have to be controlled. One such problem of concern is bromate, which is frequently detected in drinking water especially originating from process involving ozonation of bromide-containing source waters [1-3]. The World Health Organization (WHO) and United States' Environmental Protection Agency (EPA) have strictly regulated the bromate levels (provisional guideline value: 0.01 mg/L) in drinking water since the International Agency for Research on Cancer (IARC) has classified bromate as a Group 2B substance (*i.e.* possibly carcinogenic to humans) [4, 5]. This demands the development of an effective treatment method for the removal of bromate from drinking water [6]. Various techniques, such as biological [7, 8], photocatalytic [9, 10], electrochemical reduction [11] and more recently, catalytic hydrogenation [12], are available. A promising alternative for the removal of bromate pollution from drinking water is *via* heterogeneous redox catalysis without the requirement of using hydrogen [13, 14]. The main advantage of catalytic routes is the efficient and faster removal of water contaminants such as bromate, particularly when compared to the conventional physicochemical methods. Further, conventional methods concentrate removed contaminates in a secondary waste streams, which requires further treatment [15].

Review of literature cites only limited articles [13, 14] regarding the catalytic removal of BrO_3^- from aqueous solutions. It is reported by Grätzel *et al.* [13] that BrO_3^- ion decomposition is thermodynamically allowed *via* red-ox reactions involving oxidation of water and subsequent reduction of bromate as below,



However, bromate ions are very stable in aqueous solutions, especially in the absence of oxidisable impurities or when protected from UV light. A dilute aqueous HBrO_3 solution does not undergo any decomposition even after several months of storage. The slow kinetics of the bromate reduction *via* the above redox cycle may be

due to the difficulty in the transfer of charges which can be facilitated by the presence of connected electrodes. Accordingly, in the presence of typical electrode materials, in this case a Ru catalyst, RuO₂/TiO₂ [13], oxygen evolution was observed. Based on their studies with labeled oxygen (80% H₂¹⁶O and 20% H₂¹⁸O) and observing that 20% ³⁴O₂ was formed, they concluded that water was oxidized and was the source of oxygen.

However, Mills *et al.* [14] show that kinetics of the oxidation of water even in the presence of a RuO₂ catalyst is kinetically very slow (0.05·10⁻⁶ mol dm⁻³ s⁻¹ at 30°C). Presence of an easily oxidizable water soluble organic component, *e.g.* MeOH or EtOH, in the reaction medium enhances the rate of bromate decomposition. They report that in the presence of MeOH a forty times improvement in rates in bromate conversion was observed compared to the situation when only water was present [14].

Carbon nanofiber supported ruthenium catalyst layers (Ru/CNF) present a novel option for treating bromate polluted water resources. In such a reactor, Ru metal particles are placed in space in the porous CNF layer, as in a frozen fluidized bed. Such an arrangement is expected to offer enhanced contact between bromate, reductant and Ru catalyst. Bromate reduction is carried out in the microreactor module described in chapter 5 and containing Ru/CNF catalyst, in order to establish advantages over conventional fixed bed catalytic reactor systems.

In chapter 4 (*i.e.* part-I) details of the (*i*) preparation of stable and entangled CNF layers (*ii*) functionalization of the CNF surface and incorporation of Ru nanoclusters, and (*iii*) preparation of CNF supported ruthenium catalyst layers inside the flow channels of a silicon-based microreactor, have been presented. Here, the catalytic performance of these Ru/CNF containing microreactors is attempted for aqueous phase reduction of bromate ions.

6.2 Experimental

6.2.1 Preparation of Ru/CNF and Ru on Activated Carbon (AC) catalysts

The preparation of these catalysts was achieved using an aqueous phase homogeneous deposition precipitation (HDP) method, of which details are given in chapter 4. AC from Norit (RO 0.8H, 100-125 μm) was used. The Ru loading and particle size were tailored to be similar to that of Ru/CNF layers in microreactors in order to be able to make reasonable comparisons (see *Table 6.1*). The prepared powdered catalyst was tested in a fixed bed reactor placed in the same oven as used for the microreactors, and flow rates of 100 μL/min were used to achieve a similar contact time of the reactants.

The fixed bed of Ru/AC particles was prepared by diluting them with inert quartz particles of similar size.

6.2.2 Fluidic set-up and procedure

The microreactor chips with a Ru/CNF layer were fixed in a homemade Teflon (PTFE) holder provided with inlet and outlet fluid flow connections (see *Figure 5.1* in *Chapter 5*). The module was placed in an oven (Binder GmbH) and the reaction temperature controlled accurately (± 0.5 °C) over the range 30 - 50 °C. A syringe pump (Cole-Parmer® Multi-Syringe pump; 74900 series) was used to flow reactants into the module *via* flexible fused silica capillary tubing (Polymicro Technologies; outer diameter 360 μm , inner diameter 250 μm) at a flow rate of at 50 $\mu\text{L}/\text{min}$. Prior and post to the reaction the bromate concentrations were measured using an inline flow cell (Zeutek Opto-elektronik) coupled to an UV-Vis-NIR spectrometer (HR4000, Ocean Optics). The concentration of bromate ions was determined by measuring the absorbance at 230 nm.

The bromate (KBrO_3 ; Sigma-Aldrich, $\geq 99.8\%$) concentration in aqueous solution was varied between 384 mg/L (3 mmol/L) and 1280 mg/L (10 mmol/L). Methanol, was added to the bromate solution in a 10-fold molar excess [14], *i.e.* between 961 mg/L (30 mmol/L) and 3204 mg/L (100 mmol/L).

6.2.3 Characterization

Scanning electron microscopy (SEM) [LEO 1550] equipped with energy dispersive X-ray analysis (EDX) [Thermo Noran Vantage system] was used to study the morphology of the CNF layers, and the distribution of Ru across the thickness of the CNF layer. Cross-sections of CNF layers synthesized inside the microreactor chips were essentially obtained by breaking individual chip at multiple positions along the length of the channels. The activated carbon particles were crushed to perform EDX analysis. The BET surface areas of CNFs and activated carbon were calculated from the N_2 -adsorption isotherm measurements obtained at -196 °C (77 K) [Micromeritics Tristar]. X-ray fluorescence spectrometry (XRF) [Philips PW 1480] was used to determine the ruthenium loading. The ruthenium particle size distributions on CNF and AC supports were determined with transmission electron microscopy (TEM) [Philips CM300ST-FEG equipped with Gatan Ultrascan 1000 CCD camera]. The average particle size estimated from TEM was based on the analysis *ca.* 20 images, and this average size was used to

calculate dispersion values assuming spherical shapes using the formula described by Scholten *et al.* [16],

$$D = 10^{21} \cdot \frac{6 \cdot M \cdot \rho_{site}}{d \cdot \rho_{metal} \cdot N} \quad (6.4)$$

where, D is dispersion ($Ru_{surface}/Ru_{total}$), M is the atomic mass (101.07 g/mol for Ru), ρ_{site} is the ruthenium surface site density (16.3 Ru atoms/nm²), d is particle size (nm), ρ_{metal} is the metal density (12.3 g/cm³ for Ru) and N is the Avogadro's constant. This estimates the correlation for the Ru catalysts,

$$D = \frac{0.9}{d \text{ (nm)}} \quad (6.5)$$

X-ray photoelectron spectroscopy (XPS) [Quantera SXM Physical Electronics] was performed to determine the oxidation state of ruthenium prior and post to the bromate reaction. Solutions collected after reaction at the outlet of microreactor were analyzed to investigate Ru leaching using Inductively Coupled Plasma (ICP) spectrometer [Thermo Scientific iCAP 6500] using a Ru plasma standard solution, Specpure®, Ru 1000µg/ml from Alfa Aesar for determining the calibration line.

6.3 Results and discussion

6.3.1 Mass transfer issues in microreactors with Ru/CNF

Before attempting reaction with bromate, it is useful to state experiments that were carried out (in previous chapter 5) for the catalytic hydrogenation of nitrite using Pd (a kinetically facile reaction) to sort out issues related to mass transfer in CNF layers in microchannels [15]. From these experiments it followed that external mass transfer problems (varying linear velocity while keeping space velocity constant) could be avoided at the selected value for linear velocities of 90 cm/min (50 µL/min), whereas internal mass transfer problems (varying CNF layer thickness maintaining constant catalyst loading) could be avoided on CNF layers with a thickness of 13 µm or less. The latter implies that spacing between the cylindrical structural features in the microreactors should be less than of 26 µm so that growth from both sides can fill the space with CNFs. Overall, the flow rate for the Ru-catalyzed bromate reduction reaction was limited to 50 µL/min, and the cylinder-spacing to 20 µm.

6.3.2 Microreactors with Ru/CNF for bromate reduction

The bromate reduction was carried out in the microreactor containing Ru/CNF layers. CNF-layers with thicknesses of 12 to 13 μm (with $\sim 300\text{ }\mu\text{g}$ of carbon deposited over 10 min. of CNF growth time) were chosen for catalytic reduction of bromate (see *Fig. 6.1*, reproduced for clarity). HDP method was used to prepare the well dispersed and distributed Ru on CNF layers. The actual Ru loading on the CNF layers in microreactors after reduction was *ca.* 2.3 wt. %, as analyzed by XRF, accounting for $\sim 7\text{ }\mu\text{g}$ Ru for each microreactor, based on total amount of carbon in the reactor channel. TEM analysis estimated the average Ru particle size typically around *ca.* 1.7 nm (*Table 6.1*). The dispersion of Ru was estimated to be around 78 %, based on TEM and formula described previously [16].

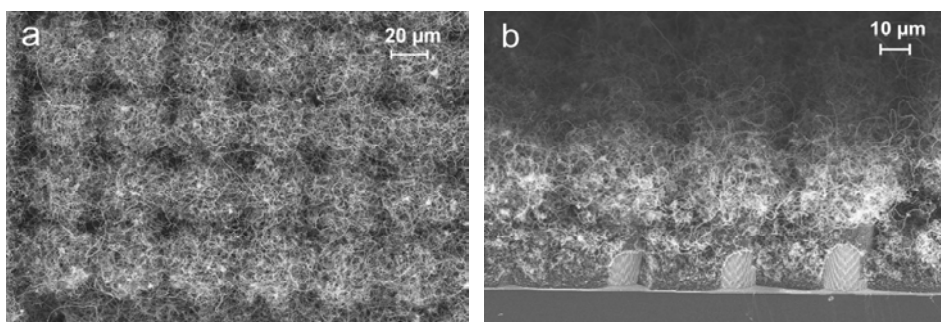


Figure 6.1: SEM images showing (a) top view of microchannel with a CNF layer on the internals (with interpillar spacing of $20\text{ }\mu\text{m}$), and (b) cross sectional view: complete filling of the channel volume with CNFs (CNF growth conditions: 25% C_2H_4 and 25% H_2 in balance N_2 at 100 mL/min total flow rate, $T = 635\text{ }^\circ\text{C}$, growth time = 10 min).

The kinetics of bromate reaction was investigated spectrophotometrically using UV-Vis-NIR spectrometer. In order to exclude the influence of catalyst deactivation on kinetic studies, all experiments were carried with fresh catalyst and values extrapolated to initial time on stream. The influence of variation of initial concentration of bromate as well as temperature was studied to probe the kinetics of reduction of bromate. The bromate conversions varied between 50-70 mol.% in these experiments. Analysis of the data using integral method (*Fig. 6.2*) showed first order dependence of rates in bromate concentrations and ' k ' value of 1.86 min^{-1} at $40\text{ }^\circ\text{C}$. An activation energy of 33.4 kJ/mol was measured in the temperature range $30 - 50\text{ }^\circ\text{C}$. For an unsupported RuO_2 catalyst a higher value of 47 kJ/mol is reported by Mills *et al.* [14].

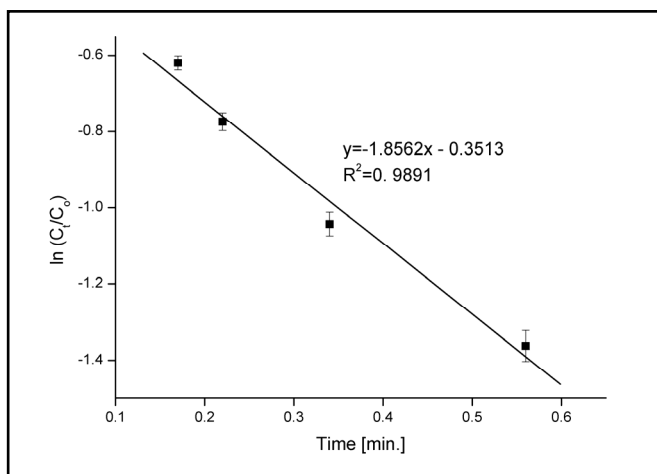


Figure 6.2: A plot of $\ln(C_t/C_0)$ as function of time with slope 'k' (reaction conditions: 2.3 wt.% Ru/CNF, bromate concentration 1 to 10 mM, reaction temperature 40 °C).

Table 6.1: Properties of ruthenium catalyst material supported on carbon nanofibers and activated carbon and prepared by homogeneous deposition precipitation method; activation treatment: reduction in dilute H_2 at 500 °C for 90 min.

Catalyst	Amount of CNF and/or AC [μ g]	Ru loading [wt.%]	Ru particle mean diameter [nm] ^a	Ru Dispersion [%] ^b
Ru/CNF	300	2.3	1.7	78
Ru/AC	500	2.9	1.9	70

^a Determined from TEM, ^b Estimated using derivation of Scholten *et al.* [16]

6.3.3 Fixed bed with Ru/AC catalyst for bromate reduction

In order to compare the performance of Ru/CNF catalyst with that of conventional microporous carbon supported catalysts, ruthenium on activated carbon (Ru/AC) was used for the bromate reduction (Ru/AC in a fixed bed). For the Ru/AC catalyst, the average particle size of Ru based on TEM was found to be 1.9 nm (*Table 6.1*), and a Ru loading of *ca.* 2.9 wt.%. Based on the equation of Scholten *et al.* [16], the dispersion of Ru/AC was estimated to be 70%.

The bromate conversions varied between 24-40 mol.% in these experiments. Analysis of the data using integral method (*Fig. 6.3*) also showed first order dependence of rates in bromate concentrations and ' k ' value of 0.46 min^{-1} at 40°C .

A comparison in catalytic performance of Ru catalyst supported on AC and CNFs for the aqueous phase bromate reduction is given in *Fig. 6.4* in terms of the TOF-values (*i.e.* mole of bromate converted per mole of surface ruthenium per second). Ru/AC has a significantly lower intrinsic catalytic activity (Ru/AC: 0.019 s^{-1} and Ru/CNF: 0.032 s^{-1}). These results indicate that in case of microporous support materials, such as activated carbon, mass transfer limitations occur, which make it difficult for bromate molecules to access all active surface Ru sites, resulting in lower conversions for Ru/AC. The superior performance of Ru/CNF is obvious.

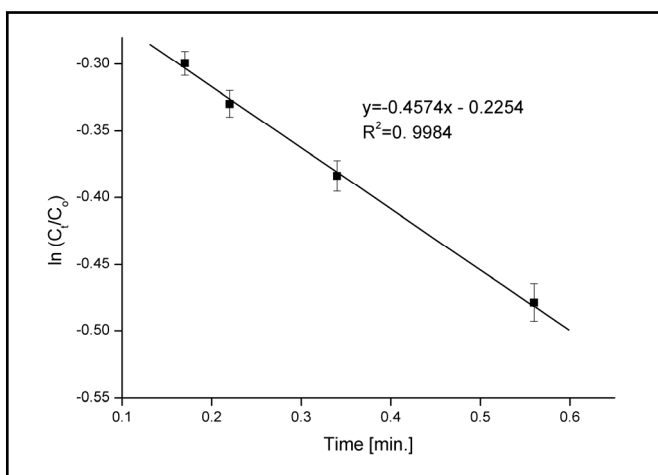


Figure 6.3: A plot of $\ln(C_t/C_0)$ as function of time with slope ' k ' (reaction conditions: 2.9 wt.% Ru/AC, bromate concentration 1 to 10 mM, reaction temperature 40°C).

BET surface area and pore volume measurements for both catalyst supports are tabulated in *table 6.2*. It is evident from the values for micropore volumes, that CNF layers have negligible fraction of micropores (*i.e.* pores with sizes below 2 nm; these pores possibly exist only in the thin, dense 'carbon-like' layer present near the interface of the CNF layer and the substrate [17, 18]. AC contains a larger fraction of micropores. The presence of micropores results in a very high surface area for AC, and this contribution is low for CNFs. The BET surface area for CNF is the summation of the micropore area and the geometrical external surface area of the fibers [19, 20]. The ratio

of external surface to micropore surface is a good indication for possible mass transfer issues: small values are undesired. In *table 6.2* calculated values are given, and these were found to be >1 for CNFs and $<<1$ for activated carbon. These ratios underline the improved mass transfer properties of the macroporous (open) structure of the entangled carbon nanofibers offering low tortuosity and easy accessibility to all active Ru sites.

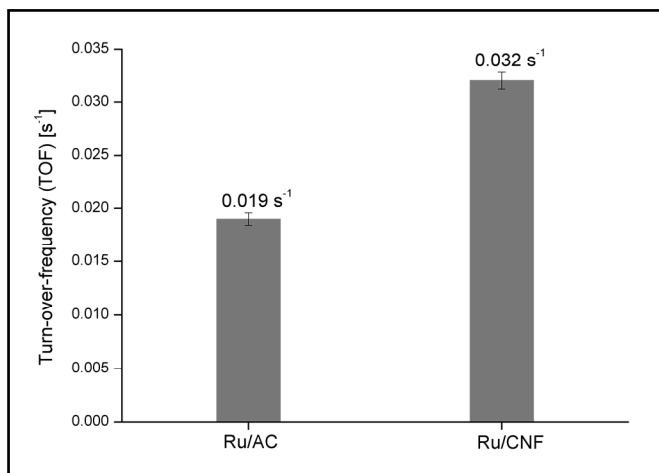


Figure 6.4: Turn-over-frequencies for bromate removal using Ru supported on AC and CNFs (reaction conditions: bromate concentration 5 mM, temperature 30°C).

Table 6.2: BET surface areas and related properties of carbon nanofiber and activated carbon catalyst support materials

Support material	BET surface area (m ² /g) ^a	Micropore volume (cm ³ /g) STP	Ratio of external surface area: micropore area
CNF	136	0.03	1.27
AC	1125	0.5	0.07

^a Measured after oxidation treatment with HNO₃ acid

6.3.4 Stability of Ru/CNF catalyst

As shown in the previous section, Ru/CNF catalyst layers show high catalytic activity for the aqueous phase bromate reduction reaction. However, the initially high activity

showed a gradual decrease during an on stream operation of *ca.* 5h, *i.e.* catalyst deactivation.

This deactivation demanded further investigation, as well as determination of possible origins for deactivation of Ru/CNFs for BrO_3^- conversion. TEM analysis was used to probe any variation in average particle size of “aged” catalyst: it was found that an increase of the Ru particle size had occurred from 1.7 nm to 2.2 nm (after 5h of use). This emphasizes that sintering occurs during the used experimental conditions. The most likely pathway for sintering is migration of active Ru ions *via* Ostwald ripening [21], which involves detachment of Ru from smaller crystallites and subsequent capture by larger crystallites [22]. Other pathways for sintering are less likely, because the reaction temperature is low, as for most liquid phase reactions over supported metal catalysts. Therefore, temperature driven migration and/or coalescence of metal particles can not take place. The consequence of particle growth occurring here is 2-fold: the amount of highly dispersed fine crystallites/particles is lowered, and the surface area of Ru available for bromate reduction decreases, which together results in a lower catalyst activity.

A series of experiments were performed to study ways to (partially) regenerate deactivated catalyst, *i.e.* 1h treatments of deactivated catalyst with air (oxidizing atmosphere; 300 °C) or hydrogen (reducing atmosphere; 500 °C).

6.3.4.1 Regeneration of deactivated Ru/CNF catalyst with an oxidizing atmosphere (air)

Exposure of deactivated Ru/CNF catalyst to an oxidizing atmosphere was intended to remove any coke and/or amorphous carbonaceous deposited from the surface of active sites, and which might have been formed during the conversion of organic species *e.g.* MeOH. A temperature of 300 °C was used to avoid oxidative damage of the CNF support. TEM analysis confirmed that the structural properties (morphology) of CNFs did not alter during this oxidation step, normally CNF are stable up to 400 °C in air [18, 23]. Due to the higher degree of crystallinity of CNFs with respect to any coke or amorphous carbon, it is expected that this treatment selectively burns away the latter. From *figure 6.5*, it can be observed that this oxidizing treatment did not restore the initial activity levels of the Ru/CNF catalyst, in fact, a further loss of activity was registered. TEM analysis of the calcined catalyst revealed that average Ru particle size had increased to *ca.* 5 nm. This can be due to sintering caused by the burn off of the non fibrous

carbon formed during the CNF growth. It is difficult to separate this effect from any coke formed from organic species during bromate reduction. This is in agreement with literature: metals sinter relatively rapid in oxidizing atmospheres (O_2) compared to reducing atmospheres (H_2) [21]. Thus, a loss of available Ru surface during oxidation treatment leads to further lowering of catalyst activity, and hence a lower bromate conversion.

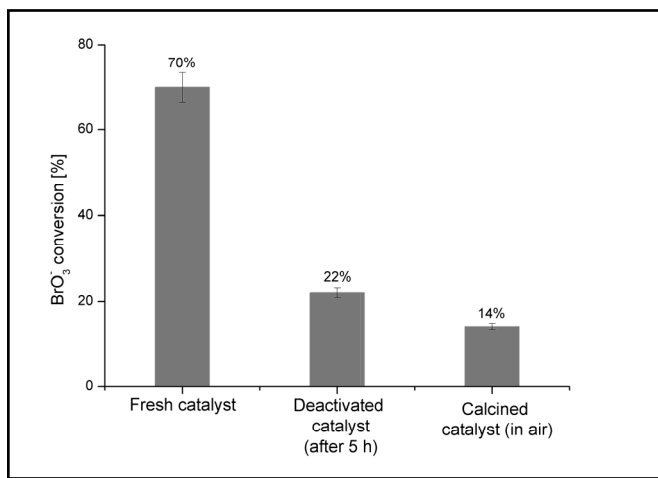


Figure 6.5: Initial bromate conversion level of Ru/CNF catalyst, after 5h of operation, and after calcination with air (reaction conditions: 5 mM bromate, temperature 50 °C).

6.3.4.2 Regeneration of deactivated Ru/CNF catalyst with a reducing atmosphere (H_2)

Deactivated Ru/CNF catalyst was also treated with a reducing hydrogen atmosphere (500 °C; 1.5 h). This treatment resulted in partial regeneration of the catalyst activity: up to 60% of the initial catalytic activity could be regained (*Fig. 6.6a*). TEM images of reduction-regenerated Ru/CNF revealed that the average Ru particle size was *ca.* 2.3 nm, which is nearly similar to the particle size on spent Ru/CNF. When deactivated Ru/CNF catalyst was subjected to consecutive reduction treatments cycles of bromate reaction-and-regeneration, no variation was observed in the catalyst activity; a constant 40% bromate conversion was measured (see *Figure 6.6b*). This figure reveals an interesting aspect: although the particle size does not vary after each reduction treatment and each reduction-regeneration step yields a bromate conversion of ~40% directly after regeneration, the conversion level of 5h-reaction periods decreased (*Fig. 6.6b*). This

indicated that there was an additional mechanism participating in the deactivation of catalyst during time on stream operating conditions.

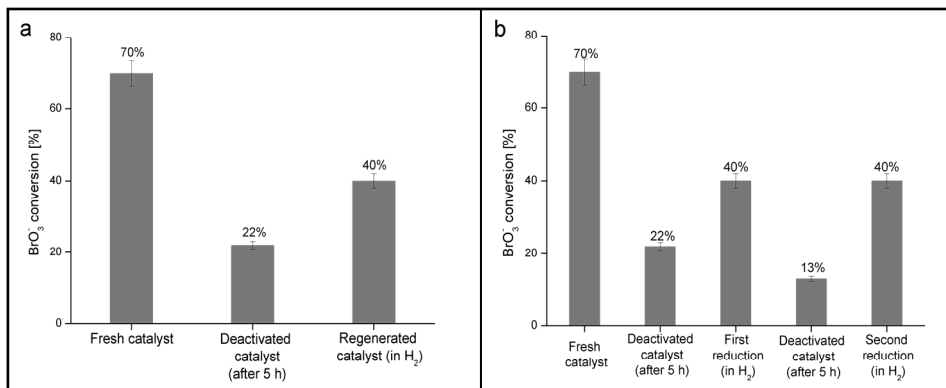


Figure 6.6: (a) Initial bromate conversion level of Ru/CNF catalyst, after 5h of operation, and after reduction with diluted hydrogen; (b) bromate conversion levels after two consecutive reduction cycles (reaction conditions: 5 mM bromate, temperature 50 °C).

6.3.4.3 Deactivation of Ru/CNF catalyst

A recent study suggests that the formation of Ru(OH)_x surface species is responsible for catalyst deactivation during liquid phase reduction reactions, particularly in presence of water [24]. Manyar *et al.*, indicate that temperatures above 400 °C are required to reduce Ru(OH)_x species [24]. This was further supported with a temperature programmed reduction (TPR) study of Ru supported on graphite support, where it was found that a temperature of 500 °C was adequate to reduce Ru in the HDP prepared catalyst. Although this temperature-requirement is fulfilled during reduction-regeneration of deactivated Ru/CNF in our case, complete regeneration of the initial activity is not still achieved. This implies that the irreversible sintering of the Ru particles is the main reason for deactivation. Leaching of active (Ru) metal or CNF support might lead to the loss of catalyst activity during the first reaction period of 5h. However, the ICP analysis of solutions collected after reaction did not indicate presence of Ru. Additionally, the constant bromate conversion level of ~40% (as measured directly after each regeneration treatment) indicates that leaching is not a major issue. Ru is also known to be one of the metals least susceptible to leaching [22]. Thus, catalyst deactivation after the first regeneration treatment (bromate conversion from 22% to 13%) could be due to

formation of inactive species such as $\text{Ru}(\text{OH})_x$. Indeed, XPS analysis (*Fig. 6.7*) of deactivated catalyst (after 5h of bromate conversion) indicates the presence of surface hydroxide: the deconvoluted O1s spectrum contains a fitting curve with a binding energy around 531-532 eV, which is attributed to hydroxide species [25, 26]. In conclusion, the catalytic activity of Ru/CNF catalyst during bromate reduction shows that Ru active phase deactivates due to irreversible sintering (*via* Ostwald ripening), as well as formation of catalytically inactive surface species ($\text{Ru}(\text{OH})_x$) during long(er) on stream operation times. However, oxidation of Ru *via* bromate can not be ruled out as one of the reasons of catalyst deactivation.

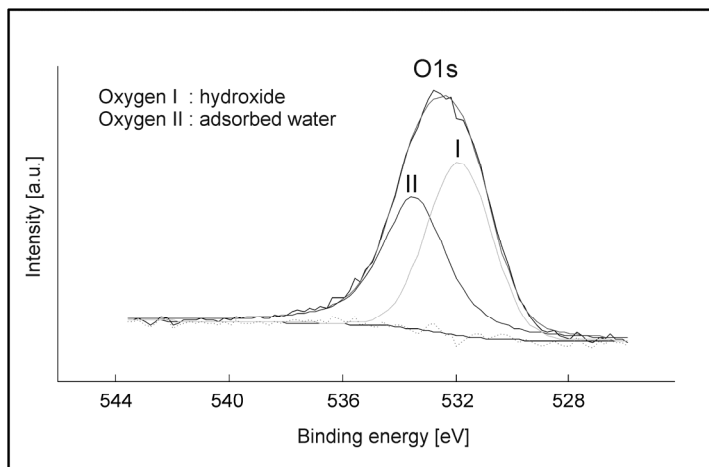


Figure 6.7: XPS spectrum of deactivated Ru/CNF catalyst after 5 h time on stream operation: deconvoluted O1s peak.

By controlling the interaction of water with surface Ru, the amount of $\text{Ru}(\text{OH})_x$ formed can be lowered. A method to achieve this is by creating a (partially) hydrophobic environment near the catalyst surface. In this context higher alcohols are known to be less hydrophilic than MeOH [24]. A series of experiments was carried out to test the influence of substituting methanol by 2-propanol and 2-butanol during the aqueous phase reduction of bromate. *Figure 6.8* shows the normalized activity of Ru/CNF catalyst as function of time on stream operation time. Clearly, the catalyst activity in the case of 2-butanol is substantially more stable with respect to time than in the presence of methanol. Methanol is hydrophilic and easily soluble in water due to its polar nature.

However, the polar nature of an alcohol molecule diminishes with increasing number of carbon atoms (*i.e.* the length of alkyl group), which makes longer alcohols less hydrophilic and hence less soluble in water. This effect explains the trend seen in *Figure 6.9*. 2-butanol has an increased hydrophobicity with respect to methanol, and thus 2-butanol resulted in a more stable catalytic activity. Moreover, the CNF support material is hydrophobic, since the catalyst activation step (reduction at 500 °C) removed the majority of oxygen containing groups, and this favors the formation of a high concentration alcohol layer near the catalyst surface that protects Ru from deactivation *via* hydroxylation.

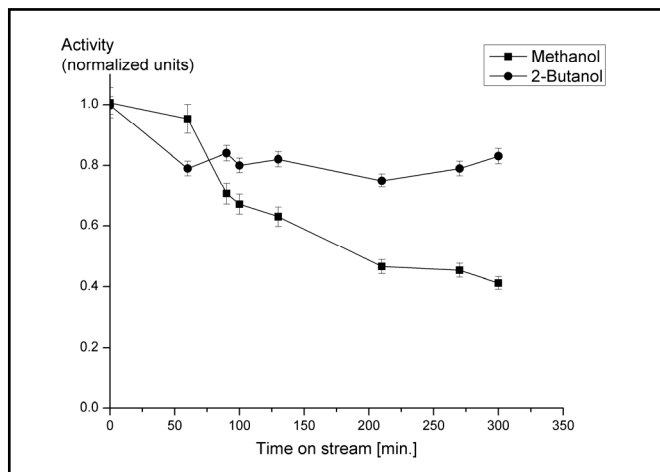


Figure 6.8: Normalized Ru/CNF catalyst activity for a primary alcohol (*i.e.* methanol) and a secondary alcohol (*i.e.* 2-butanol) (reaction conditions: 5 mM bromate, temperature 50 °C).

However, although use of higher alcohols improves the stability of the catalyst, the use of these alcohols also results in lower initial conversions for bromate reduction. *Figure 6.9* shows the initial bromate conversion levels observed for three alcohols: this lowering is due to the fact that MeOH competes favorably with water for the hydrophobic CNF surface in comparison to higher alcohols [24]. We believe that the presence of 2-butanol molecules near/on the surface of the catalyst somewhat hampers/delays the access of bromate molecules to the Ru active sites due to this hindrance, resulting in mass transfer limitations and hence lower initial conversion level, despite the more stable in-time catalytic behavior. However, differences in

activities might also be originating from the difference in reduction capabilities of various alcohols.

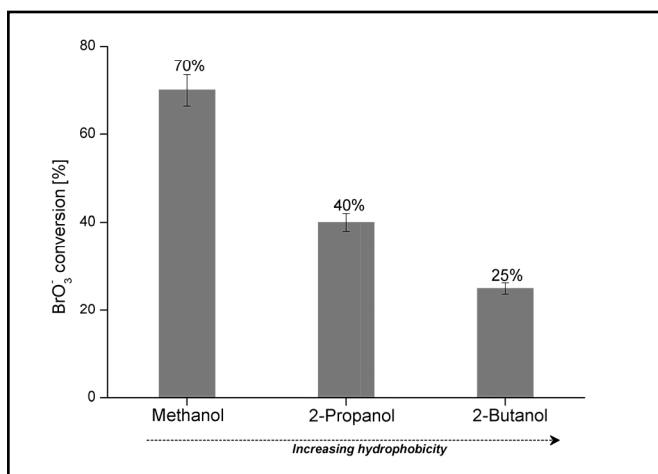


Figure 6.9: *Ru/CNF catalyst activity for bromate reduction for different alcohols: methanol, 2-propanol, and 2-butanol (reaction conditions: 5 mM bromate, temperature 50 °C).*

6.3.5 Reaction sequences for bromate reduction

Aqueous phase bromate reduction *via* heterogeneous redox catalysis has been proposed previously in literature [14]. The analysis of Ru/CNF catalyst at various stages, *i.e.* of fresh, and after reaction, was performed using XPS. *Figure 6.10a* shows the XPS spectrum of fresh catalyst. The most prominent peak observed was Ru 3d_{5/2} (more commonly seen Ru 3p_{3/2} peak exhibited extremely weak signal). The insets shown in *figure 6.10a* illustrate the magnified portion of Ru 3d_{5/2} peak overlapping with C1s peak of carbon. After appropriate curve fitting procedure the estimated value of binding energy turn out to be 280.7 eV. This corresponds with that reported for RuO₂ [27]. In the case of a used catalyst Ru 3d_{5/2} (*Fig. 6.10b*) binding energy was found to shift to higher value by almost 1.5 eV indicating presence of higher oxidation state between RuO₂ and RuO₃ (282.3 eV) [27]. These results show that Ru in fresh Ru/CNF catalyst still consists of oxidized Ru species, *i.e.* RuO₂. Eventhough the catalyst was prerduced at 500 °C, exposure to air at ambient oxidizes Ru, in agreement with literature [24].

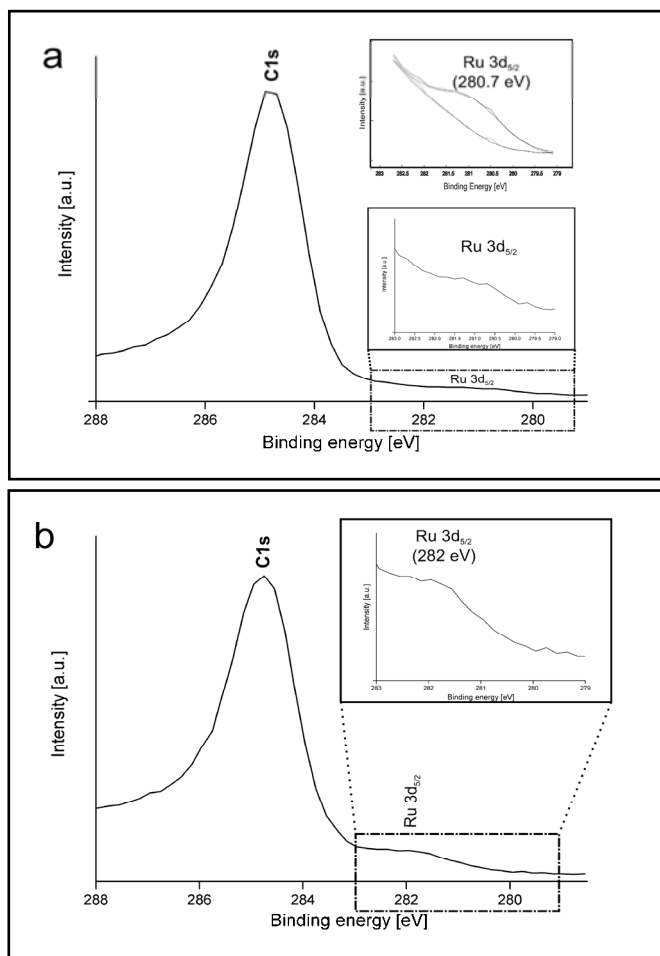


Figure 6.10: XPS spectrum of fresh (a) and spent Ru/CNF catalyst (b).

Oxidized Ru species, RuO_2 reduces bromate to bromide (particularly at higher pH values [13]) and in the process oxidizes itself to higher oxidation state, most probably to RuO_3 , Eq. (6.6). Once RuO_3 is formed it further oxidizes alcohol present in the reaction mixture and gets reduced to RuO_2 , Eq. (6.7), to recycle for next catalytic redox cycle. This can result in simultaneous formation of alkoxy species. It has been observed in literature previously, that platinum group metals served in formation of such species from aqueous phase solutions [24, 28]. However, as outlined earlier, simultaneous gradual hydroxylation to $\text{Ru}(\text{OH})_x$ deactivates Ru/CNF catalyst during time on stream operation.

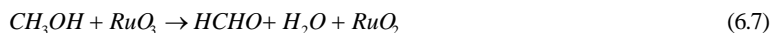


Figure 6.11 shows the simplified schematic representation of aqueous phase bromate reduction *via* heterogeneous redox catalysis mediated by Ru/CNF catalyst layers in microreactor.

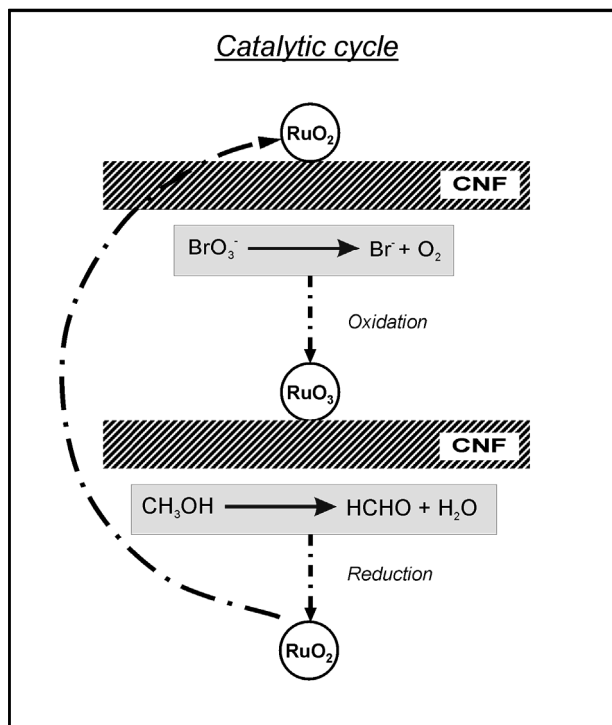


Figure 6.11: Proposed reaction sequence for aqueous phase bromate reduction over a Ru/CNF catalyst layer in the flow channel of a silicon-based microreactor.

6.4 Conclusions

Carbon nanofiber supported ruthenium catalyst layers integrated in silicon based microreactors showed promising catalytic performance in eliminating bromate contamination from aqueous solutions. It was demonstrated that CNF based catalyst are indeed highly active for bromate reduction, resulting in TOFs larger in comparison to conventional powdered catalyst *i.e.* activated carbon. This enhance catalytic

performance is due to improved mass transfer properties of entangled CNF layers with macroporous (open) structure, which offer low tortuosity and subsequently enhanced accessibility to all the Ru active sites in contrast to the poor accessibility of active sites in the case of AC support material. This benefit is crucial in particular for heterogeneously carried liquid phase reaction where mass transfer limitations are important factor. Although a high catalytic activity was shown a gradual deactivation of Ru/CNF catalyst was observed under current experimental conditions. Further investigation of spent catalyst showed that severe sintering took place leading and confirming no deposition of coke or amorphous carbon deposits on Ru catalyst. Specific characterization using XPS indicated the formation of $\text{Ru}(\text{OH})_x$ species as an additional cause of deactivation. The use of higher alcohols indeed limited the extent of deactivation by controlling hydroxylation of Ru. It is proposed that aqueous phase bromate removal is carried out by heterogeneous redox catalysis *via* bromate reduction to bromide mainly by RuO_2 which itself get oxidized to a higher oxidation state and react with alcohol to be recycled after being reduced in the process. In general, Ru supported on CNF layers inside microreactor systems offers a promising option in terms of efficient and green way for removal of drinking water pollutants such as bromate.

Acknowledgements

This work was performed with the financial support from MicroNed program, under cluster-II of Smart Microchannel technology (SMACT) and work package II-G-2 and 3 (Smart Micro Reactors). The authors gratefully acknowledge Dr. M. Smithers for SEM and TEM analysis, Dr. G. Kip for XPS analysis, J.A.M. Vrieling for XRF, and B. Geerdink for technical support. We would like to acknowledge Dr. A. Zwijnenburg for fruitful discussions and Dr. A. Tepass (Johnson Matthey Chemicals GmbH, Emmerich am Rhein, Germany) for ICP analysis.

References

- [1] H.S. Weinberg, C.A. Delcomyn, V. Unnam, Environ. Sci. Technol. 37 (2003) 3104-3110.
- [2] W.R. Haag, J. Hoigne, Environ. Sci. Technol. 17 (1983) 261-267.
- [3] M.S. Siddiqui, G.L. Amy, Journal American Water Works Assoc. 85 (1993) 63-72.

- [4] IARC, *Potassium Bromate (Summary Data Reported and Evaluation)*, IARC, Lyon, 1999.
- [5] World Health Organization, *Bromate in Drinking-water. Background Document for Preparation of WHO Guidelines for Drinking-water Quality*, World Health Organization Press, Geneva, 2005.
- [6] R. Butler, A. Godley, L. Lytton, E. Cartmell, Crit. Rev. Environ. Sci. Technol. 35 (2005) 193-217.
- [7] W.A.M. Hijnen, R. Voogt, H.R. Veenendaal, H. Vanderjagt, D. Vanderkooij, Appl. Environ. Microbiol. 61 (1995) 239-244.
- [8] C.G. van Ginkel, A.M. van Haperen, B. van der Togt, Water Res. 39 (2005) 59-64.
- [9] M. Siddiqui, W.Y. Zhai, G. Amy, C. Mysore, Water Res. 30 (1996) 1651-1660.
- [10] W.J. Huang, L.Y. Chen, Environ. Technol. 25 (2004) 403-412.
- [11] N. Kishimoto, N. Matsuda, Environ. Sci. Technol. 43 (2009) 2054-2059.
- [12] H. Chen, Z.Y. Xu, H.Q. Wan, J.Z. Zheng, D.Q. Yin, S.R. Zheng, Appl. Catal. B 96 (2010) 307-313.
- [13] D.H. Dung, W. Erbs, S.B. Li, M. Gratzel, Chem. Phys. Lett. 95 (1983) 266-268.
- [14] A. Mills, G. Meadows, Water Res. 29 (1995) 2181-2185.
- [15] J.K. Chinthaginjala, J.H. Bitter, L. Lefferts, Appl. Catal. A 383 (2010) 24-32.
- [16] J.J.F. Scholten, A.P. Pijpers, A.M.L. Hustings, Catal. Rev. – Sci. Eng. 27 (1985) 151-206.
- [17] D.B. Thakur, R.M. Tiggelaar, J.G.E. Gardeniers, L. Lefferts, K. Seshan, Chem. Eng. J. (2010) 899-908.
- [18] J.K. Chinthaginjala, D.B. Thakur, K. Seshan, L. Lefferts, Carbon 46 (2008) 1638-1647.
- [19] C. Pham-Huu, N. Keller, L.J. Charbonniere, R. Ziessle, M.J. Ledoux, Chem. Commun. (2000) 1871-1872.
- [20] F. Salman, C. Park, R.T.K. Baker, Catal. Today 53 (1999) 385-394.
- [21] C.H. Bartholomew, Appl. Catal. A 212 (2001) 17-60.
- [22] M. Besson, P. Gallezot, Catal. Today 81 (2003) 547-559.
- [23] C.W. Huang, S.C. Chiu, W.H. Lin, Y.Y. Li, J. Phys. Chem. C 112 (2008) 926-931.
- [24] H.G. Manyar, D. Weber, H. Daly, J.M. Thompson, D.W. Rooney, L.F. Gladden, E.H. Stitt, J.J. Delgado, S. Bernal, C. Hardacre, J. Catal. 265 (2009) 80-88.
- [25] M. Vukovic, T. Valla, M. Milun, J. Electroanal. Chem. 356 (1993) 81-91.

- [26] J.F. Moulder, W.F. Stickle, P.E. Sobol, K.D. Bomben, *Handbook of X-ray Photoelectron Spectroscopy*, Perkin-Elmer, Physical Electronics Division, 1992.
- [27] D. Briggs, M.P. Seah, *Practical surface analysis: by auger and x-ray photoelectron spectroscopy*, John WILEY & SONS, 1993.
- [28] P. Gao, C.H. Lin, C. Shannon, G.N. Salaita, J.H. White, S.A. Chaffins, A.T. Hubbard, *Langmuir* 7 (1991) 1515-1524.

Chapter 7

Conclusions and Recommendations

Abstract

The work presented in this thesis highlights the use of carbon nanofibers (CNFs) as structured support materials for catalytic phase. Integration of such layers inside the structured channels of microreactor module was the main task of this thesis. In previous chapters systematic study of the various aspects, including synthesis, morphology, surface chemistry and catalytic performance of CNF layers, was presented. This chapter summarizes main conclusions of the work carried out in this thesis followed by some recommendations for future research.

In **Chapter 2**, synthesis of carbon nanofibers on fused silica substrates coated with nickel based thin-films using thermal catalytic chemical vapor deposition of ethylene (700 °C, 1h growth time) was investigated. Three different adhesion layers were used under the nickel layer. Although CNFs could be synthesized on 25 nm nickel with a titanium adhesion layer (10-200 nm), titanium is not a good adhesion material. The use of a 10 nm thick adhesion layer of titanium-tungsten or tantalum resulted in the formation of well-attached CNF-layers. The carbon nanofibers in these layers were entangled, quasi-crystalline and showed tip-type growth mode. For both metal layer configurations, *i.e.* Ni/Ti-W and Ni/Ta, the thickness of the CNF layer was $\sim 3.5 \mu\text{m}$, whereas the diameter of the fibers was smaller in case of Ni/Ta (20-50 nm) compared to Ni/Ti-W (80-125 nm). This is related to the grain size of the nickel nanoparticles formed during the reduction treatment prior to the CNF synthesis step. The presented results on the adhesion and properties of CNF-coatings synthesized on nickel based thin-films on fused silica yields important knowledge for the fabrication of CNF-based catalyst support layers to be used in microreactors for multiphase reactions.

In **Chapter 3**, the synthesis and characterization of carbon nanofiber (CNF) layers on fused silica and oxidized silicon substrates using nickel-based thin-films (*i.e.* Ni/Ti-W and Ni/Ta) is described. By means of high-resolution SEM imaging the influence of various growth parameters on the morphology of catalytic thermal chemical vapour deposited CNF-coatings is studied. It was found that the most important parameters were ethylene concentration and addition of hydrogen to the reactant mixture. In case of Ni/Ti-W and Ni/Ta thin-films (25 nm Ni, 10 nm Ti-W or Ta) on flat fused silica or oxidized silicon substrates, open, entangled ‘jungle’ CNF layers were found for ethylene concentrations $\geq 25 \text{ vol.}\%$. Moreover, addition of hydrogen to ethylene significantly enhances the rate of formation of CNFs, and reduces the average diameter of the fibers. When Ti-W is used as adhesion material for Ni, the concentrations of ethylene and hydrogen should not exceed 25 vol.% and 6.25 vol.%, respectively, in order to avoid the existence of a thick ‘dense’ C-layers between the substrate and the ‘open’ CNF layer. However, for similar synthesis conditions this C-layer is absent when Ta is used as adhesion material.

CNF layers are to be used as a structured catalyst support in microreactors. The ‘optimal’ C-TCVD conditions (*i.e.* C_2H_4 with H_2 and a Ni/Ta thin-film) resulted in a good thickness uniformity of CNFs synthesized on the sidewalls of oxidized silicon micropillar arrays. The CNF layers filled the complete space between the pillars, which

is important for performing gas-liquid-solid reactions. Catalytic metal particles were successfully pulsed laser deposited on such rigid, open-structure CNF-coatings, and the particles were homogeneously dispersed over the complete CNF layer. Despite the visually ‘open, entangled jungle’ character of the CNF layer and the homogeneous distribution of the nanoparticles across its thickness, prior to use of functionalized CNFs in microreactors issues such as mass transfer need to be verified experimentally. These aspects were investigated for liquid phase reactions with Pd and/or Ru anchored to the CNF-layer.

In **Chapter 4**, ruthenium catalytic nanoparticles on carbon nanofiber support layers were realized *via* homogeneous deposition precipitation and pulsed laser deposition. CNF layers are functionalized by oxidation with nitric acid to facilitate Ru deposition. Besides removal of exposed nickel (used for CNF-growth), acid treatment forms oxygen-containing groups on the surfaces of CNFs (mainly carboxyl and hydroxyl groups).

Ruthenium was anchored on oxidized CNF layers by means of HPD and PLD. Critical issues for a good dispersion of the particles and a sharp size distribution are the pH of the precursor solution (HDP) and the reduction treatment after deposition (PLD). Both optimized deposition methods resulted in a ruthenium loading of 2.3 ± 0.1 wt.% (HDP had a narrower particle size distribution). The presence of nanoparticles across the complete thickness of the CNF layers was found to be uniform when HDP was used to deposit Ru on CNF layers. Using the optimal CNF-growth settings such that the spacings between cylinders in a silicon-based microreactor channel were completely filled with an open, entangled jungle CNF layer, these CNF layers were successfully functionalized and well dispersed ruthenium clusters grown. A catalytic microreactor module containing Ru particles attached to carbon nanofibers which fill the entire reactor volume keeping the highly porous and/or open structure, is achieved.

In **Chapter 5**, Carbon nanofiber supported palladium (Pd) catalyst layers synthesized inside silicon based microreactors were used for studying the reduction of aqueous nitrite solution. Nitrite hydrogenation is known to be kinetically fast reaction, hence ideal for demonstrating performance of synthesized CNF layers inside microreactor systems. The catalyst layers were prepared *via* incipient organic impregnation method using palladium acetylacetonate precursor solution in toluene. A relatively large average particle size of Pd (~7-9 nm) was obtained with uniform

distribution across the CNF layers. The mass transfer properties, both external and internal, were probed and the intrinsic rates of nitrite conversion (TOF) were found to be independent of the, (i) linear velocity higher than 90 cm/min (flow rate of 50 $\mu\text{L}/\text{min}$ for the current microreactor module), and (ii) CNF layer thickness below $\sim 13\text{ }\mu\text{m}$, indicating the absence of any mass transfer limitations. Thus optimized CNF layers then can be applied for performing relevant aqueous phase reactions, such as aqueous phase bromate reduction.

In **Chapter 6**, carbon nanofiber supported ruthenium catalyst layers integrated in silicon based microreactors showed a promising catalytic performance in eliminating bromate contamination from aqueous solutions. It was demonstrated that a CNF based catalyst is indeed highly active for bromate reduction, resulting in TOFs larger in comparison to conventional powdered catalyst *i.e.* Ru/activated carbon. This enhanced catalytic performance is due to improved mass transfer properties of entangled CNF layers with macroporous (open) structure, which offer low tortuosity and subsequently enhanced accessibility to all the Ru active sites, in contrast to the poor accessibility of active sites in the case of microporous AC support material. This benefit is crucial to in particular heterogeneously carried liquid phase reactions where mass transfer limitations are important factor. Although a high catalytic activity was shown, a gradual deactivation of the Ru/CNF catalyst was observed under current experimental conditions. Further investigation of used catalyst showed that severe sintering took place and confirmed no deposition of coke or amorphous carbon on Ru catalyst. Specific characterization using XPS indicate the formation of $\text{Ru}(\text{OH})_x$ species as an additional cause of deactivation. The use of higher alcohols indeed limited the extent of deactivation by controlling hydroxylation of Ru.

It is proposed that aqueous phase bromate removal is carried out by heterogeneous redox catalysis *via* bromate reduction to bromide, mainly by RuO_2 which itself gets oxidized to a higher oxidation state and react with alcohol to be recycled after being reduced in the process. In general, Ru supported on CNF layers inside microreactor systems offers a promising option in terms of efficiency and offer a “green” method for removal of drinking water pollutants such as bromate.

Recommendations

It has been shown in this thesis that stable CNF layers with an open, entangled morphology can be synthesized on the structured internals of silicon based microreactor channels using Ni thin films. However, deposition of CNF growth metal in pillared microchannels, particularly with high aspect ratios and small inter pillar spacing can pose a challenge in terms of obtaining a uniform thickness of Ni across the pillar height. This consequently can result in non-uniform growth of CNFs, as also described in chapter 3 of this thesis. Though this issue has been effectively dealt in this work by optimizing growth conditions, the metal PVD deposition technique does need further optimization. One way to overcome this issue can be carrying out deposition at an angle with respect to the substrate/wafer. This would reduce the non-uniformity in the thickness of deposited metal film on the pillar sidewalls, and thus be beneficial for synthesizing a uniform CNF layer thickness. Obviously, the use of large(r) pillar spacing and limited pillar height also helps.

The pillars fabricated in microchannels can be utilized for distributive gas injection along the microchannel length for multiphase (gas-liquid-solid) reactions. The reactor configuration described so far is suitable for operation in heterogeneously catalyzed liquid phase and/or gas-saturated liquids (as shown in chapter 6 and chapter 5, respectively). Measures can be taken to introduce gas in the reactor along the length of microchannels *via* hollow porous pillars, mimicking a membrane reactor configuration. This can be an important aspect in terms of product distribution as conversions in such reactions are found to be very sensitive to concentration gradients typically occurring along used microchannel lengths. Such CNF-microreactors can be evaluated to introduce gas to the reactor and to optimally mix gas and liquid phase. However, the spatial synthesis of CNF layers on these porous cylinders has to be optimized to be able to inject the gas through hollow porous pillars.

PLD has been utilized as one of the methods to anchor catalytic active sites on CNF layers in microreactor channels. As already mentioned in chapter 4, it could provide various possibilities for exploring active metal deposition. It could be possible with this method to perform multi-component deposition, maintaining required stoichiometry to obtain bi-metallic/oxidic catalytic materials [1, 2]. However, obtaining uniform deposition of active metal on each individual fiber across the entire CNF layer thickness would be difficult. This uncertainty indeed motivated to opt for liquid phase deposition techniques in this work (chapter 5 and 6). Nevertheless a further tuning

and/or optimization of parameters during PLD deposition can be a way to utilize this method effectively to anchor active metal sites on CNF layers. Parameters such as target-substrate distance, the spot size of laser beam, the laser fluency and frequency, the gas pressure (*e.g.* Ar atmosphere) in deposition chamber and controlling the temperature of substrate *via* holder heater can be some important parameters that can affect the overall quality of deposition of active metal on the CNF layers. It would also be useful to vary and/or optimize CNF bulk density (amount of CNFs per unit microchannel volume) accordingly to minimize shadow effect of entangle morphology of CNF in terms of exposing individual fiber to the flux of active metal. This has to be supported with appropriate characterization to investigate the degree of uniformity of metal deposition on isolated spots across the CNF layer thickness.

The application of CNF supported catalysts for nitrite and bromate removal inside structured microreactors has been shown in this thesis. Comparable system configurations can be applied for carrying out other reaction of similar requirements, particularly reactions with facile kinetics. For example alkyne hydrogenation (*e.g.* using Pd) which has a selectivity issue, that is alkene product can be further hydrogenated to alkane. The benefit of open-structure support materials such as CNFs can be demonstrated for such reactions. Diffusion limitations which can lead to loss in selectivity of alkene can be avoided. The presence of nickel (in trace amounts also) is not an issue since the commercial alkyne selective hydrogenation catalyst also contains nickel which is seen beneficial. The comparison with a mesoporous catalyst support such as $\gamma\text{-Al}_2\text{O}_3$ can be used to highlight the advantages of microreactor with CNF to achieve better accessibility of catalytic sites. Eventually role of CNFs (when hydrophobic, non-acidic) itself in altering (*i*) activity of metal for alkyne conversion and (*ii*) selectivity to alkenes, has to be investigated and elucidated further for better insights.

The configuration of pillars arranged inside microreactor channel can be tested with different designs.

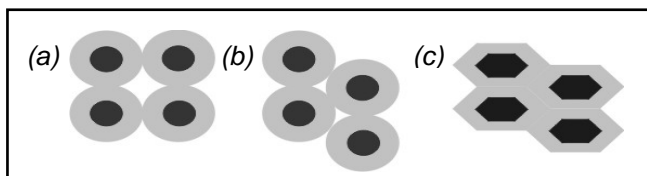


Figure 7.1: Schematic representation of various arrangements of arrays of pillars micromachined inside reactor channels. (black portion is a pillar, grey portion is CNF-layer anchored on sidewalls of pillars).








Figure 7.1 shows some possible options. An array of diamond-shaped pillars can be the preferred one to obtain even more efficient CNF-filling, provided that the Ni is uniform on all sides.

In this work the use of stable thin metal films for synthesizing well attached CNF layers has been demonstrated. Porous ceramic layers deposited/prepared on flat surfaces of microreactor channels can also facilitate the integration of catalytic CNF layers into microreactors. The layers of γ -alumina deposited for example by sol-gel method can be prepared on microreactor channel internals. Thus prepared layers can further be impregnated with nickel particles *via* classical impregnation techniques which will further act as nucleation sites for CNF growth using catalytic thermal chemical vapor deposition (C-TCVD) of carbon containing gases. γ -Al₂O₃ is a promising candidate due to high surface area, high thermal stability and controllable surface acidity [3]. Important parameters that needed to be optimized are for example, stability and thickness of ceramic layer and porosity, since penetration of nickel particles and subsequent mechanical attachment of later synthesized CNF layers can be dependent on it. Additionally, loading of Ni deposited on alumina layer has to be optimized to control CNF growth later. Moreover, CNF growth parameters during C-TCVD (as described in chapter 3) have to be re-evaluated to avoid any problems with CNF layer stability as well as morphology.


References


- [1] G. Koster, *Artificially layered oxides by pulsed laser deposition*, PhD Thesis, University of Twente, Enschede, The Netherlands, 1999.
- [2] G. Rijnders, *The initial growth of complex oxides: study and manipulation*, PhD Thesis, University of Twente, Enschede, The Netherlands, 2001.
- [3] R.A. van Santen, P.W.N.M. van Leeuwen, J.A. Moulijn, B.A. Averill, *Catalysis: An Integrated Approach*, Stud. Surf. Sci. Catal., Elsevier publishing (1999) 439-442.


List of Publications


-  **D.B. Thakur**, R.M. Tiggelaar, J.G.E. Gardeniers, K. Seshan, L. Lefferts
Synthesis of carbon nanofibers as support layer for metal catalyst in a microreactor for three-phase reactions,
Adv. Sci. Technol. 54 (2008) 231-236.
-  J.K. Chinthaginjala, **D.B. Thakur**, K. Seshan, L. Lefferts
How carbon nano-fibers attach to Ni foam,
Carbon 46 (2008) 1638-1647.
-  **D.B. Thakur**, R.M. Tiggelaar, J.G.E. Gardeniers, L. Lefferts, K. Seshan
Growth of carbon nanofiber coatings on nickel thin films on fused silica by catalytic thermal chemical vapor deposition: On the use of titanium, titanium-tungsten and tantalum as adhesion layers,
Surf. Coat. Technol. 203 (2009) 3435-3441.
-  **D.B. Thakur**, R.M. Tiggelaar, J.G.E. Gardeniers, L. Lefferts, K. Seshan
Carbon nanofiber based catalyst supports to be used in microreactors: Synthesis and characterization,
Chem. Eng. J. 160 (2010) 899-908.
-  **D.B. Thakur**, R.M. Tiggelaar, T.M.C. Hoang, J.G.E. Gardeniers, L. Lefferts, K. Seshan
Ruthenium catalyst on carbon nanofiber support layers for use in Si-based structured microreactors, Part I: Preparation and characterization
Appl. Catal. B – Environmental (2010) submitted.
-  **D.B. Thakur**, R.M. Tiggelaar, Y. Weber, J.G.E. Gardeniers, L. Lefferts, K. Seshan
Ruthenium catalyst on carbon nanofiber support layers for use in Si-based structured microreactors, Part II: Catalytic reduction of bromate contaminants in aqueous phase
Appl. Catal. B – Environmental (2010) submitted.
-  R.M. Tiggelaar, **D.B. Thakur**, H. Nair, K. Seshan, L. Lefferts, J.G.E. Gardeniers
Growth of carbon nanofiber coatings on nickel thin films by catalytic thermal chemical vapor deposition: Influence of pretreatment conditions and adhesion layer on the CNF coating,
(*in preparation*)


Conference Presentations


-  **D.B. Thakur**, R.M. Tiggelaar, J.G.E. Gardeniers, L. Lefferts, K. Seshan. Synthesis of carbon nanofibers as support layer for metal catalysts in a microreactor for three-phase reactions, IMRET-10: 10th International Conference on Microreaction Technology, AIChE Spring National Meeting, New Orleans, 2008, United States of America.


-  J.K. Chinthaginjala, **D.B. Thakur**, K. Seshan, L. Lefferts. How Carbon-Nano-Fibers attach on Ni foam, 9th Netherlands Catalysis and Chemistry Conference, Noordwijkerhout, 2008, The Netherlands.


-  **D.B. Thakur**, R.M. Tiggelaar, J.G.E. Gardeniers, L. Lefferts, K. Seshan. Effect of growth conditions on carbon nanofibers grown on fused silica substrates using nickel thin-film catalyst, CARBON'08: International Conference on Carbon, Nagano, 2008, Japan.


-  **D.B. Thakur**, R.M. Tiggelaar, J.G.E. Gardeniers, L. Lefferts, K. Seshan. Carbon nanofibers as structured catalyst supports for microreactors, Annual meeting of MESA+ Institute for Nanotechnology, Enschede, 2008, The Netherlands.


-  **D.B. Thakur**, R.M. Tiggelaar, S.R.A. de Loos, H. van den Vlekkert, M.H.J.M. de Croon, J. Van der Schaaf, J.C. Schouten, J.G.E. Gardeniers, L. Lefferts, K. Seshan. Development of smart microreactors, Netherlands MicorNano Conference '08, Ede, 2008, The Netherlands.


-  **D.B. Thakur**, R.M. Tiggelaar, J.G.E. Gardeniers, L. Lefferts, K. Seshan. Synthesis of carbon nano fiber (CNF) based structured catalyst support layers on fused silica and silicon substrates: model systems towards multi-phase microreactors. 10th Netherlands Catalysis and Chemistry Conference, Noordwijkerhout, 2009, The Netherlands.


-  **D.B. Thakur**, R.M. Tiggelaar, J.G.E. Gardeniers, L. Lefferts, K. Seshan. Carbon nanofibers as catalyst supports for microreactors, 2nd International Conference on Frontiers in Nanoscience and Technology- CochinNano'09, Cochin, 2009, India.

-  **D.B. Thakur**, R.M. Tiggelaar, J.G.E. Gardeniers, L. Lefferts, K. Seshan. Carbon nanofibers (CNFs): A novel structured catalyst support layer for multi-phase microreactors, 2nd FERMaT-IMPACT Meeting, Enschede, 2009, The Netherlands.

-  **D.B. Thakur**, T.M.C. Hoang, R.M. Tiggelaar, J.G.E. Gardeniers, L. Lefferts, K. Seshan. Structured catalyst layer based on carbon nanofibers (CNFs) for multi-phase microreactors, 11th Netherlands Catalysis and Chemistry Conference, Noordwijkerhout, 2010, The Netherlands.

-  **D.B. Thakur**, R.M. Tiggelaar, J.G.E. Gardeniers, L. Lefferts, K. Seshan. Development and application of carbon nanofiber based nanostructured catalyst support layer for microreaction systems, The Annual World Conference on Carbon, CARBON'10, Clemson, 2010, United States of America.

-  **D.B. Thakur**, T.M.C. Hoang, R.M. Tiggelaar, J.G.E. Gardeniers, L. Lefferts, K. Seshan. Structured features in micro catalytic reactor – preparation of ruthenium catalyst on carbon nanofibers, The 10th International Symposium on the “Scientific Bases for the Preparation of Heterogeneous Catalysts”, Louvain-la-Neuve, 2010, Belgium.

-  **D.B. Thakur**, R.M. Tiggelaar, J.G.E. Gardeniers, L. Lefferts, K. Seshan. Carbon Nano Fibers (CNFs) as ‘open-structured’ catalyst support for aqueous phase reactions in microreactors, 3rd FERMaT-IMPACT-GIMFus Meeting, Seville, 2010, Spain.

Acknowledgements

Now coming to a non-scientific part of this thesis book (which indeed benefited in realizing previously presented scientific part), that is expressing my sincere gratitude to all who supported and contributed either directly or indirectly to make my journey enjoyable during last more than four years to achieve this milestone in my life.

Initially, I would like to express my deepest gratitude to my promoter Prof. Leon Lefferts for giving me an opportunity to perform my PhD work in CPM group. Leon, I will always be grateful for your critical and insightful contribution in the realization of my PhD thesis. Apart from our progress meetings, the annual group gatherings at your residence and group trips rendered me an opportunity to know you more through our open discussions about various interesting topics including social trends. Your visit to my home during your stay for a conference in Pune is a rare and pleasant memory for me.

It would be rather unrealistic to put in few words or lines the support and contribution given by my daily supervisor Dr. K. Seshan in helping to make this thesis a reality. Seshan, your ever enthusiastic attitude to always go farther in a quest to know the details not only taught me to find new avenues in scientific research but also thinking with broader perspectives. As someone has rightfully said, "The dream begins with a teacher who believes in you, who tugs and pushes and leads you to the next plateau, sometimes poking you with a sharp stick called "truth"". You along with Jayanthi played various roles in my life for past more than four years including that of teachers, guardians, and friends. Jayanthi, thanks for all the delightful gatherings with testy food at you place, which really made me feel at home during my stay in Enschede.

It would not have been possible to realize this project to its fullness without my collaborator at MCS group and friend Dr. Roald Tiggelaar. Roald, your aptitude for novel ideas was a crucial factor for reaching to this stage. I greatly appreciate your resourcefulness and readiness to help. It was a joyful venture for me to write all the manuscripts with you which are the result of our collaboration. With our numerous sessions of fruitful discussions I enriched myself with an ability to analyze the results critically and report the facts clearly. Your passion for biking gave me the glimpse of Dutch love for bicycle. I appreciate your assistance in proofreading my thesis manuscript and helping in translating the English summary into Dutch language.

I would like to thank my project collaborators Prof. Han Gardeniers at the University of Twente, Prof. Jaap Schouten and Ir. Stijn de Loos at the Technical University of Eindhoven (TU/e) and Mr. Hans van den Vlekkert at LioniX BV, Enschede for fruitful discussions on various aspects of project work whenever needed.

I would also like to extend my special thanks for the team from MESA+ who certainly was instrumental in obtaining valuable characterization results during my PhD thesis work. Thank you Mark for numerous SEM and TEM analysis sessions and patiently obtaining fabulous images

and data. Rico, thanks for timely discussions of TEM results. Gerard, I appreciate your help in performing XPS analysis.

Igor, I had a great time all these years in CPM with you. Memories of Friday borrels which we had in Langezijds will stay with me for long time, including your adventure of building tallest stack of beer bottles (the record still remains unbeaten and I believe will remain so in future☺). I along with Aabha, definitely enjoyed the very Ukrainian hospitality at the ceremony of silver jubilee of your marriage to Jana. Thanks for all these pleasant memories.

Barbara, it was always been pleasant to have you around with your jolly personality. Your unique approach to science as well as life has always motivated me positively. I always enjoyed the home made apple tarts frequently made by you, which along with fresh home grown fruits helped to make our coffee breaks healthier for me. Dr. Jan van Ommen, thanks for all our occasional light discussions either in group trips or in the corridors of CPM. I would also like to extend my thanks to Dr. Arie van Houselt for being an encouraging colleague and for his always ready to help attitude. I also like the way you bring a light mood around with your unique jokes and belly laughter. Dr. A. (Bart) Zwijnenburg, thanks for the support and understanding during the time, which coincided with my new assignment in CPM. Your practical inputs and proactive help in characterization were quite useful. Bert'olino, it was a great pleasure to spend last more than four year of my stay in CPM with you. Your vast practical knowledge and long experience with labs is certainly a crucial factor for any research project in CPM to reach its successful end and it is true in my case as well. Thank you very much for all the help you provided throughout my PhD journey. Apart from that, you were a connecting link between me and various Dutch organizations, whether it was health insurance, immigration office or tax office. I still remember the persuasive communication (of almost more than two years) we both had with tax office for my rightful tax returns, which at last ended positively.

I found my self fortunate to be supported by not one but three group secretaries. Lianne, Sabine, and Lidy, thank you all for supporting me at various stages of my stay here in Enschede during PhD. Karin, thanks for your kind help in lab and interesting discussions on coffee table and during borrels. I appreciate your several initiatives in organizing group dinners. Louise, your lively presence around is appreciable. Thanks for all the measurements, even at short notice.

Now it's time to express my gratitude to all my former and current CPM colleagues and friends, without their continuous support and enjoyable companionship it would not have been easy to accomplish my PhD journey. Dejan, thanks a lot for being a warm hearted colleague and a good friend. Your persuasive and passionate nature constantly motivated me. I still remember the parties at your place especially with the testy traditional Serbian food made by your mother. The Keukenhof trip together with you, your mother and Cassia still holds a pleasant memory in my mind. Cristiano, thanks for being a wonderful friend and an enthusiastic colleague. You have a great zeal for science and a unique way to simplify and explain the difficult things. I experienced the glimpse of the very Italian things in your personality *i.e.* fashion, football and cars. It was wonderful time when we used to spend the long working hours in labs in Langezijds. Khalid,

thanks for being helpful and cheerful colleague. My first day in CPM (during my interview) I spent with you and was the beginning of my successful venture at CPM. It was a pleasure to be one of your paranymphs as well.

Kumar, thanks for being a great friend to me and a supporting colleague. Your support during the first years of my PhD not only helped me to enrich myself with professional attitude but also assisted in socializing. As they rightfully say about you, one of the most 'European Indian' around, I had a great time with you in CPM and outside. Particularly, all the trips to various European destinations still hold a cherishing memory in my mind. Davide, being officemate I spent quite some time with you during my PhD. It was wonderful to experience your Sicilian spirit during this time through your vibrant personality. I enjoyed all those potluck evenings at your place together with other CPM members. Thanks for creating a lively atmosphere in the office as well as in lab with your talkative presence. Berta, you were always an inspiring colleague to me with your fighting nature and not giving up attitude. Your chatty personality virtually made you CPM's spokesperson, making the coffee table and Friday borrels conversations sometimes very 'interesting'. Cassia, we started our PhD work in CPM around same time. Thanks for sharing the joyful and difficult moments of our PhD journey. Your diligence to tackle the difficult times effectively, constantly inspired me to keep my strengths together. Your inclination towards performing arts is unique in its own way. I wish you and Bedo a prosperous future. I would also like to thank some of my former colleagues Sune, Hans, Patrick, Anil, Joreon who also directly or indirectly made my PhD journey unforgettable.

Though time has passed and many colleagues have left the group after successfully completing their endeavor in CPM, fortunately many new colleagues have joined in and made the absence of long time buddies feel less painful. I would like to express my gratitude to all of them. Sergio, I had a nice time with you in lab and around. Your humor has its own shade which some times relieved stressful moments in my later years of PhD. Hrudya, your innocent smile keeps the atmosphere light and fresh. Thanks for being an encouraging friend and colleague. Marijana, thanks for your cheering words and for a pleasant company during long working hours in labs, which were routine during last months of my PhD. Son, thanks for being a helpful and jovial colleague; also sharing the room either in NCCC or in group trips. Dennis, I had numerous discussions with you on all sorts of topics from shooting to politics, which also made my time in CPM exciting.

Željko, it has been my pleasure to have you as my officemate for last almost two years, which subsequently resulted in meeting a compassionate friend. Your proactive and modest nature is unique and highly appreciable. I would like to express my gratitude for all the help which enriched me in numerous ways. Thanks for being my Paranymph. I wish you all the happiness in your life you deserve. Inga, your presence in CPM was pleasant. I not only appreciate our interesting conversations as members of CNF team but also which we had in numerous group gatherings. Chris, your style to crack sharp jokes is unique in itself. Thanks for your lively presence around in CPM. Martine, Arturo, Yingnan, Masoud, Shilpa, Koteswara, Yejun it is great

pleasure to have you all around in recent months. Our occasional discussions regarding science and other topics, made last months of my PhD unforgettable. Tom, your crispy jokes make the atmosphere light from time to time. Ruben, I appreciate your friendly attitude and cooperative nature. Joline, thanks for your important contribution to my project during your bachelors assignment. I enjoyed working with you and wish you all the best for your PhD endeavor in CPM.

I would like to express my thanks to Chau and Yasmin for their contribution in my project, which consequently assisted in realizing this thesis book to its fullness. Thank you very much to both of you for this valuable contribution. Chau, it was very enjoyable to have numerous sessions of discussions with novel ideas to implement in the project. Your aptitude for testing new things and diligently performing experimental work definitely obtained valuable results. Yasmin, you have been tremendously helpful in accomplishing last necessary part of experimental work for the thesis. Your dedication was undoubtedly exceptional to make things happen in lab in very last months of my PhD work. I would like to thank you for the valuable time you did invest in finishing experiments including the weekends and daily extended hours. I wish you all the best for your career. Can, even though I met you late in my stay here, I always enjoyed your company ever since we started our collaboration. Even though you are not officially in CPM, your constant presence in our lab made you virtually a CPM member☺, which definitely benefited me. I found our conversations invigorating and I highly appreciate your always ready to help attitude.

Being abroad for such a long time would never have been so easy for me in first three and half years and for Aabha for last one year without the emotional and moral support of my Indian friends. They filled the void of social variation and provided us the much needed intervals of relaxation. One of the best thing happened to me after coming to Netherlands is that I met Chandu, Sameer and Pramodji. Dear Chandu, as we share the same zodiac, I guess we also understand each other very good. Thanks for being a true and understanding friend. You and Meenakshi were extremely helpful to make our life enjoyable here. Thanks for being my Paranymp. Sameer, you have been a motivating friend to me whose companionship enriched me in various ways. Thanks for being a supportive and caring friend. Pramodji, your thoughtful and understanding nature has always been a big boost to me in all situations. You, Vishakha and Vibhor created a homely atmosphere away from India for me and Aabha. Thanks for all. I would like to take this opportunity to also thank Ravi and Madhavi for their wonderful company during initial years of my PhD. Ambati-Sangeeta, thanks for your pleasant friendship and interesting discussions from politics to mathematics. Ambati, I appreciate your passion for cooking and hope to be your guest for many more evening dinners☺.

I would like to express my sincere thanks to 'Aadhaar', a small family of like-minded people inspired with the common goal of welfare in India, of which I am a member from the beginning of my stay here in Enschede. It offered a rare opportunity to contribute the best possible way towards the welfare of underprivileged in India. I would like to thank all Aadhaar members, including Parmaji, Letteke, Sandeep-Jalaja, Srivatsa, Karina, for a wonderful time and fruitful meetings with diverse projects.

I truly believe this achievement is not for me alone. My family, who is the essential reason for me to be where I am today, indeed deserves the gratitude for this success. It is beyond words to appreciate their contribution to my life. Their devotion and numerous sacrifices all the way long ultimately helped to achieve this success. I will remain indebted to my mother for instilling an inspiration to see dreams and determination to fulfill them and to my father for his everlasting kind support. I would like to thank my sister Shraddha for her continual loving support. Aabha, you were always there for me in testing moments. Your ceaseless faith in me and love made this happened. I owe you special thanks for your patience and understanding, particularly during last days of my PhD.

Digvijay Bhagwan Thakur
Enschede, October 2010



Digvijay Bhagwan Thakur, was born on April 24th, 1979 in Nasik, India. In 2001 he graduated in Petrochemical Engineering from Maharashtra Institute of Technology, University of Pune. In October 2003 he joined the masters course in Chemical and Process Engineering at the Otto-von-Guericke University of Magdeburg, Germany. He was awarded the degree of M. Sc. in Chemical and Process Engineering in November 2005 after completing the master thesis work titled 'Structure-activity relations in the catalytic oxidation of hydrocarbons'. The work was carried out under the supervision of Prof. A. Seidel-Morgenstern at The Max Planck Institute for Dynamics of Complex Technical Systems, Magdeburg.

In February 2006, he started his PhD at the University of Twente in Catalytic Processes and Materials group on the project titled 'Smart Micro Reactors', under the guidance of Prof. L. Lefferts and Dr. K. Seshan. This thesis is focused on realizing microreaction systems for heterogeneously catalyzed liquid phase reactions, particularly using carbon nanofiber supported catalyst layers on structured internals of microreactors. From May 2010, he is working as a post doctorate in the same group.

